Doctoral Dissertation

Development and application of dual fluorescence-linked immunosorbent assay for the quantification of full and empty particles of adeno-associated virus vectors

SOTH SEREIRATH

September 2024

Laboratory of Macromolecular Biotechnology,
Department of Biotechnology,
Graduate School of Engineering,
Osaka University

Table of Contents

Abbreviation

AAV	adeno-associated virus
Ads	adenoviruses
AAP	assembly-activating protein
BS-AUC	band sedimentation analytical ultracentrifugation
BSA	bovine serum albumin
CRISPR	clustered regularly interspaced short palindromic repeats
cp	capsid particle
CMV	cytomegalovirus promoter
CV	coefficient of variation
DNA	deoxyribonucleic acid
dPCR	digital polymerase chain reaction
dsDNA	double-strand DNA
dFLISA	dual fluorescence-linked immunosorbent assay
ELISA	enzyme-linked immunosorbent assay
EP	empty particle
ExP	extrafilled particle
Ex	excitation wavelength
Em	emission wavelength
EGFP	enhanced green fluorescent protein
FP	full particle
FIX	factor IX
GuHCl	guanidine hydrochloride
QC	quality control
HRP	horseradish peroxidase
HCRhAAT	hepatic control region and human a1 antitrypsin promoter
HSV	herpes simplex viruses
ITR	inverted terminal repeat
LOQ	limit of quantification
LV	lentivirus
LNP	lipid nanoparticles
MP	mass photometry
MAAP	membrane-associated AAV protein
OD	optical density
ORF	open reading frame
PP	partially filled particle
PBS	phosphate-buffered saline

pA	polyA
qPCR	quantitative polymerase chain reaction
rAAV	recombinant adeno-associated virus
SD	standard deviation
ssDNA	single-stranded DNA
scDNA	self-complementary DNA
siRNA	small interfering RNAs
TMB	3,3′,5,5′-tetramethylbenzidine
UV-Vis	ultra violet-visible
vg	viral genome
VP	viral protein
VP1u	unique N-terminal region of VP1

List of Figures

List of Tables

Table 1. DNA/RNA/Primer/Promoter

Reagent	Source; Identifier
ssDNA ladder	PerkinElmer, Waltham, MA, USA
ITR forward primers	Hokkaido System Science
ITR forward primers	Hokkaido System Science
ITR probe	Hokkaido System Science

Table 2. Dyes

Reagent	Source; Identifier
SYBR Gold Nucleic Acid Gel staining solution	Invitrogen, Thermo Fisher Scientific (Eugene, OR, USA); S11495

Table 3. Antibodies

Reagent	Source; Identifier
CaptureSelect Biotin Anti-AAVX Conjugate (VHH)	Thermo Fisher Scientific (Eugene, OR, USA); 7103522100
Goat anti-mouse IgG H&L (Alexa Fluor 647)	Abcam (Cambridge, UK); ab150115
Lyophilized mouse anti-AAV8 monoclonal antibody (ADK8)	Progen, (Heidelberg, Germany); 610160
Lyophilized mouse anti-AAV2 monoclonal antibody (A20)	Progen, (Heidelberg, Germany); 61055

Table 4. Reagents

Reagent	Source; Identifier
BupH carbonate-bicarbonate buffer packs	Thermo Fisher Scientific (Eugene, OR, USA); 28382
Cesium chloride (CsCl)	Nacalai Tesque (Kyoto, Japan)
Bovin Serum Albumin (BSA)	Sigma Aldrich (St.Louis, MO, USA); A7030-10
DNase I Kit	Takara (Shiga, Japan); ALG1425A
0.5M EDTA (pH8.0)	Nippongene (Tokyo, Japan); 311-90075
Poloxamer-188	BASF Japan (Japan, Tokyo)
Phosphate buffered saline (PBS)	Thermo Fisher Scientific(Waltham, MA, USA); 70011044
Poly-L-lysine solution	Sigma Aldrich (St.Louis, MO, USA); P4707

QuantStudio Absolute Q Isolation Buffer	Thermo Fisher Scientific (Waltham, MA, USA); A52730
Sodium chloride (NaCl)	FUJIFILM Wako Pure Chemical (Osaka, Japan)
Stop solution (2M Sulfuric acid)	Thermo Fisher Scientific (Waltham, MA, USA); N600
Tween 20	Sigma Aldrich (St.Louis, MO, USA); P7949
TE buffer pH8.0	Vitrogen; AM9849

Table 5. Instruments

Instrument	**Source; Identifier**
Analytical ultracentrifugation AUC)	Beckman Coulter (Indianapolis, IN, USA)
Band Sedimentation-analytical ultracentrifugation (BS-AUC)	Beckman Coulter (Indianapolis, IN, USA)
AquaMax 4000: Microplate washer	Molecular Devices (Silicon Valley, LA, USA)
Clear Flat-Bottom Immuno Nonsterile 96-Well Plates	Thermo Fisher Scientific (Eugene, OR, USA); 442404
Nunc MaxiSorpTM flat-bottom 96-well plate Black 96-Well Immuno Plates	Thermo Fisher Scientific (Eugene, OR, USA); 437111
Matrix ™ Reagent Reservoir	Thermo Fisher Scientific (Eugene, OR, USA); 8093
Microplates (96 well, 200 µL, Black, Polypropylene (PP), Flat-Bottom, Greiner Bio-One)	Sigma Aldrich (St.Louis, MO, USA); M5811-40EA
Mass Photometry (TwoMP)	Refeyn Ltd,Oxford, UK
QuantStudio Absolute Q MAP16 Plate Kit	Thermo Fisher Scientific (Eugene, OR, USA); A52688
Absolute Q Digital PCR Master Mix (5x)	Thermo Fisher Scientific (Eugene, OR, USA); A52490
MicroAmp™Optical Adhesive Film	Thermo Fisher Scientific (Eugene, OR, USA); 4311971
Multi-channel precision pipettor	Eppendorf (Humburg, Germany)
Eppendorf ThermoMixer® C	Eppendorf (Humburg, Germany)
Micromixture E-36	TAITEC corporation (Saitama, Japan)
Spectramax^{R} i3x	Molecular Devices (Silicon Valley, LA, USA)
UV-Vis Spectrophotometer (Biomate 160)	Thermo Fisher Scientific (Eugene, OR, USA); 9A5Y041036

Abstract

Chapter 1: General Introduction

Gene therapy is the treatment of a genetic disease by the introduction of specific cell function-altering therapeutic gene into a patient's body. Adeno-associated virus (AAV) vector is one of the most advanced platforms for gene therapy because of its low immunogenicity, non-pathogenicity, and ability to substantiate long-term gene expression in different tissues. The concentrations of both AAV vector empty particles (EPs), which do not contain DNA and do not show any efficacy, and AAV vector full particles (FPs), which contain DNA, are important quality attributes. During the upstream process, it is difficult to completely remove EPs by purification because the physicochemical properties of EPs are only slightly different from those of FPs.

Analytical ultracentrifugation (AUC) is the gold standard for characterizing AAV vectors and can quantify FPs, EPs and ExPs. Mass photometry (MP) is a method that measures the mass of individual particles and provides the percentage of the particles against total counts (% counts). However, these analytical methods have limitations, especially in the case of crude sample. For example, it is burdensome that prior purification is required before using these analyses. A combination of enzyme-linked immunosorbent assay (ELISA) and polymerase chain reaction (PCR), which do not require purification before analysis, is a conventional method to quantify capsid and genome titers and to calculate FP ratios. However, the combination of ELISA and PCR is subject to inherent drawbacks of error and variability because it relies on data from two independent quantitative analyses which are based on different principles, and capsid and genomic titers must be quantified separately using non-identical samples.

In my study, I aimed to establish a dual fluorescence-linked immunosorbent assay (dFLISA) as an analytical method capable of simultaneously quantifying viral capsid and genomic titers in a single analysis using the same 96-well plate. This method is primarily based on ELISA followed by genome staining where two different fluorescent dyes are employed to quantify full and empty AAV vector particles and the FP ratio. After the addition of fluorescent dye conjugated secondary antibody, the plate was subjected to heat treatment to release the genome from the capsid before the introduction of the second fluorescent dye with.

Chapter 2: Development, validation, and comparison of dFLISA

In **Chapter 2**, a novel method named dual fluorescence-linked immunosorbent assay (dFLISA) was developed. Analytical conditions, such as genome detection following release from the capsid and the detection wavelength, were optimized. The dFLISA results for capsid titer, genomic titers and FP ratio were comparable to the expected values. Therefore, dFLISA allows the determination of the FP ratio in a simple way with high precision, high accuracy, and high sensitivity.

In addition, the developed method was validated successfully such as limitation of quantification (LOQ) and linearity, as well as in comparison with orthogonal methods. These results demonstrated that the good linear correlation between dFLISA and AUC was well observed with respect to FP ratio and other orthogonal methods including AUC, MP, and rather than the combination of ELISA and dPCR. This validates the robustness and reliability of the dFLISA method.

Chapter 3: Application of dFLISA

dFLISA was successfully developed, allowing the determination of capsid and genome

titers as well as the FP ratio in a simple way with high precision, high accuracy, high sensitivity and good linearity. The production of AAV vectors is a complex process influenced by multiple factors such as cell line or plasmid ratios. It is not only FPs that are generated, but also EPs, ExPs, and PPs. Remarkably, there is no existing methods that can quantify the full particle ratio of AAV vectors before purification in one assay. Considering this complexity, it is essential to apply the dFLISA method for the quantification of diverse AAV vectors in both purified and crude lysate samples.

In this **Chapter 3**, I also investigated on the application of dFLISA to determine if dFLISA can be used to quantify the FP ratio for different AAV serotypes. The results showed that dFLISA can be easily modified to measure other AAV vector serotypes. Moreover, the fluorescence intensity of the AAV vector varies with different genome lengths, and this factor is also relevant to dFLISA. I further performed the dFLISA analysis to compare the fluorescence intensity between AAV vectors with different genome lengths.

Another application of dFLISA focused on the analysis of crude lysate samples; the recovery efficiency of spiking levels was also evaluated to determine if dFLISA could be used to analyze crude samples without purification, despite the presence of host cell DNA and proteins that could potentially interfere with measurements. The results showed that dFLISA could accurately detect capsid and genome titers without interference from the sample matrix, whether it was purified or crude lysate. Subsequently, I evaluated the ability of dFLISA to quantify capsids/genomes in the presence of untreated crude lysate sample and compared the results with other methods such as ELISA and dPCR. The results showed that dFLISA could assess both capsid and genomic titers without purification. The capsid titer determined by dFLISA was comparable to that determined by ELISA whereas the genomic titer results with dFLISA were higher than those from dPCR. Therefore, dFLISA results are relatively unaffected

by matrix interference or impurities from the crude lysate.

The applicability of dFLISA as the developed method for the quantification of FP and EP in AAV vector samples, including other AAV vector serotypes and AAV vectors with different genome lengths, was demonstrated. Notably, since a potential advantage of dFLISA is to be applicable for the crude samples, spike recovery test was performed using crude lysate to evaluate the capability of dFLISA for capsid/genome quantification without interference the impurities from crude lysate. Thus, the result shown that dFLISA could accurately quantify the titer of crude samples, making it uniquely capable of directly quantifying the genomic titer and FP ratio of crude sample. dFLISA could be easily modified for measuring other AAV vector serotypes and AAV vectors with different genome lengths. These features made dFLISA a valuable tool for the future development of AAV-based gene therapies.

Chapter 4: General conclusion and future perspective

Through the **Chapter 2** and **Chapter 3**, the correlation between dFLISA and BS-AUC proved robustness and the reliability of the dFLISA for both full and empty capsids. dFLISA results also corresponded with those of other orthogonal techniques, including MP and a combination of ELISA and dPCR. Remarkably, dFLISA showed significant potential for evaluating the capsid and genome titers of unpurified samples and different AAV vector serotypes, making it a reliable analytical technique for AAV vector particle analysis.

In addition, I also viewed the future perspective with several promising directions for future developments and applications of dFLISA. Firstly, dFLISA has the potential to significantly increase throughput, making it an ideal solution for large-scale screening in pharmaceutical and clinical laboratories. Secondly, while this study concentrated on AAVs,

the principles of dFLISA could be applicable to other viral vectors, including lentiviruses (LVs) and adenoviruses, thereby broadening its applicability in gene therapy research. Thirdly, non-viral vectors such as lipid nanoparticles (LNPs), including liposomes or solid lipid nanoparticles, would encounter similar challenges and could be evaluated using a method like dFLISA. Fourthly, the combination of dFLISA with advanced imaging techniques or next-generation sequencing could provide comprehensive insights into viral vector characteristics and improve the precision of quantification. In sum up, it is expected that this work represents an exploration and generation of a novel method with significant implications for AAV quantification, offering substantial benefits for the advancement of AAV-based gene therapy in the future.

Chapter 1. General introduction

1. Gene therapy

Genetic diseases occur because of an alteration in our genetic material or DNA. The discovery of DNA as the biomolecule of genetic inheritance and disease has opened up the possibilities for therapies in which mutant or damaged genes could be altered for improving the human health.[1] If these mutant genes could be completely fixed, the disease could be treated at the molecular level, and in the best-case scenarios, potentially be cured. Recently, researchers have been able to rapidly and cost-effectively examine specific mutations or variations in DNA sequences that may cause disease.[2] They also investigate protein-coding regions that affect protein function, regulatory elements (such as promoters, enhancers, and silencers) that control gene expression, and non-coding regions (such as intronts) that help regulate gene expression and maintain genomic stability.[3] This approach enables the identification of disease-related genes and contributes to the development of targeted therapies.[4]

Therefore, in recent years, gene therapy is the treatment of a genetic disease by the introduction of specific cell function-altering genetic material into a patient, has been attracting attention as a method of fundamentally treating such genetic diseases.[5–7] Gene therapy is broadly categorized into two main types. The first one is *in vivo* gene therapy, in which normal genes are delivered directly into the patient's body, typically using vectors, which are carriers that transport the genetic material into the cells. These vectors are often modified viruses that have been engineered to safely deliver the genes without causing disease. Once inside the cells, the therapeutic genes can correct or compensate for genetic defects, potentially leading to improved health outcome and *ex vivo* gene therapy, in which normal genes are introduced into cells taken from the patient, modifying them with the

therapeutic gene outside the patient's body. The therapeutic genes are introduced into these cells using vectors, which then alter the cell's genetic modification. After the cells are successfully modified, they are returned to the patient's body (**Figure 1A**). In both types of gene therapy, vectors are required to carry and deliver the genes and introduce them into the cells.[8] In both *in vivo* and *ex vivo* gene therapy, vectors play a crucial role. These vectors are responsible for delivering the therapeutic genes into the target cells. They are designed to overcome various cellular barriers and ensure that the genetic material reaches the appropriate location within the cell. The choice of vector and the method of delivery can vary depending on the type of genetic disease, the specific therapeutic goal, and the characteristics of the target cells (**Figure 1A** to **Figure 1C**).

2. Viral vectors for gene therapy

Recombinant viral vectors are often used as vectors in gene therapy. The recombinant viral vectors are suitable as gene carriers because viruses originally have the ability to introduce their own DNA or RNA into host cells. Non-viral vector-based gene therapies including the lipid nanoparticles (LNPs), antisense oligonucleotides, siRNAs or cell-based CRISPR genome editing are also being developed actively.[1] Compared to non-viral vectors, viral vectors are characterized by a longer expression period of the transgene and a higher rate of gene delivery. Thus, modern gene therapies predominantly employ viral vectors such as retroviruses, lentivirus (LVs), adenoviruses (Ads), herpes simplex viruses (HSV), poxviruses, vaccina virus or adeno-associated viruses (AAVs) vector[9,10] (**Figure 1B** and **Figure 1C**).

Nevertheless, gene therapy still requires for more functional full particles of AAV vectors, especially when it comes to undergo of clinical trials testing, including *in vivo* performance (**Figure 1C**) and avoidance of neutralizing antibodies, although it has a lower number of clinical trials, and is one of the leading platforms for the development of gene therapy drugs.

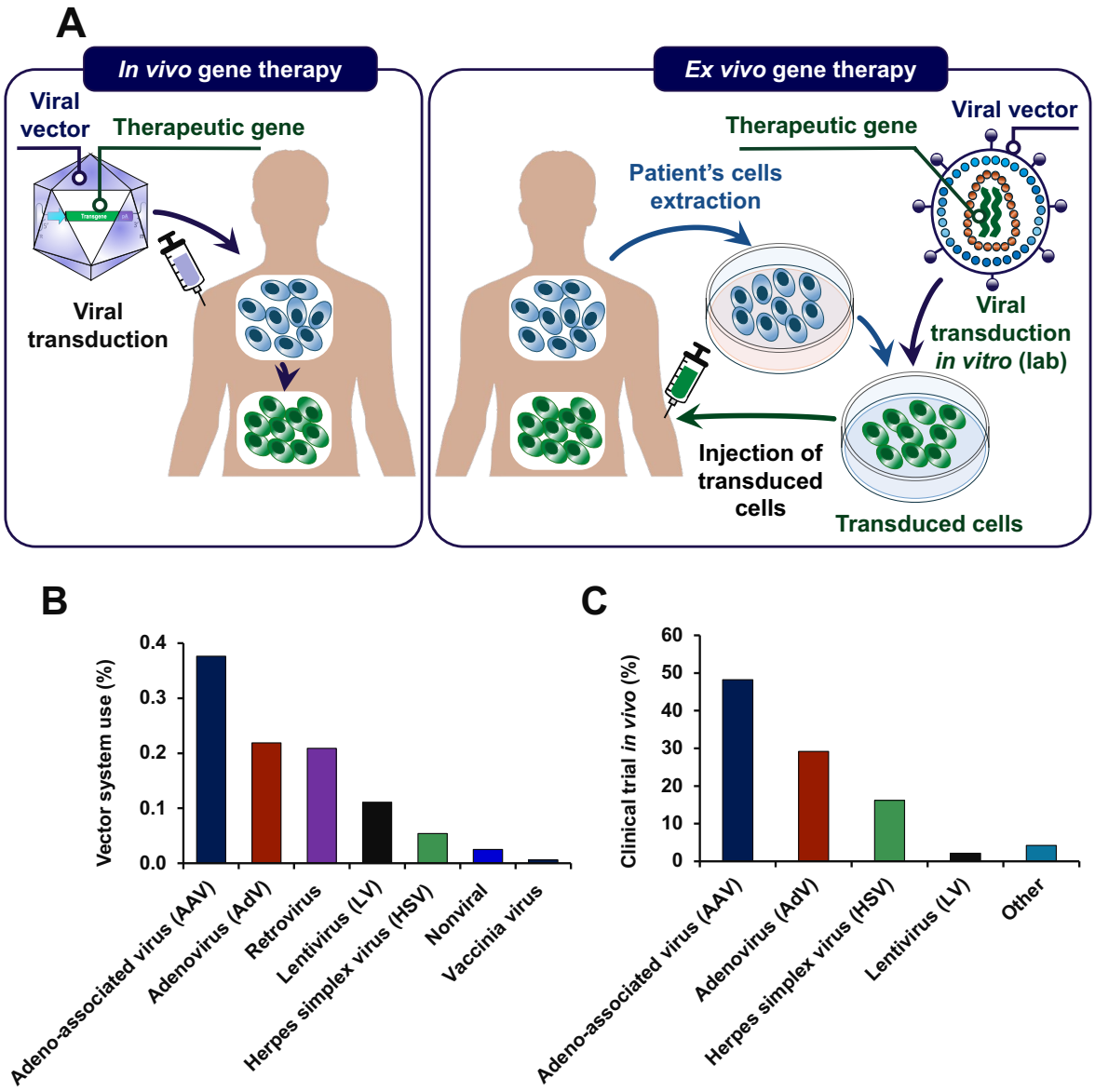

Figure 1. Viral vectors in gene therapy

(A) Schematic diagram of gene therapy using viral vector.

(B) Distribution of the different vector systems used in the gene therapy clinical trial.

(C) Major viral vectors system used in clinical trials *in vivo*.

3. Adeno-associated virus (AAV)

Adeno-associated virus (AAV) was originally discovered in 1960s, as contaminant of adenovirus preparation, and it was later discovered to also be present in infection with other such as adenovirus, human papilloma virus, vaccinia virus or HSV.[1] Due to its dependence

on the other viruses for replication, AAV is classified as genus of *Dependoparvovirusm,* which dependent on adenovirus or herpesvirus for helper-dependent replication, which is a non-enveloped virus that belongs to the family of *Parvoviridae*.[11]

AAV is a small, approximately 26 nm in diameter,[12] with an icosahedral capsid composed of three viral proteins (VP1, VP2, VP3) in an estimated ratio of 5:5:50.[13] These viral proteins assemble to form the T=1 icosahedral capsid consisting of 60 VPs. Additionally, there is an alternative open reading frame within the cap gene that expresses an assembly-activating protein (AAP), which is essential for capsid assembly[12,14–17] (**Figure 2A** to **Figure 2B**).

AAV packages a single-stranded DNA (ssDNA) genome size of approximately 4.7 kilo bases (kb)[12,14,15].The genome contains two open reading frames (ORF) for the rep gene and cap gene between two 145 bp long inverted terminal repeat (ITR) sequences which form T-shaped hairpin structure. The ITR sequences compose of an enhancer, a promoter, a gene of interest sequence, and a polyA sequence and two ITR sequences are located at the 5'and 3' ends termini of the genome and assist in forming the genome structure by forming concatemer.[18,19]

The Rep gene encodes the non-structural proteins Rep78, Rep68, Rep52, and Rep40, which are responsible for viral genome replication, transcription regulation and packaging [12,14,15,21].The Cap gene transcribes mRNA via the p40 promoter, which is further spiced into three viral proteins (VP1, VP2, and VP3).[12,14,15,21] VP1spans the entire VP2 sequence in addition to a ~ 130-amino-acid N-terminal region, and VP2 protein contains VP3 sequence in addition to a ~ 60-amino-acid N-terminal region. Sixty copies of proteins at a ratio of approximately 5:5:50 for VP 1–3 assemble into the characteristic icosahedral capsid.[12,14,15,17] Specifically, the icosahedral capsid is assembled by the common region of VP3, while the N-terminal extensions of VP1 and VP2 are essential for endosomal trafficking and escape, nuclear

localization and genome release.[11]

The three capsid protein subunits have a shared C-terminal sequence region of VP3. The overlapping area of VP1 and VP2, which is absent in VP3, includes two basic regions functioning as a nuclear localization signal (NLS) during AAV infection.[10] Additionally, the unique N-terminal region of VP1 (VP1u) contains a phospholipase A2 (PLA2) domain essential for the infection process. The assembly activating protein (AAP) is also expressed from a frameshift of the cap gene[12] (**Figure 3A** to **Figure 3C**). Previous reported have known that AAP is essential for capsid assembly. However, its mechanistic roles in assembly and how they might differ among AAV serotypes remain elusive.[22] Recently, another open reading frame (ORF) in the VP1/2 region of the cap gene, coding for a protein called membrane-associated accessory protein (MAAP), has been discovered.[23] MAAP localizes to the plasma membrane, perinuclear membrane structures, the nuclear membrane, and it has been reported to play a role in infectivity, replication, and egress from infected cells[24] (**Figure 2C** and **Figure 3A** to **Figure 3C**).

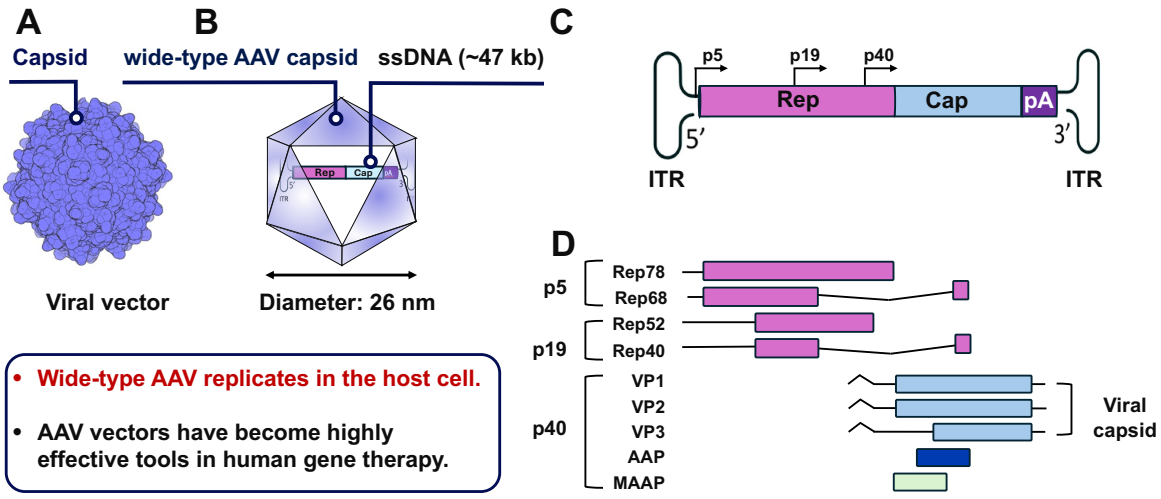

Figure 2. Outline of AAV vector structure.

(A**)** AAV structures were prepared using PyMOL[25]

(B) Schematic diagram of wild-type AAV.

(C) AAV2 genome organization including two inverted terminal repeats (ITR) flanking the rep and cap genes, polyA (p5, p19, and p40).
(D) Transcriptional map of AAV structural (VP1, VP2, and VP3) and non-structural proteins (Rep78, Rep68, Rep52, Rep40, AAP, and MAAP).
VP, viral protein; AAP, assembly-activating protein; MAAP, membrane-associated AAV protein; wtAAV, wide-type AAV

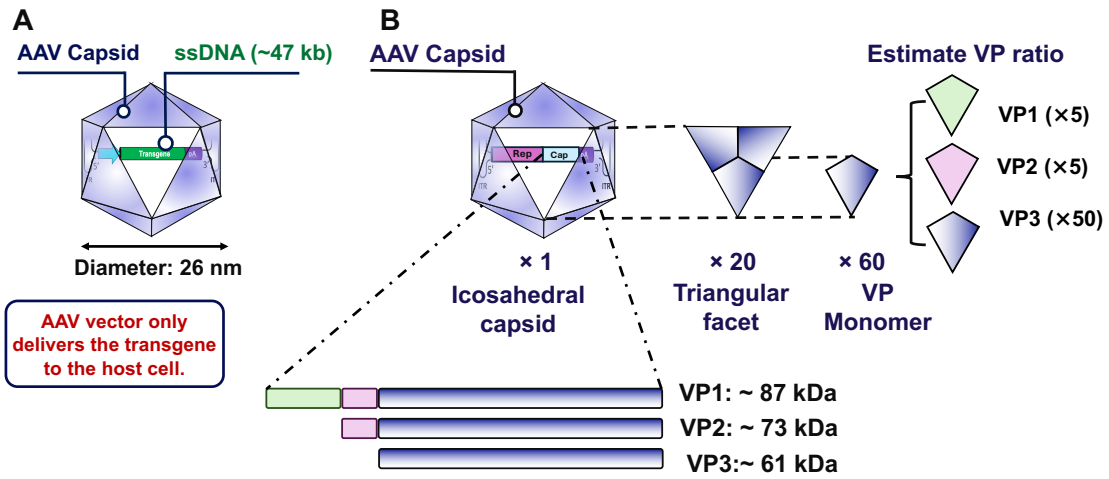

Figure 3. Recombinant AAVs are used for gene therapy

(A) Recombinant capsid of AAV particle with the AAV single-stranded genome (ssDNA).
(B) Schematic representation of each VP sequence encoded by the cap gene of AAVs.
AAV serotypes are conventionally classified according to differences in VP sequences, and the major serotypes are AAV1 to AAV12.
VP1 and VP2 were crucial role of infection while V3 is very important for capsid assembly.
VP, viral genome

4. Development of AAV vector for gene therapy

Recombinant AAV vectors have become widely utilized in human gene therapy.[5,26,27] AAV vector has emerged as the predominant vector due to many desirable attributes, including non-pathogenicity, efficient infection of both dividing and non-dividing cells and sustained maintenance of the viral genome, leading to the succession of the clinical stage for many different genetic and acquired diseases.[12,14,15,17,20,21] AAV vector has multiple serotypes showing different tissue tropisms. To date, 12 known serotypes and 100 variants of AAV vector are known[12,14,15,17] each capable of variable binding to host cell glycoprotein receptors.[28,29]

Several AAV-based gene therapy treatments already approved by the European Medicines Agency (EMA) and US Food and Drug Administration (FDA).[15,17,20,21,26] Notable examples such as Glybera (uniQure) in 2012[15,17,21,30] is the 1st AAV1 product for familial lipoprotein lipase deficiency[31], Luxturna (Spark Therapeutics) in 2017 is an AAV2 product for retinal dystrophy which treats patients with RPE65-associated Leber congenital amaurosis, Zolgensma (Novartis) in 2019 is an AAV9 product for spinal muscular atrophy, Roctavian (BioMarin) in 2023 is an AAV5 product for severe hemophilia A, Elevidys (Sarepta Therapeutic) in 2023 is an AAV9 product for duchenne muscular dystrophy (DMD), and Beqvez (Pfizer) in 2024 is an AAVRhvar product for severe hemophilia B[15,17,20,21] **(Figure 1D)**. In addition, more than 100 clinical trials and more than 4700 National Institute of Health (NIH)-listed clinical trials are ongoing in the file of gene therapy (GT).[14,21,30,31]

5. Challenging of using AAV vector

AAV vectors have become highly effective tools in human gene therapy primarily because of the exceptional properties of AAV vector.[32,33] Other advantages of AAV vectors are that there are several serotypes,[34–36] each with different tissue tropisms.[19] Despite the advantages of using AAV vectors for therapeutic purposes, there are several challenges to be overcome. Empty AAV vector particles (EPs), partial particles (PPs), which lack therapeutic deoxyribonucleic acid (DNA) or only contain fragments of the genome,[37,38] and extra filled particles (ExPs) (**Figure 6**), which contains higher numbers of DNA, are generated in upstream production processes, as up to 95% of the capsid generated in the this process,[39] and complete removal of the particles in downstream processes is impractical because of their physicochemical similarity to full particles (FPs), which contain therapeutic DNA.[40–42] EPs and PPs are considered impurities that potentially trigger adverse immunogenic reactions.[37,43–45] Furthermore, these impurities may compete with FPs for binding to target cell receptors, potentially reducing their therapeutic efficacy.[46–48] The

clinical impact of EPs is not fully understood, but they are recognized to be significant obstacles affecting FPs biodistribution and potentially provoking immune responses (**Figure 4**).

In the recent timeline, several analytical techniques to evaluate the purity of AAVs are crucial for AAV vector development.[48] At the same time, demonstrating robustness and consistency across the various AAV vector contents examined to date, including differences in AAV serotypes, genomic titer, full capsid ratio and genome lengths, those current techniques must address the inherent limitations of each method.[49] For example, some analytical methods are available to assess the contents of FPs and EPs. Combination of genome quantitation by quantitative polymerase chain reaction (qPCR) and capsid quantitation by enzyme-linked immunosorbent assay (ELISA) has been conventionally employed for the estimation of FP ratio. Now, band sedimentation analytical ultracentrifugation (BS-AUC) is recognized as the gold standard for the size distribution analysis of AAV vectors and can quantify FPs, EPs, PPs, and ExPs with high precision.[50,51] Charge-detection mass spectrometry and transmission electron microscopy could be orthogonal methods for the size distribution analysis. They are able to quantify FP ratio[39,52,53] and furthermore could provide aggregation, fragmentation, and mass distribution of packaged DNA.[54] Mass photometry (MP) is a method that measures the mass of individual particles and provides the percentage of each kind of particle against total counts (% counts).[55,56] Nonetheless, these analytical methods have limitations[39], especially in the case of crude samples. For example, it is burdensome that prior purification is required before using these analyses. A combination of ELISA and qPCR[57,58] which do not require purification before analysis has been used to quantify capsid and genome titers, respectively, and to calculate FP ratios. Besides qPCR, digital or digital droplet PCR (dPCR or ddPCR) are used for detecting the genomic titer of the viral vector.[59–62] However, the combination of ELISA and PCR is subject to inherent drawbacks of error and variability[63–65] because it relies on data from two independent quantitative analyses that use different mechanisms, and FPs and EPs

must be quantified separately using non-identical samples.[66–69]

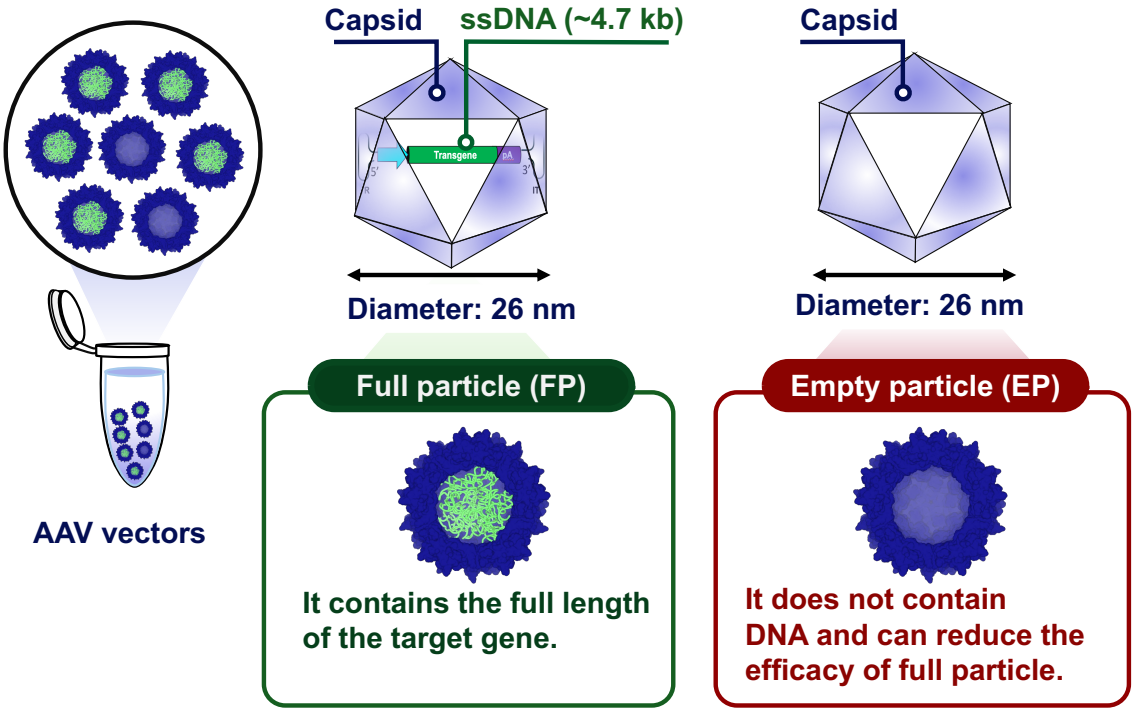

Figure 4. Illustration of the particle distribution in an AAV vector sample, which is specifically focused on the full and empty particles

Full particles (FPs), empty particles (EPs) and full particle (FP) ratio are particulary used as critical quality attributes (CQAs) in quality control (QC) of gene therapy products.

6. Objective of this study

In this dissertation, my objective is to develop a useful method that can be applicable to the gene therapy developments. Importantly, it would be highly beneficial to quantify and control the content of full and empty particles for successful AAV vector development with high efficiency and safety. In my road trip study, I aimed to establish a dual fluorescence-linked immunosorbent assay (dFLISA) as an analytical method capable of simultaneously quantifying viral capsid and genomic titers in a single analysis **(Figure 14)**.

First, a novel method named dual fluorescence-linked immunosorbent assay (dFLISA) was developed. This method is primarily based on ELISA,[68,70] followed by genome staining where two different fluorescent dyes are employed to quantify full and empty AAV vector

particles and the FP ratio. After the addition of a secondary antibody conjugated to one fluorescent dye, the plate is subjected to heat treatment to release the genome from the capsid before the introduction of the second fluorescent dye. dFLISA allows the determination of the FP ratio in a simple way with high precision, high accuracy, and high sensitivity. Analytical conditions such as genome dectection condition were optimized in **Chapter 2**. In addition, the developed method was validated, and precision, accuracy, limit of quantification (LOQ), linearity and comparison with other orthogonal methods were also evaluated successfully in **Chapter 2**. Since the production of AAV vectors is a complex process influenced by multiple factors such as cell line or plasmid ratios. It is not only FPs that are generated, but also EPs, ExPs and PPs. Currently, no existing methods that can quantify the full particle ratio of AAV vectors before purification in one assay.dFLISA method is one of the most essential for accurately quantifying diverse AAV vectors in both purified and crude lysate samples. Considering this complexity, it is essential to apply the dFLISA method for the quantification of diverse AAV vectors in both purified and crude lysate samples as indicated in **Chapter 3**.

In **Chapter 3**, the applicability of the developed method for the quantification of FP and EP in AAV vector samples, including other AAV vector serotypes and AAV vectors with different genome lengths, was evaluated. Notably, since a potential advantage of dFLISA is to be applicable for the crude samples, spike recovery test was performed using crude lysate to evaluate the capability of dFLISA for capsid/genome quantification without interference the impurities from crude lysate.

In **Chapter 4**, I summarized the results obtained in **Chapter 2** and **Chapter 3** and discussed the directions for the development of the method for quantifying AAV vectors in gene therapy. This work represents an exploration and generation of a novel method with significant implications for AAV vector quantification, offering substantial benefits for the advancement

of AAV-based gene therapy in the future. The flow of this study is summarized in **Figure 5**. In addition, I have also considered the future perspectives of dFLISA, such as its potential to become an ideal solution for large-scale screening in pharmaceutical and clinical laboratories. Beyond AAVs, the principles of dFLISA could be applied to other viral vectors, including lentiviruses (LVs) and adenoviruses, thus broadening its applicability in gene therapy. Furthermore, non-viral vectors like lipid nanoparticles (LNPs), which may present similar challenges, could also be evaluated using dFLISA.

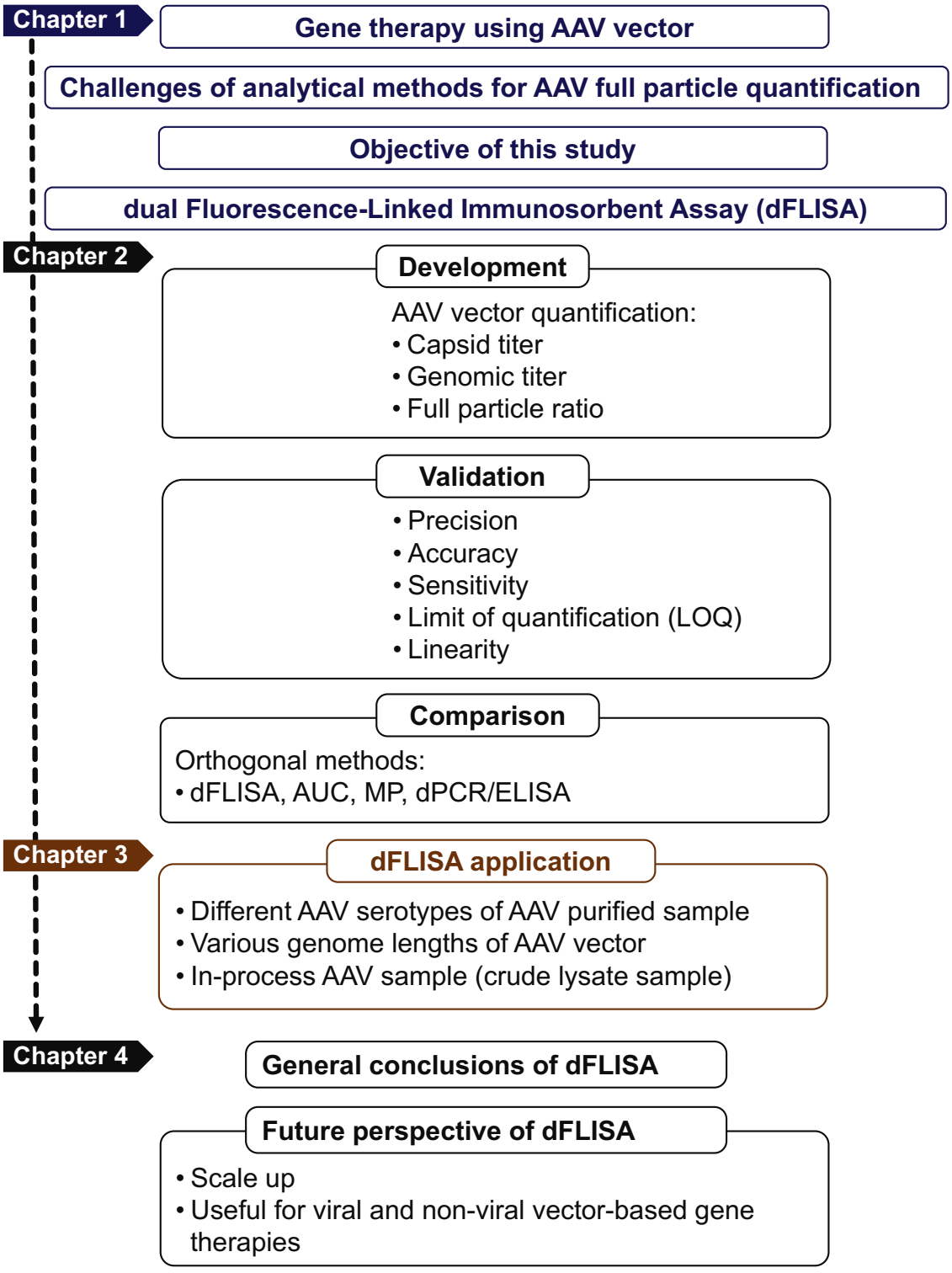

Figure 5. Flow of this study

Gene therapy is the treatment of genetic diseases by introducing therapeutic genes into the body of the patient, with AAV vectors being a leading platform due to their low immunogenicity and non-pathogenicity. This dissertation focuses on developing a useful method named dual fluorescence-linked immunosorbent assay (dFLISA) as an analytical method capable of simultaneously

quantifying viral capsid and genomic titers in a single analysis. This method allows for the straightforward measurement of total capsid, genomic titer, and the determination of the full particle (FP) ratio in a simple way. The dFLISA method was initially validated, and its performance was evaluated in terms of precision, accuracy, sensitivity, limit of quantification (LOQ) and linearity. It was also compared with other orthogonal methods such as AUC, MP, dPCR/ELISA. Subsequently, the applicability of dFLISA for the quantification of FP and EP in various AAV vectors, including different serotypes and genome lengths, was evaluated. The method was also tested for spike recovery using crude lysate samples. In addition, these results were discussed in the light of future perspectives of dFLISA, including the potential for scaling up and applying it to both viral and non-viral vectors in gene therapy.

AUC, analytical ultracentrifugation; dPCR, digital polymerase chain reaction; EP, empty particle; ELISA, enzyme liked-immunosorbent assay; FP, full particle; MP, mass photometry

Chapter 2. Development, validation and comparison of dFLISA

1. Introduction

Dual florescence-linked immunosorbent assay (dFLISA), which has capability of simultaneously quantifying viral capsid and genomic titers in a single analysis, was developed in this chapter. The dual florescence-linked immunosorbent assay (dFLISA) is a developed analytical method capable of simultaneously quantifying viral capsid and genomic titers in a single analysis (**Figure 14**). dFLISA is primarily based on ELISA,[68,70] followed by genomic staining where two different fluorescent dyes are employed to quantify full and empty AAV vector particles and the FP ratio. First, after the addition of a secondary antibody conjugated with red fluorescent dye, second, the micro well plate is subjected to heat treatment to release the genome from the capsid before the introduction of the green, fluorescent dye. These strategies make this method unique and distinguish it from other conventional methods such as analytical ultracentrifugation (AUC), digital polymerase chain reaction (dPCR), Enzyme liked-immunosorbent assay (ELISA), mass photometry (MP), and others. There are different parameters for the assay development need to be discussed.

Determining the optimal conditions, including the appropriate antibodies for coating and

detection, their concentrations, and the conditions for genome release, is required. Accordingly, I evaluated the efficacy of the biotinylated anti-AAV VHH antibody in binding with the AAV capsid, a comprehensive analysis involving techniques such as enzyme-linked immunosorbent assay (ELISA) and biolayer interferometry (BLI) is necessary. In this **Chapter 2**, the screening of the initial condition for method development were conducted. First, BLI was performed for characterizing the binding kinetics and affinity of AAV vector with anti-AAV VHH antibody fragment, which has been reported to bind to the near fivefold axis of AAV2 capsid.[71] Next, the conditions for genome release at various times and temperatures during the heating of the AAV capsid were evaluated. Furthermore, the development of dFLISA was assessed using the standard derived from BS-AUC analysis. Additionally, this development process included comparing the concentration of anti- AAV VHH antibody immobilized on the AAV capsid, evaluating the detection wavelength for both the capsid and genome of AAV capsid, and measuring the fluorescence intensity in black and clear microwell plates for the capsid and genome.

Subsequently, after successfully developing the dFLISA, its validation is critically conducted using parameters such as linearity, precision, accuracy, and limit of quantification (LOQ). Additionally, I determined the full-to-empty ratio of AAV vector by dFLISA and compared it with orthogonal methods such as BSA-AUC, MP, and the combination of dPCR and ELISA to ensure its robustness and reliability.

To this end of this chapter, the dFLISA allows the determination of the FP/EP ratio in a simple way with high precision, high accuracy, and high sensitivity. The capsid and genomic titers, and full capsid ratios were comparable to the expected values. Moreover, the good linear correlation between dFLISA and AUC was well observed regarding FP/EP ratio as well as other orthogonal techniques.

2. Experimental materials and methods

2-1. Recombinant AAV samples

Two recombinant adeno-associated virus serotype 2 were used: AAV2-LotA, which was purchased from (VectorBuilder, Chicago, USA) (**Table 6)**, AAV2-LotB, which was provided by the Manufacturing Technology Association of Biologics (Tokyo, Japan) (**Table 7**). AAV2-LotC, which was purchased from Virovek (Houston, USA) (**Table 8**). Samples were formulated in PBS, 200 mM NaCl, 0.001% poloxamer-188 and stored at -80ºC until use.

Other in-house three AAV8 vectors (**Table 10**) including AAV8-Lot1, AAV8-Lot2, and AAV8-Lot3, were generated using triple-plasmid co-transfection. Briefly, pAAV-Rep&Cap (Serotype 8), pAd helper, and transgene plasmids (CMV-EGFP or AAT-FIX) were co-transfected into suspended HEK293T or VPC 2.0 (Thermo Fisher Scientific, Waltham, MA, USA) cells. The transfected cells were cultured, and the medium and cell lysate were harvested (it was collected as a crude sample). Thereafter, the samples were purified via affinity chromatography using AAVX columns (Thermo Fisher Scientific). Bulk AAV samples were purified using affinity chromatographic purification followed by a CsCl ultracentrifugation (UC) or an anion exchange column to separate full and empty particles. Purified samples (AAV8-Lot1 and AAV8-Lot2) were centrifuged at 25,000 rpm in an Optima XE-90 (Beckman Coulter, Inc., Brea, CA, USA) using a Beckman SW41Ti rotor at 20°C for 42 h. For AAV8-Lot3, purified sample was centrifuged at 34,000 rpm at 20°C for 72 h. The virus bands generated by UC were collected by using a piston fractionator (BioComp Instruments Ltd., Fredericton, Canada) equipped with a UV monitoring apparatus (Triax flow cell, BioComp Instruments Ltd.). For the anion exchange chromatography, the samples were applied to a CIMmultus QA column (Sartorius, Göttingen, Germany) and eluted with a linear gradient of 0–250 mM NaCl in bis-tris-propane buffer (pH 9.0). Then the virus fractions were dialyzed in Slide-A-Lyzer 10K (Thermo Fisher Scientific). AAV vector samples were analyzed by BS-

AUC prior to analysis (**Figure 6**). The representative sedimentation coefficient distributions for AAV2 vector and AAV8 vector in PBS/D2O + 0.001% poloxamer-188 determined by BS-AUC, are also described in **Figure 9** to **Figure 11**. **Table 10** summarizes the information on the in-house AAV8 vectors used in this study.

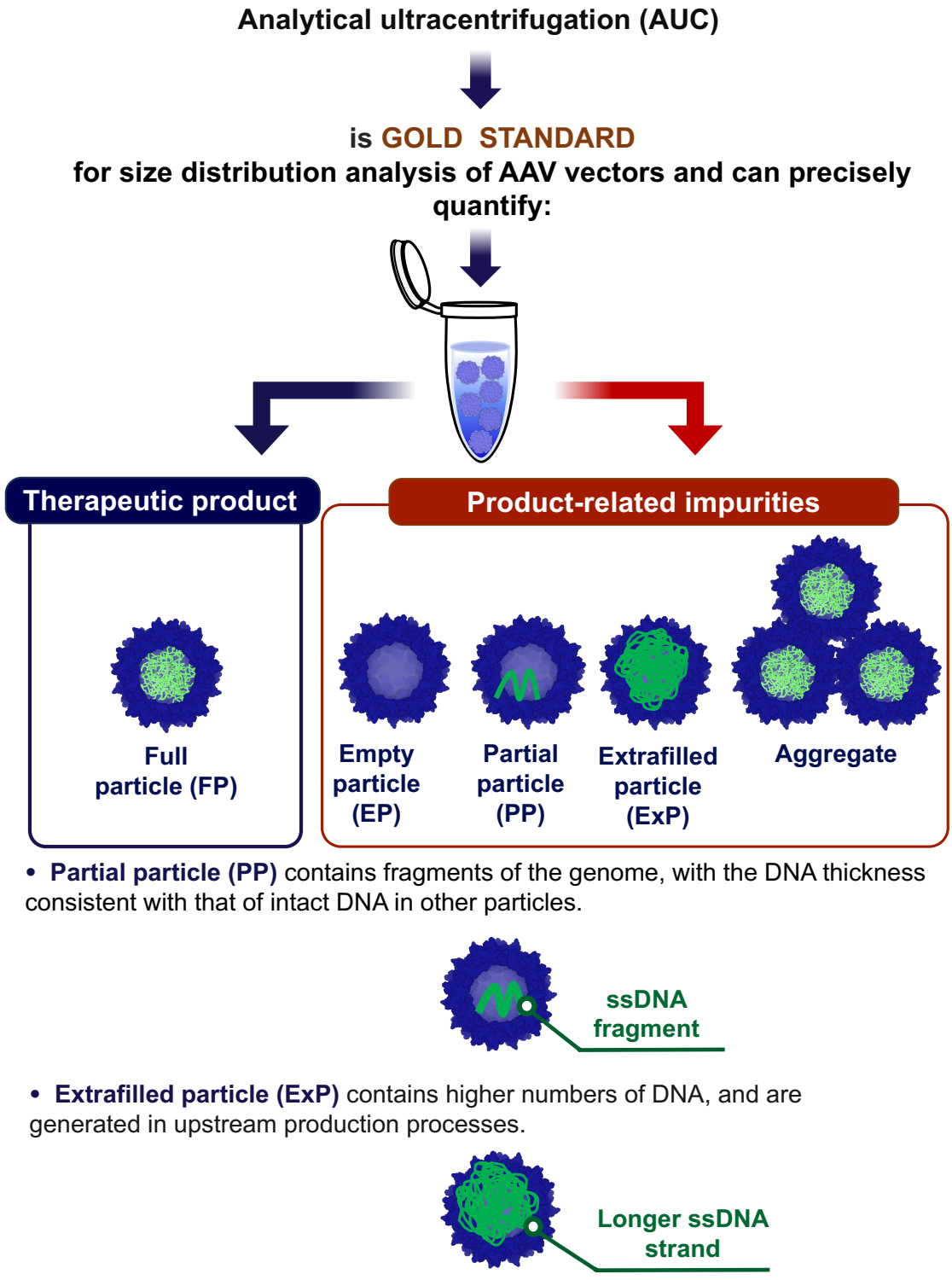

Figure 6. Therapeutic products and product-related impurities were quantified using AUC.

Table 6. Summary of AAV vectors purchased from VectorBuilder used in BLI analysis

Sample name	Serotype	Promoter	GOI	Number of nucleic acids	EP (10^{11} cp/mL)	Sample preparation
AAV2-LotA	2	na	na	na	2.50	Sample

CMV, cytomegalovirus promoter; cp, capsid particle; EP, empty particle; GOI, gene of interest

Table 7. Summary of AAV vectors purchased from Takara used in this study, as provided by the Manufacturing Technology Association of Biologics (Tokyo, Japan)

Sample name	Serotype	Promoter	GOI	Number of nucleic acids	FP (10^{12} vg/mL)	Sample preparation
AAV2-LotB	2	CMV	ZnGreen	2521	1.46	Standard

GOI, gene of interest; CMV, cytomegalovirus promoter; FP, full particle; vg, viral genome

Table 8. Summary of AAV vectors purchased from Virovek used in this study

Sample name	Serotype	Promoter	GOI	Number of nucleic acids	FP (10^{12} vg/mL)	Sample preparation
AAV2-LotC	2	CMV	ZnGreen	2521	7.03	Sample

CMV, cytomegalovirus promoter; FP, full particle; vg, viral genome; GOI, gene of interest

2-2. Screening the initial conditions for assay development

2-2-1. Binding kinetics and affinity of AAV2 vector with anti-AAV VHH antibody by BLI

Biolayer Interferometry (BLI) measurement[63,72] was conducted for binding kinetics and affinity of AAV2 vector with anti-AAV VHH antibody analysis. This assay was performed on Octet HTX system (Sartorius, Goettingen, Germany). Octet SAX biosensors (Sartorius) were hydrated by immersion in 1× PBS for at least 10 min prior to use. Biotinylated anti-AAV VHH antibody (CaptureSelect™ Biotin Anti-AAVX Conjugate, Thermo Fisher Scientific) was diluted to 0.01 μg/mL and immobilized on the SAX biosensors. AAV2 vector samples were diluted in a 2-fold dilution series from 2.50×10^{11} vg/mL to 1.56×10^{10} vg/mL with Octet sample diluent (Sartorius). After the baseline measurement using Octet sample diluent, association and dissociation of AAV2-LotA with the anti-AAV VHH antibody were measured at 30°C in an Octet 384-well tilted-bottom microplate (Sartorius) while shaking at 1000 rpm. Octet Analysis Studio software (ver. 12.2) was used for data analysis. The interaction between anti-AAV VHH antibody and AAV2 vector was analyzed by 1:1 fitting.

According to the manufacturer's website of the 96-well plate, the maximum coating amount is 650 ng/cm^2. The bottom area of 96-well plates is approximately 0.33 cm^2, and the volume of AAV vector solution was 100 microliters. Thus, the coated concentration of VHH, whose molecular weight is 14 kDa, would be 150 nM. Using these values and the result of BLI, I calculated the binding efficiency of AAV vector based on the following **Equation 1** and **Equation 2**:

$$[\text{Complex}] = \frac{(K_D+[AAV]+[VHH])-\sqrt{(K_D+[AAV]+[VHH])^2-4[AAV][VHH]}}{2} \quad \textbf{(Equation 1)}$$

$$\text{Binding efficiency} = \frac{[Complex]}{[AAV]} \times 100 \quad \textbf{(Equation 2)}$$

2-2-2. Comparison of the genome detection after release from AAV vector at different times and temperatures

This experiment was conducted to monitor the condition for the genome release from the AAV vector capsid. First, fluorescent dye, SYBR Gold Nucleic Acid Gel Stain solution was diluted 500-fold with 1 × PBS (pH 7.4). The AAV2-LotB vector sample was diluted with 10-fold, in 1 × PBS (pH 7.4). Diluted vector sample solution was loaded into microplates (96 well, 200 µL, black, polypropylene (PP), flat-bottom, (Greiner Bio-One) (Sigma Aldrich) for 100 µL per well. AAV2 samples were incubated at five different conditions from 10 min at 80°C, 15 min at 80°C, 15 min at 85°C, 10 min at 90°C, 30 min at 90°C and 30 min at 90°C for detecting the genome after releasing from AAV2 capsid particles. Furthermore, the intensity of the green fluorescence emanating from SYBR gold[73,74] to detect the released genome using an excitation wavelength of 495 nm and an emission wavelength of 540 nm were measured. A standard curve was generated using a four-parameter curve-fitting algorithm with the SpectraMax i3x microplate reader (Molecular Devices, CA, USA).

2-3. Development of dFLISA

2-3-1. Standards and samples quantification determined by BS-AUC

The standard of capsid and genomic titer of dFLISA were derived by the BS-AUC. Experiments and analyses of band sedimentation analytical ultracentrifugation (BS-AUC) were performed according to the previous study.[75] Briefly, a buffer or AAV vector sample at a volume of 15 µL were loaded into a reference or sample reservoir well with a 12-mm band-forming centerpiece (Spin Analytical, South Berwick, ME, USA) equipped with sapphire windows. A volume of 250 µL of PBS/D_2O containing 0.001% of poloxamer-188 was loaded into the reference or sample sector, respectively. In-house AAV8-Lot1 to AAV8-Lot3 and outsourced (VectorBuilder, Chicago, USA) AAV2-Lot1 to AAV2-Lot4 and AAV8-Lot5 to AAV8-Lot6

were used. Data were collected at 20°C using Optima AUC (Beckman Coulter, Indianapolis, IN, USA) at 20,000 rpm using a UV detection system, with the detection wavelength set at 280 nm. Data points were collected with a radial increment of 10 μm at an interval of 150 sec.

Sedimentation data were analyzed using the analytical zone centrifugation c(s) model of the program SEDFIT (version 16.2b),[76] in which parameters such as lamella width, frictional ratio, meniscus, time-invariant noise, and radial-invariant noise were adjusted and a regularization level of 0.68 was used. The s-value range of 0–175 S was evaluated with a resolution of 350. The SEDNTERP program facilitated the calculation of buffer density and viscosity for the solvent loaded in the sectors.[77] The apparent sedimentation coefficient for FPs was converted to the sedimentation coefficient in water at 20°C, ($s_{20,w}$). This conversion used the partial specific volume of the FPs, determined according to the procedure described in a previous study,[78] in conjunction with the buffer density and buffer viscosity. Subsequently, figures showing the c(s) distribution were generated using the program GUSSI (version 1.3.2).[79] Particle concentrations of were calculated by dividing the FP, EP and ExP peak areas by respective molar extinction coefficient at the detection wavelength. The genomic titer was calculated by the sum FPs and ExPs while the capsid titer was calculated by the sum of of FPs, EPs, and ExPs. Therefore, the full particle ratio was calculated by dividing the sum of FPs and ExPs by the sum of FPs, EPs, and ExPs. The mean sedimentation coefficient in water at 20°C, ($s_{20,w}$), full particle ratio, and standard deviation of each parameter were also calculated based on the results obtained from the experiment.

2-3-2. Comparison of VHH antibody immobilized with AAV8 vector by dFLISA

Black, 96-well, flat-bottomed MaxiSorp surface-treated immunoplates (Thermo Fisher Scientific) were used. These plates were coated with CaptureSelect Biotin Anti-AAVX Conjugate, a 14-kDa recombinant single-domain antibody fragment (VHH affinity ligand). For

1st and 2nd experiment, the anti-AAV VHH antibody was diluted at two concentrations: 10 µg/mL (100-fold) and 20 µg/mL (50-fold), respectively, using BupH carbonate-bicarbonate buffer. The plates were then incubated for 16 hours at 4°C. The plates were washed three times with 0.05% Tween 20 in 1 × PBS (pH 7.4). Prior to sample addition, addition of 200 µL of 1% BSA in 1 × PBS was performed for blocking. An AAV vector samples in a formulation consisting of 1 × PBS, 200 mM NaCl, and 0.001% (w/v) poloxamer-188 was used as samples. AAV8-Lot5 (**Table 11**) with a 2521 base genome was used as a standard. AAV8-Lot6 (**Table 11**) was diluted to a concentration of 1.95×10^{11} cp/mL and 1.49×10^{11} vg/mL in 0.05% Tween 20 in 1 × PBS and then serially diluted at a 1:2 ratio to generate a calibration curve. Subsequently, 100 µL of that diluted sample solutions were added to each well of the plate. To remove unbound components, the plate was subjected to a wash with 0.05% Tween 20 in 1 × PBS. The lyophilized mouse monoclonal anti-AAV8 antibody, ADK8, was reconstituted with 1 mL of Milli-Q water. For 1st and 2nd experiment, ADK8 antibody was diluted was diluted at two different concentrations:1 µg/mL (50-fold) and 10 µg/mL (5-fold), respectively, using 1 × PBS buffer at pH 7.4 containing 0.09% sodium azide and 0.5% BSA, followed by incubation at 37°C for 1 h, and three washes. The secondary antibody, goat anti-mouse IgG H&L (Alexa Fluor 647), was diluted to a concentration of 4 µg/mL (500-fold) and added for labeling. The plate was then sealed with adhesive foil and incubated for 1 h at 37°C with shaking at 300 rpm. Following incubation, the plate was washed with wash buffer. Next, 100 µL of 1 × PBS was added to each well, and plates were incubated at 85°C for 15 min. This process disrupted the viral capsid structure and released the ssDNA. Afterward, samples were allowed to cool at room temperature for 5 min. SYBR Gold Nucleic Acid Gel Stain solution was diluted 1000-fold with 1 × PBS. Subsequently, 10 µL of the diluted SYBR Gold solution was added to individual wells, followed by a 5 minutes incubation at room temperature. Finally, fluorescence measurements were then performed. The intensity of the red fluorescence emanating from second antibody conjugated with goat anti-mouse IgG H&L (Alexa Fluor 647) at a final

concentration of 4 ug/mL was measured using an excitation wavelength of 652 nm and an emission wavelength of 680 nm to quantify the capsid titer. Additionally, the intensity of the green fluorescence emanating from SYBR gold was measured to quantify the released genome, using an excitation wavelength of 495 nm and an emission wavelength of 530 nm. A standard curve was generated using a four-parameter curve-fitting algorithm with the SpectraMax i3x microplate reader (Molecular Devices, CA, USA).

Capsid and genomic titers of standards were calculated based on the results of BS-AUC (**Table 10**). Because the concentrations of ExPs and PPs were lower than LOQ of BS-AUC,[80] a sum of EPs and FPs, was considered as capsid titer, and FPs was considered as genomic titer. FP ratio was then calculated by dividing genomic titer by capsid titer. The amount of capsid protein (cp) and vector genome (vg) per milliliter were then determined using the standard curve. Finally, the comparison of the signal-to-background noise ratio of both experiments was determined. The signal background ratio was calculated by dividing the signal the lowest florescence intensity (S) by the background noise (N), which was derived from the blank value (**Equation 3**).

$$\text{S/N ratio} = \frac{[\text{S}]}{[\text{N}]} \times 100 \quad \textbf{(Equation 3)}$$

2-3-3. Comparison of detection wavelength for capsid and genome quantification of AAV2 vector by dFLISA

Black, 96-well, flat-bottomed MaxiSorp surface-treated immunoplates (Thermo Fisher Scientific) were used. These plates were coated with CaptureSelect Biotin Anti-AAVX Conjugate, a 14-kDa recombinant single-domain antibody fragment (VHH affinity ligand), at a concentration of 10 μg/mL (100-fold dilution) with BupH carbonate-bicarbonate buffer and the plates were incubated for 16 h at 4°C. The plates were washed three times with 0.05%

Tween 20 in 1 × PBS (pH 7.4). Prior to sample addition, addition of 200 µL of 1% BSA in 1 × PBS was performed for blocking. An AAV2 vector samples in a formulation consisting of 1 × PBS, 200 mM NaCl, and 0.001% (w/v) poloxamer-188 was used as samples. AAV2-LotC (**Table 8**) with a 2521-bp genome was used as a standard. AAV2-LotC was diluted to a concentration of 7.03×10^{10} vg/mL in 0.05% Tween 20 in 1 × PBS and then serially diluted at a 1:2 ratio to generate a calibration curve. Subsequently, 100 µL of that diluted sample solutions were added to each well of the plate. To remove unbound components, the plate was subjected to a wash with 0.05% Tween 20 in 1 × PBS. The lyophilized monoclonal anti-AAV2 antibody, A20, was reconstituted with 1 mL of Milli-Q water. A20 was diluted to a concentration of 1 µg/mL (50-fold dilution) with 1 × PBS buffer at pH 7.4 containing 0.09% sodium azide and 0.5% BSA, followed by incubation at 37°C for 1 h, and three washes. The secondary antibody, goat anti-mouse IgG H&L (Alexa Fluor 647), was diluted to a concentration of 4 µg/mL (500-fold dilution) and added for labeling. The plate was then sealed with adhesive foil and incubated for 1 h at 37°C with shaking at 300 rpm. Following incubation, the plate was washed with wash buffer. Next, 100 µL of 1 × PBS was added to each well, and plates were incubated at 85°C for 15 min. This process disrupted the viral capsid structure and released the ssDNA. Afterward, samples were allowed to cool at room temperature for 5 min. SYBR Gold Nucleic Acid Gel Stain solution was diluted 1000-fold with 1 × PBS Subsequently, 10 µL of the diluted SYBR Gold solution was added to individual wells, followed by a 5-min incubation at room temperature. For the 1st and 2nd experiments, the wavelength detection of the capsid titer was prepared at two different wavelengths: 652 nm_{Ex}/ 680 nm_{Em} and 662 nm_{Ex}/ 700 nm_{Em}, respectively. For the 1st and 2nd experiments, the wavelength detection of the genomic titer was prepared at two different wavelengths: 495 nm_{Ex}/ 500 nm_{Em} and 500 nm_{Ex}/ 535 nm_{Em}, respectively. In addition, a standard curve was generated using a four-parameter curve-fitting algorithm with the SpectraMax i3x microplate reader (Molecular Devices).

Capsid and genomic titers of standards were calculated based on the results of BS-AUC

(**Table 10** and **Table 11**). The sum of EPs and FPs was considered as capsid titer, and FPs was considered as genomic titer. FP ratio was then calculated by dividing genomic titer by capsid titer. The amount of capsid protein (cp) and vector genome (vg) per milliliter were then determined using the standard curve. Finally, the comparison of the signal-to-background ratio of both experiments was determined. **Equation 3** was employed to calculate the signal background ratio (S/N) of low concentration sample.

2-3-4. dFLISA analysis

The dFLISA method was developed successfully, and the optimal standard curve with a schematic illustrating of dFLISA was shown in **Figure 14.** Black, 96-well, flat-bottomed MaxiSorp surface-treated immunoplates (Thermo Fisher Scientific) were used. These plates were coated with CaptureSelect Biotin Anti-AAVX Conjugate, a 14-kDa recombinant single-domain antibody fragment (VHH affinity ligand), at a concentration of 10 µg/mL (100-fold dilution) with BupH carbonate-bicarbonate buffer and the plates were incubated for 16 h at 4°C. The plates were washed three times with 0.05% Tween 20 in 1 × PBS (pH 7.4). Prior to sample addition, addition of 200 µL of 1% BSA in 1 × PBS was performed for blocking. An AAV vector samples (**Table 10**) in a formulation consisting of 1 × PBS, 200 mM NaCl, and 0.001% (w/v) poloxamer-188 was used as samples. AAV8-Lot1 with a 2521 base genome was used as a standard. AAV8-Lot1 was diluted to a concentration of 2.38×10^{11} cp/mL and 2.18×10^{11} vg/mL in 0.05% Tween 20 in 1 × PBS and then serially diluted at a 1:2 ratio to generate a calibration curve. Subsequently, 100 µL of sample and standard solutions were added to each well of the plate. To remove unbound components, the plate was subjected to a wash with 0.05% Tween 20 in 1 × PBS. The lyophilized monoclonal anti-AAV8 antibody, ADK8, was reconstituted with 1 mL of Milli-Q water. ADK8 was diluted to a concentration of 1 µg/mL (50-fold dilution) with 1 × PBS buffer at pH 7.4 containing 0.09% sodium azide and 0.5% BSA, followed by incubation at 37°C for 1 h, and three washes. The secondary antibody, goat anti-

mouse IgG H&L (Alexa Fluor 647), was diluted to a concentration of 4 μg/mL (500-fold dilution) and added for labeling. The plate was then sealed with adhesive foil and incubated for 1 h at 37°C with shaking at 300 rpm. Following incubation, the plate was washed with wash buffer. Next, 100 μL of 1 × PBS was added to each well, and plates were incubated at 85°C for 15 min. This process disrupted the viral capsid structure and released the ssDNA. Afterward, samples were allowed to cool at room temperature for 5 min. SYBR Gold Nucleic Acid Gel Stain solution was diluted 1000-fold with 1 × PBS. Subsequently, 10 μL of the diluted SYBR Gold solution was added to individual wells, followed by a 5-min incubation at room temperature. Finally, we measured the intensity of the red fluorescence emanating from the proteins labeled with goat anti-mouse IgG H&L (Alexa Fluor 647) to quantify the capsid titers using an excitation wavelength of 652 nm and an emission wavelength of 680 nm. Additionally, we measured the intensity of the green fluorescence emanating from SYBR gold[74,81] to quantify the released genome using an excitation wavelength of 500 nm and an emission wavelength of 530 nm. A standard curve was generated using a four-parameter curve-fitting algorithm with the SpectraMax i3x microplate reader from Molecular Devices (CA, USA). Capsid and genomic titers of standards were calculated based on the results of BS-AUC. Because the concentrations of PPs were lower than LOQ of BS-AUC,[80] a sum of EPs, FPs, and ExPs was considered as capsid titer, and a sum of FPs and ExPs was considered as genomic titer. FP ratio was then calculated by dividing genomic titer by capsid titer. The amount of capsid protein (cp) and vector genome (vg) per milliliter were then determined using the standard curve. Correction of SYBR gold intensity was not performed if the % difference in genome length between the standard and the sample was within ±10%. The schematic illustration of dFLISA as shown in **Figure 15**.

2-4. Validation of dFLISA

2-4-1. Precision and accuracy and LOQ of dFLISA measurement

dFLISA was analyzed as above described in **2-3-4** of development step. Similarly, AAV8-Lot2 with a 2712-base gene of interest (GOI) was diluted 400-fold to a concentration of 1.54 × 10^{11} cp/mL and 1.39 × 10^{11} vg/mL in 0.05% Tween 20 in 1 × PBS. Subsequently, serial dilutions at a 1:2 ratio were carried out to ensure precision, accuracy, and LOQ calculations. Measurements were conducted for three consecutive days (days 1–3) under identical operating conditions at short intervals using the same sample conditions and without any freeze–thaw cycles. The repeatability percentage was calculated by dividing the SD by the mean of three independent dFLISA results obtained by the same operator over three days (**Equation 4**):

$$\%CV = \frac{[\text{Mean of SD}]}{[\text{Mean of result}]} \times 100 \quad (\textbf{Equation 4})$$

Accuracy was calculated by finding the percentage difference between the value of capsid and genomic titer, as measured by dFLISA, and their expected values, as determined by BS-AUC. **Equation 5** was used with ±10% of expected values as the recovery percentage criteria for this calculation:

$$\%\ \text{of accuracy} = \frac{[\text{Experimental value}]}{[\text{Expected value}]} \times 100 \quad (\textbf{Equation 5})$$

2-5. Comparison of full particle ratio determination of AAV8 vector by orthogonal methods

2-5-1. Determination full particle ratio of AAV8 vector by dFLISA

Linearity of FP ratio is critical in dFLISA to achieve optimal assay performance. I investigated precision, accuracy, linearity, and LOQ of FP ratio determined by dFLISA. The representative dFLISA procedure described above was used. Specifically, AAV8-Lot1 was diluted 60-fold to obtain a concentration of 2.38 × 10^{11} cp/mL and 2.18 × 10^{11} vg/mL with 0.05% Tween 20 in 1 × PBS. Further serial dilutions were performed at a 1:2 ratio to construct

a calibration curve. AAV8-Lot2 and AAV8-Lot3 were concentrated by ultrafiltration. I then mixed these concentrated samples at various ratios containing the following expected percentages of full capsids: 0%, 10.5%, 31.5%, 52.3%, 73.1%, and 90.1% of FPs. The mixed sample was then diluted 320-fold with 0.05% Tween 20 in 1 × PBS. All samples were tested in duplicate. Each well of the plate was filled with 100 µL of the prepared sample solutions. The back-calculated concentrations of the calibration standards were maintained within ± 25% of the value at the LOQ and within ± 20% at all other levels.[82] The anchor calibrators (<LOQ) did not require acceptance criteria because they were beyond the quantifiable range of the curve.

2-5-2. Determination of full particle ratio of AAV8 vector by BS-AUC

Experiments and analyses of BS-AUC were performed according to our previous study.[75] Briefly, a buffer or AAV sample at a volume of 15 µL were loaded into a reference or sample reservoir well with a 12-mm band-forming centerpiece (Spin Analytical, South Berwick, ME, USA) equipped with sapphire windows. A volume of 250 µL of PBS/D_2O containing 0.001% of poloxamer-188 was loaded into the reference or sample sector, respectively. Mixed samples (full particles in six prepared spike ratios, specifically, 90.1%, 73.1%, 52.1%, 31.5%, 10.5%, and 0% FPs) of AAV8 vectors were used. Data were collected at 20°C using Optima AUC (Beckman Coulter) at 20,000 rpm using a UV detection system, with the detection wavelength set at 280 nm. Data points were collected with a radial increment of 10 µm at an interval of 150 seconds.

Sedimentation data were analyzed using the analytical zone centrifugation c(s) model of the program SEDFIT (version 16.2b),[76] in which parameters such as lamella width, frictional ratio, meniscus, time-invariant noise, and radial-invariant noise were adjusted and a regularization level of 0.68 was used. The s-value range of 0–175 S was evaluated with a resolution of 350. The SEDNTERP program facilitated the calculation of buffer density and viscosity for the

solvent loaded in the sectors.[77] The apparent sedimentation coefficient for FPs was converted to the sedimentation coefficient in water at 20°C, ($s_{20,w}$). This conversion used the partial specific volume of the FPs, determined according to the procedure described in a previous study,[78] in conjunction with the buffer density and buffer viscosity. Subsequently, figures showing the c(s) distribution were generated using the program GUSSI (version 1.3.2).[79]

Particle concentrations were calculated by dividing the FP, EP and ExP peak areas by respective molar extinction coefficient at the detection wavelength. The full particle ratio was calculated by dividing the sum of FPs and ExPs by the sum of FPs, FPs, and ExPs. The mean sedimentation coefficient in water at 20°C, ($s_{20,w}$), full particle ratio, and standard deviation of each parameter were calculated based on the results obtained from the triplicate experiments.

2-5-3. Determination of capsid titers of AAV8 vector by single ELISA

An AAV8 titration kit (PROGEN) was used to determine capsid titers. The assay was performed according to the manufacturer's instructions. A series of 2-fold dilutions of the kit's standard viruses were made to generate a capsid standard curve ranging from 7.97×10^6 to 5.01×10^8 cp/mL. Mixed samples (full capsids in six prepared spike ratios, specifically, 90.1%, 73.1%, 52.3%, 31.5%, 10.5%, and 0% FPs) of AAV8 vector were diluted with 0.05% Tween 20 in 1 × PBS. All measurements, including unknown samples and blanks, were performed in duplicate at three different dilutions. The mean value was used to calculate AAV8 titers. A prepared 100 µL sample was added to a microwell plate and incubated for 1 h at 37°C. The microwell plate was then washed three times with wash buffer. The biotinylated anti-AAV8 antibody (ADK8) was then added to the microwell plate, and the plate was incubated for 1 h at 37°C. The washing step was repeated. Streptavidin-horse radish peroxidase conjugate was added and incubated for 1 h at 37°C, followed by the washing and the addition of ready-to-use tetramethylbenzidine (TMB) solution to the wells, which were then incubated for 15 min at

room temperature. The color reaction was stopped by adding ready-to-use sulfuric acid solution. Absorbance was then measured photometrically at 450 nm with a SpectraMax 3x microplate reader. The readings of each sample were then averaged to determine the final titers using a four-parameter logistic (4PL) curve-fitting model. The 4PL standard curve was generated in Microsoft Excel by plotting the subtracted optical density measurements of the serially diluted kit controls against the corresponding AAV vector concentrations.

2-5-4. Determination of genomic titers of mixed samples of AAV8 vector using dPCR

AAV vector samples with various FP ratio (full capsids in six prepared ratios, specifically, 90.1%, 73.1%, 52.3%, 31.5%, 10.5%, and 0% FPs) were prepared as described above and then treated with DNase I (Takara Co., Ltd, Japan). The samples were then incubated at 37°C for 30 min to digest any unpackaged DNA. Subsequently, a solution of 0.25 mM ethylenediaminetetraacetic acid (EDTA) (Nippon Gene, Japan) was added. The mixture was incubated at room temperature for 5 min. Afterward, the mixture was heated to 95°C for 15 min to inactivate the DNase I enzyme and denature the viral capsid. Dilution buffer was prepared by adding poloxamer-188 to Tris-EDTA buffer to achieve a final concentration of 0.001%. This dilution buffer was used to dilute the test samples to the appropriate range for analysis. Each dPCR reaction was set up to a final volume of 10 µL consisting of 1 µL of the prepared sample solution, 2 µL of 5X dPCR QuantStudio Absolute Q Master Mix (Thermo Fisher Scientific), 1.8 µL ITR primers (forward and reverse), and 0.25 µL ITP probe mix (purchased from Hokkaido System Science); 9 µL of dPCR reaction mix were added to each well of a QuantStudio Absolute Q MAP16 Plate Kit (Thermo Fisher Scientific). Afterwards, 15 µL of QuantStudio Absolute Q Isolation Buffer (Thermo Fisher Scientific) was carefully added to each well on top of the reaction mix. The wells were sealed with QuantStudio Absolute Q Strip Caps (Thermo Fisher Scientific) and centrifuged at 1200 rpm for 1 min on a swing-out rotor. The assay was performed on a QuantStudio Absolute Q Digital PCR System (Thermo

Fisher Scientific). Thermal cycling was performed as follows: (1) preheat at 96°C for 10 min, then (2) 40 cycles consisting of denaturation at 94°C for 5 s followed by annealing/extension at 54°C for 30 s. Data and global threshold were analyzed using QuantStudio Absolute Q digital PCR software (Thermo Fisher Scientific). Sample dilutions were used to calculate AAV genomic titers.

2-5-5. Determination of full and empty ratios of AAV8 vector by MP

MP measurements were conducted using TwoMP (Refeyn Ltd,Oxford, UK). For each experiment, mixed samples (full capsids at six prepared sample ratios, specifically, 90.1%, 73.1%, 52.3%, 31.5%, 10.5%, and 0% FPs) of AAV8 vector were pre-diluted in PBS (Gibco). Precision cover glasses (ThorLabs, Tokyo, Japan) were meticulously cleaned by serial rinsing with Milli-Q water and ethanol. To create the measurement chambers, I attached a pre-cut 2 × 3 well Culture Well silicone seal (3 mm diameter × 1 mm depth, Grace Bio-Labs, Bend, OR) to the clean coverslips. The coverslips were then transferred to the MP instrument, and 18 μL of PBS buffer was added to each well. After focusing, 2 μL of each AAV vector solution was added and mixed into the wells to achieve a total filling volume of 20 μL. Each measurement was recorded for 60 s, and each sample was analyzed at least three times ($n \geq 3$). Data analysis was performed using DiscoverMP version 2.5.1 (Refeyn Ltd, Oxford, UK). A Gaussian distribution fit was applied to the histogram peaks. From these Gaussian fits, we extracted the percentage of filled and empty AAV capsid.

3. Results

3-1. Screening the initial condition for assay development

3-1-1. Binding kinetics and affinity of AAV2 vector with anti-AAV VHH antibody by BLI

To determine if efficiency of the biotinylated anti-AAV VHH antibody sufficiently binds with AAV capsid, which can be first step for method development, I conducted initial Biolayer interferometry (BLI) analysis.[72] Since BLI is an optical technique, was employed molecular interactions, which offers ease of use and delivers both kinetic and affinity data without the necessity of labeling samples. These benefits position BLI as a promising method for the kinetic characterization of interactions between AAV vector and their ligands, for anti-AAV VHH antibody as well.

The dissociation constant (K_D) of anti-AAV VHH antibody for AAV2 vector was determined as 27.3 pM using BLI. Using these values, I calculated the binding efficiency of AAV based on **Equation 1** and **Equation 2**. The calculation result shown that the binding efficiency of VHH antibody and AAV2 vector was >99% over the entire range of the standard curve. Although there is no information about the affinity of anti-AAV VHH antibody for AAV8 vector, the binding efficiency would be >98% even if K_D value of anti-AAV VHH antibody for AAV8 vector is 100 times larger than that for AAV2 vector.

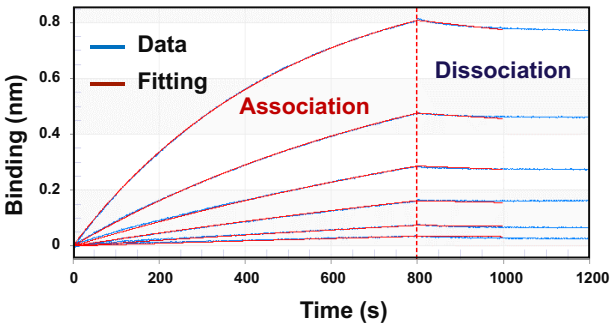

K_D (M)	k_{on} (1/Ms)	k_{off} (1/s)
2.73×10^{-11}	4.69×10^{6}	1.28×10^{-4}

Figure 7. Binding kinetics and affinity of AAV2 with anti-AAV VHH antibody measured by Biolayer Interferometry (BLI).

BLI measurement was performed on Octet HTX system (Sartorius, Goettingen, Germany).
The BLI measurements is conducted in the following steps. First, baseline measurement using Octet sample diluent. Next step is to load 0.01 µg/mL CaptureSelect™ Biotin Anti-AAVX immobilized on the SAX biosensors. Subsequently, then baseline measurement using Octed sample diluent. Furthermore, the associate of AAV2 vector with anti-AAV VHH antibody and the subsequent dissociation of AAV2 from anti-AAV VHH antibody were measured at 30°C in an Octet 384-well tilted-bottom microplate while shaking at 1000 rpm. The data were analyzed using Octet Analysis Studio software (ver. 12.2). The interaction between anti-AAV VHH antibody and AAV2 vector was analyzed by 1:1 fitting. Of note, for AAV2 vector samples were diluted in a 2-fold dilution series from 2.50×10^{11} vg/mL to 1.56×10^{10} vg/mL with Octet sample diluent and filled in the Octet® 384-well tilted-bottom microplate.
K_D, k_{on} and k_{off} are the kinetic values
K_D, dissociation constant; k_{on}, association rate constant; k_{off}, dissociation rate constant

3-1-2. Comparison of the genome detection after release from AAV vector at different times and temperatures

To ensure that AAV2 vector genome could be released by heating and detected by fluorescent dye, the preliminary experiment was performed using AAV2 vector. Previous studied have been reported that the viral protein unfolds at between 70°C and 90°C,[83] while other studied have also suggested that at the high temperatures, typically exceeding 50°C (with variations depending on the serotype), can result in capsid rupture.[84] For example, for AAV8 capsids, DNA is linearly ejected between 60°C and 70°C, with complete rupture occurring above 75°C.[85] Thus, in this experiment, to ensure that AAV vector genome could be detected

after being released from the AAV vector by heating, the sample solution was heated under five different conditions, specifically, 10 min at 80°C, 15 min at 80°C, 15 min at 85°C,10 min at 90°C, and 30 min at 90°C. After incubation, a fluorescent dye (SYBR Gold)[74,86] was added to the heated AAV2 vector solutions, and resulting fluorescent intensity was measured (**Figure 8**). The dose-response curve was successfully obtained, indicating that the AAV2 genome can be detected by heating and quantified using the fluorescent dye. By comparing these five conditions, the dose-response for 15 min at 85°C was higher than 10 min at 80°C, 15 min at 80°C, 10 min at 90°C and 30 min at 90°C incubation (**Table 9**). This suggests that the AAV genome can be fully released after heating at temperatures between 80°C and 90°C, with the optimal condition for genome detection being 85°C for 15 min. Previous reports revealed that by heating at 85°C for 20 min both AAV8 and AAV9 capsids are complexly ruptured and appropriate temperature range for the disruption of AAV capsid particles from AAV1 to AAV8 was reported to be between 66.5°C and 89.5°C ± 0.5°C, with the exception of AAV5 vector,[85,87]. Additionally, I used 85°C as the optimal temperature to genome detection of AAV after released from the AV capsid (**Figure 8**).

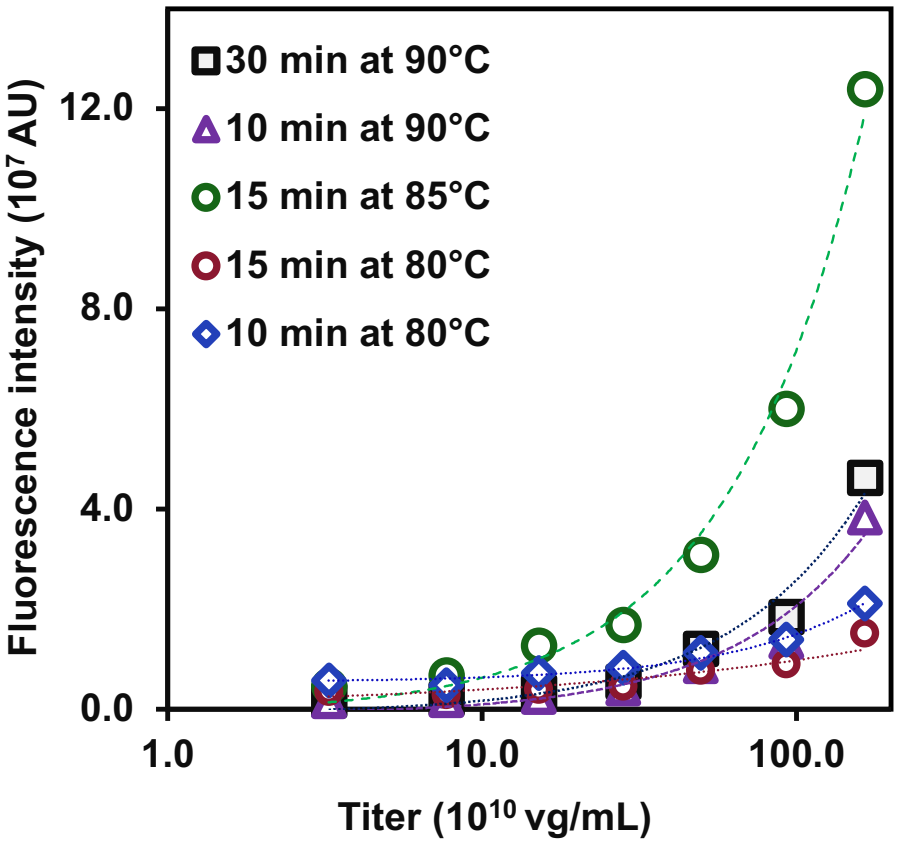

Figure 8. Result of testing the fluorescent/ temperature dye to detect genome after release from AAV2 capsid

SYBR Gold Nucleic Acid Gel Stain solution was diluted 500-fold with 1× PBS. The AAV2-LotB vector sample was diluted with 10-fold, in 1 × PBS. Diluted AAV vector sample was directly loaded into microplates for 100 µL per well. AAV2 vector samples were incubated at five different conditions from 10 min at 80°C (blue diamond), 15 min at 80°C (red circle), 15 min at 85°C (green circle), 10 min at 90°C (purple triangle), and 30 min at 90°C (black square) for disrupting the AAV 2 capsid particles. The intensity of the green fluorescence emanating from SYBR gold to quantify the released genome using an excitation wavelength of 495 nm and an emission wavelength of 540 nm. A standard curve was generated using a four-parameter curve-fitting algorithm with the SpectraMax i3x microplate reader. The resulting data were plotted on a graph, with the fluorescence intensity value on the vertical axis and the viral concentration value on the horizontal axis. The sample was analyzed in duplicate.

AU, arbitrary unit; vg, viral genome.

Table 9. Result of genome detection after releasing from AAV capsid using fluorescent dye, as used in the screening the initial conditions

Sample		Florescence intensity (AU)				
Serial dilution	Concentration (10^{10} cp/mL)	10 min at 80°C (10^7)	15 min at 80°C (10^7)	15 min at 85°C (10^7)	10 min at 90°C (10^7)	30 min at 90°C (10^7)
1:1	165	2.11	1.52	12.4	3.83	4.63
1:2	92.7	1.39	0.90	6.01	1.35	1.85
1:4	49.6	1.13	0.78	3.09	8.68	1.21
1:8	28.1	0.84	0.47	1.69	3.83	0.57
1:16	15.1	0.72	0.40	1.28	0.25	0.34
1:32	7.70	0.49	0.30	0.68	0.18	0.22
1:64	3.35	0.58	0.36	0.47	0.16	0.19

AU, arbitrary unit; cp, capsid particle

3-2. Development of dFLISA

3-2-1. Standards and samples quantification determined by BS-AUC

As BS-AUC was recently recognized as the gold standard for the size distribution analysis of AAV vectors and can quantify of partial, extra filled particles and aggregates with high precision.[78] BS-AUC experiments were conducted using different lots of AAV8-CMV- EGFP (in-house AAV8-Lot1 to AAV8-Lot3 and outsourced (VectorBuilder) AAV2-Lot1 to AAV2-Lot4, and AAV8-Lot5 to AAV8-Lot6. The concentration of each component could be determined in BS-AUC, and a high resolution could be obtained. The result shows the representative profiles of the apparent sedimentation coefficient distribution (c(s) profiles) of each sample are displayed in **Figure 9** to **Figure 11**. For **Tables 10** and **Table 11** summarize the results.

Since, AUC has potential to quantify EP, PP, FP and ExP, where the genome length of ExP is longer than that of FP. In this study, because the amount of PP was lower than the limit of quantification of AUC (6.3×10^{11} particles/mL)[80] the sum of particle concentration of EP, FP, and ExP was considered as capsid titer. For simplicity, the sum of particle concentration of FP and ExP was considered as genomic titer. FP ratio was calculated by dividing the genomic titer by the capsid titer. Thus, the potential standard for our dFLISA was derived from this BS-AUC.

Except for AAV8-Lot5 and AAV8-Lot6 because the amount of PP and ExP was lower than the limit of quantification of AUC. Therefore, the sum of particle concentration of EP and FP was considered as capsid titer, while the sum of particle concentration of only FP was considered as genomic titer. The FP ratio was calculated by dividing the genomic titer by the capsid titer.

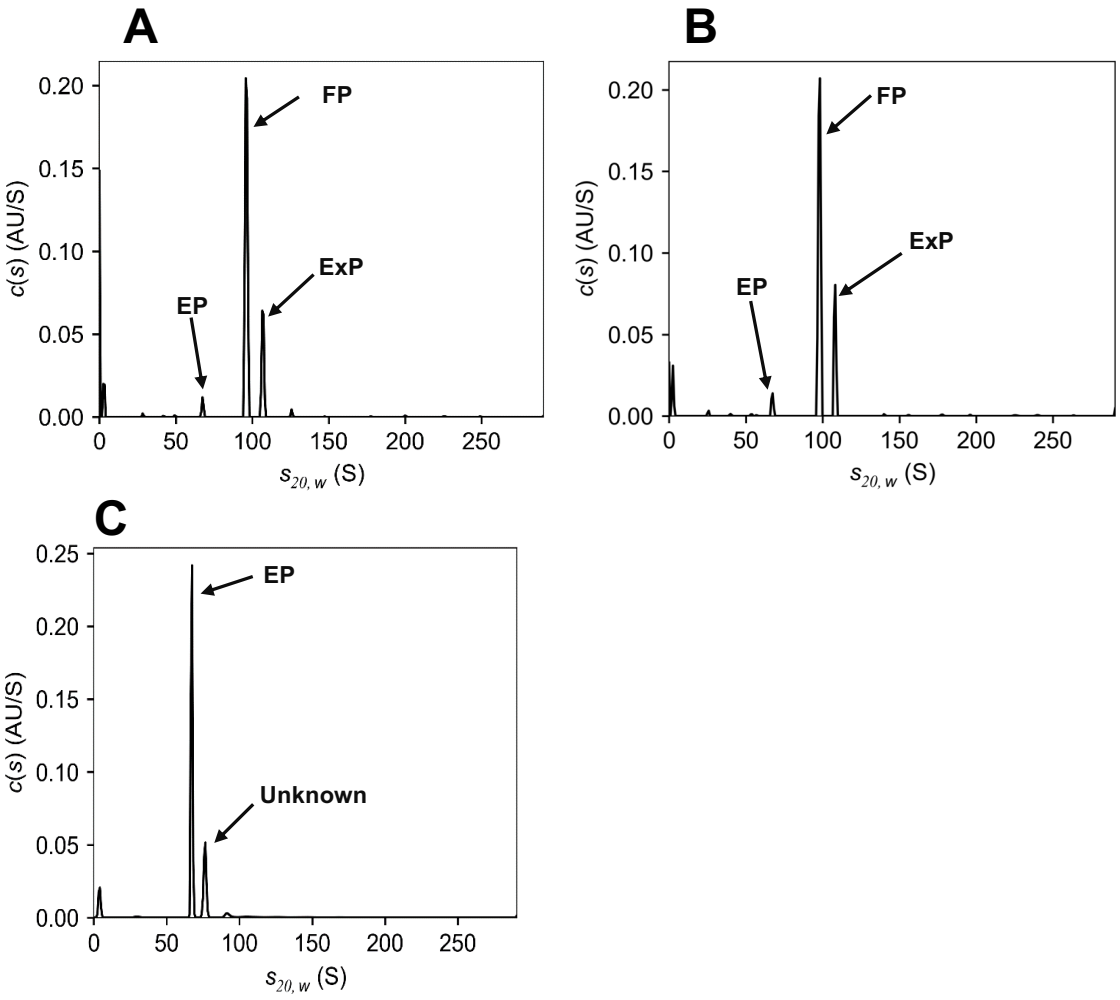

Figure 9. Representative sedimentation coefficient distributions in PBS/D2O + 0.001% poloxamer-188 for AAV8-Lot1 to AAV8-Lot3 vector samples (see in Table 10)

(A) Sedimentation coefficient distribution of AAV8-Lot1 vector sample, which is used as the standard for dFLISA analysis.

(B) Sedimentation coefficient distribution of AAV8-Lot2 vector sample, which is used as sample for dFLISA analysis.

(C) Sedimentation coefficient distribution of AAV8-Lot3 vector sample, which is used as sample for dFLISA analysis.

The observed peaks are assigned as empty particle (EP), full particle (FP), or extra filled (ExP). [80,88] It is important to note that the unknown peak was not counted as particle.

$S_{20,w}$, sedimentation coefficient in water at 20°C

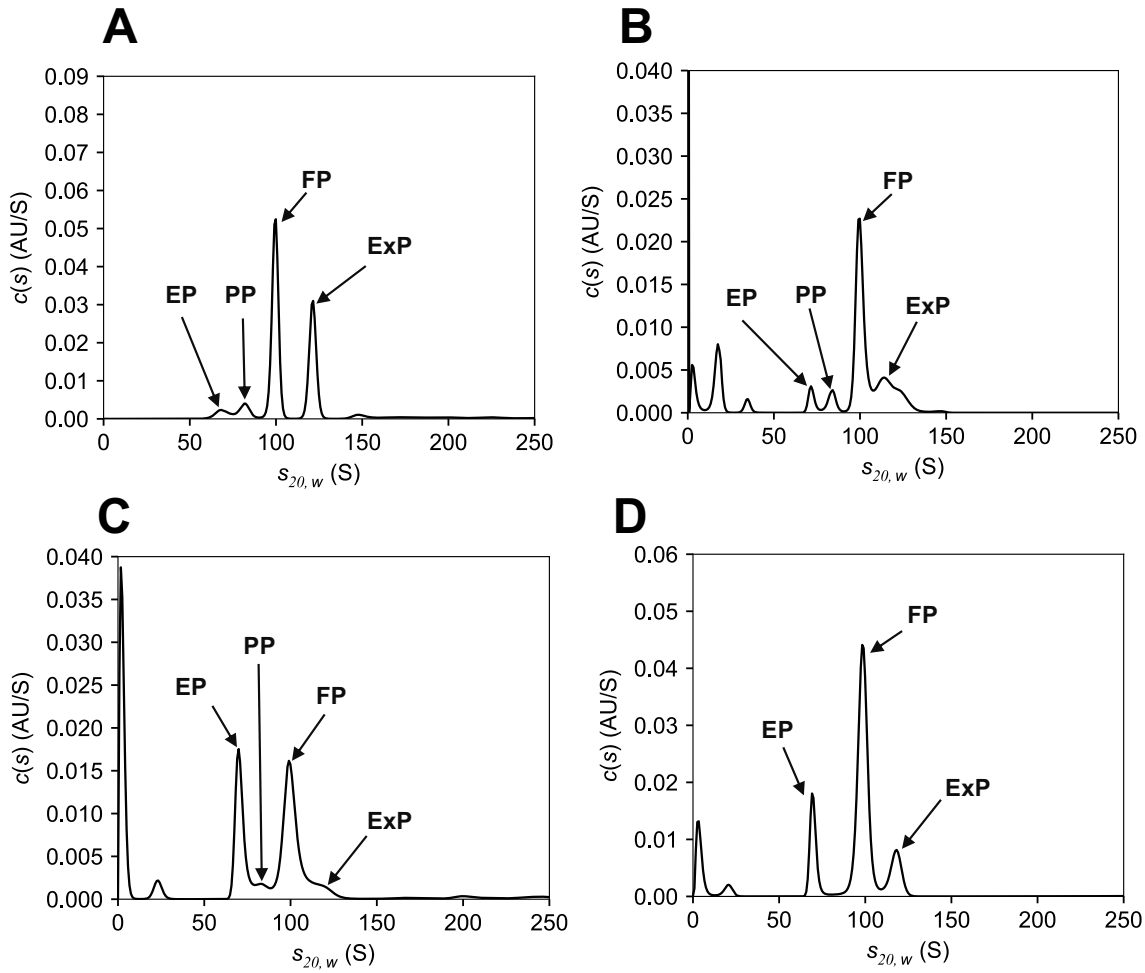

Figure 10. Representative sedimentation coefficient distributions in PBS/D2O + 0.001% poloxamer-188 for AAV2-Lot3 to AAV2-Lot4 and AAV8-Lot5 to AAV8-Lot6 and vector samples (see in Table 11)

(A) Sedimentation coefficient distribution of AAV2-Lot3 vector sample, which is used as the standard for dFLISA analysis.

(B) Sedimentation coefficient distribution of AAV2-Lot4 vector sample, which is used as the sample for dFLISA analysis.

(C) Sedimentation coefficient distribution of AAV8-Lot5 vector sample, which is used as the standard for dFLISA analysis.

(D) Sedimentation coefficient distribution of AAV8-Lot6 vector sample, which is used as the sample for dFLISA analysis.

The observed peaks are assigned as empty particle (EP), full particle (FP), extra filled particle (ExP) or partial particle (PP).

$S_{20,w}$, sedimentation coefficient in water at 20°C

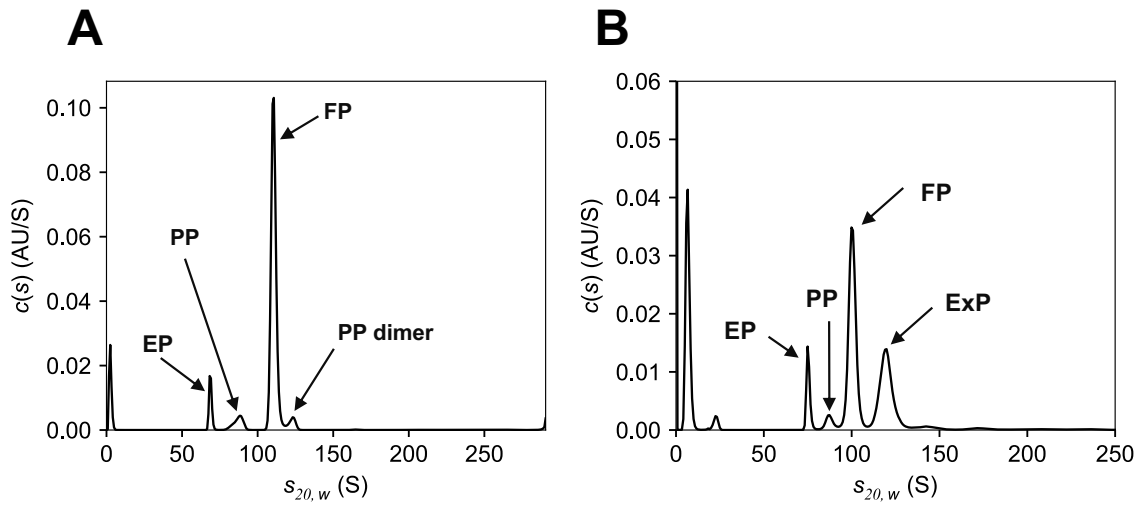

Figure 11. Representative sedimentation coefficient distributions in PBS/D2O + 0.001% poloxamer-188 for AAV2-Lot1 to AAV2- Lot2 vector samples (see in Table 11).

(A) Sedimentation coefficient distribution of AAV2-Lot1 vector sample, which is used as the standard for dFLISA analysis. The observed peaks were identified as EP, PP, FP and PP dimer. PP is higher than LOQ, and the PP dimer is lower than LOQ of BS-AUC.

(B) Sedimentation coefficient distribution of AAV2-Lot2 vector sample, which is used as standard for dFLISA analysis. The observed peaks are assigned as empty particle (EP), full particle (FP), partial particle (PP) as shown in the figures.

$S_{20,w}$, sedimentation coefficient in water at 20°C

Table 10. Summary of in-house AAV8 vectors used in this study, as determined by BS-AUC in 3-2-1

Sample name	Serotype	Promoter	GOI	Number of nucleic acids	FP (10^{13} vg/mL)	EP (10^{13} cp/mL)	ExP (10^{13} vg/mL)	PP (10^{13} vg/mL)	FP (%)	EP (%)	ExP (%)	PP (%)	FP+ExP (%)	FP+ExP (10^{13} vg/mL)	Total FP+ExP+EP (10^{13} cp/mL)	Sample preparation
AAV8-Lot1	8	CMV	EGFP	2521	1.09	0.11	0.24	<LOQ	76.10	8.23	15.67	na	91.8	1.31	1.43	Standard
AAV8-Lot2	8	HCRhAAT	FIX	2712	4.75	0.61	0.79	<LOQ	77.15	9.90	12.95	na	90.1	5.55	6.16	Sample
AAV8-Lot3	8	na	na	na	na	7.37	na	na	na	100	na	na	na	na	7.37	Sample

BS-AUC, band sedimentation analytical ultracentrifugation.

GOI, gene of interest; CMV, cytomegalovirus promoter; HCRhAAT, hepatic control region and human a1 antitrypsin promoter; EGFP, enhanced green fluorescent protein; FIX, factor IX.

cp, capsid particle; vg, viral genome; EP, empty particle; ExP, extra filled particle; FP, full particle; PP, partial particle; LOQ, limit of quantification; na, not applicable

Table 11. Summary of AAVs vectors purchased from VectorBuilder used in this study, as determined by BS-AUC in 3-2-2

Sample name	Serotype	Promoter	GOI	Number of nucleic acids	FP (10^{12} vg/mL)	EP (10^{12} cp/mL)	ExP (10^{12} vg/mL)	PP (10^{12} vg/mL)	FP (%)	EP (%)	ExP (%)	PP (%)	FP+ExP (%)	FP+ExP (10^{12} vg/mL)	Total FP+ExP+EP (10^{12} cp/mL)	Sample preparation
AAV2-Lot1	2	CMV	EGFP	2521	1.87	0.27	0.94	<LOQ	60.5	8.9	30.9	na	91.1	2.82	3.09	Sample
AAV2-Lot2	2	CMV	EGFP	3681	3.33	0.40	<LOQ	<LOQ	89.1	10.9	na	na	89.1	3.33	3.73	Sample
AAV2-Lot3	2	CMV	EGFP	2521	10.3	1.21	6.12	<LOQ	58.5	6.9	34.6	na	93.1	16.5	17.7	Standard
AAV2-Lot4	2	CMV	EGFP	2521	6.12	0.75	2.76	<LOQ	63.6	7.8	28.6	na	92.2	8.88	9.63	Sample
AAV8-Lot5	8	CMV	EGFP	2521	7.43	2.34	<LOQ	<LOQ	72.2	22.7	na	na	77.3	7.95	10.3	Standard
AAV8-Lot6	8	CMV	EGFP	2521	7.83	6.60	<LOQ	<LOQ	53.6	45.1	na	na	54.9	8.02	14.6	Sample

BS-AUC, band sedimentation analytical ultracentrifugation. GOI, gene of interest; CMV, cytomegalovirus promoter; EGFP, enhanced green fluorescent protein; cp, capsid particle; vg, viral genome; EP, empty particle; ExP, extra filled particle; FP, full particle; LOQ, limit of quantification; PP, partial particle; na, not applicable

3-2-2. Comparison of anti-AAV VHH antibody immobilized with AAV2 vector by dFLISA

The results of BLI measurements, using an in-house established method, analyzed the binding affinity of the anti-AAV VHH antibody with AAV vectors. The findings demonstrated that for AAV2 vector, the binding efficiency between anti-AAV VHH antibody and AAV2 vector was >99% over the entire range of the standard curve, while for the affinity of AAV8 vector, the binding efficiency would be >98% even if K_D value of anti-AAV VHH antibody for AAV8 vector is 100 times larger than that for AAV2 vector.

The objective of the dFLISA experiment was to determine the appropriate concentration of VHH binding ligand for sufficient binding to the AAV capsid. To achieve this, two different concentrations of the anti-AAV VHH antibody were applied. In the 1st and 2nd experiments, the anti-AAV VHH antibody was prepared at concentrations of 10 μg/mL and 20 μg/mL, respectively. The AAV8-Lot5 vector, with a genome length of 2521 bases, was used in this study. The results showed that the capsid quantification fluorescence intensity was higher in the 1st experiment than in the 2nd. Conversely, the genomic titer showed a lower fluorescence intensity in the 1st experiment than in 2nd. However, in the 1st experiment, both the capsid and genomic signal-to-noise of background ratios (S/N) were higher in the 1st than in the 2nd experiment. Since the higher S/N ratio is a criterion of dFLISA method, the concentrations of the anti-AAV VHH antibody and anti-AAV8 antibody (ADK8) were set at 10 μg/mL and 1 μg/mL, respectively, for further experiments in this study (**Figure 12**).

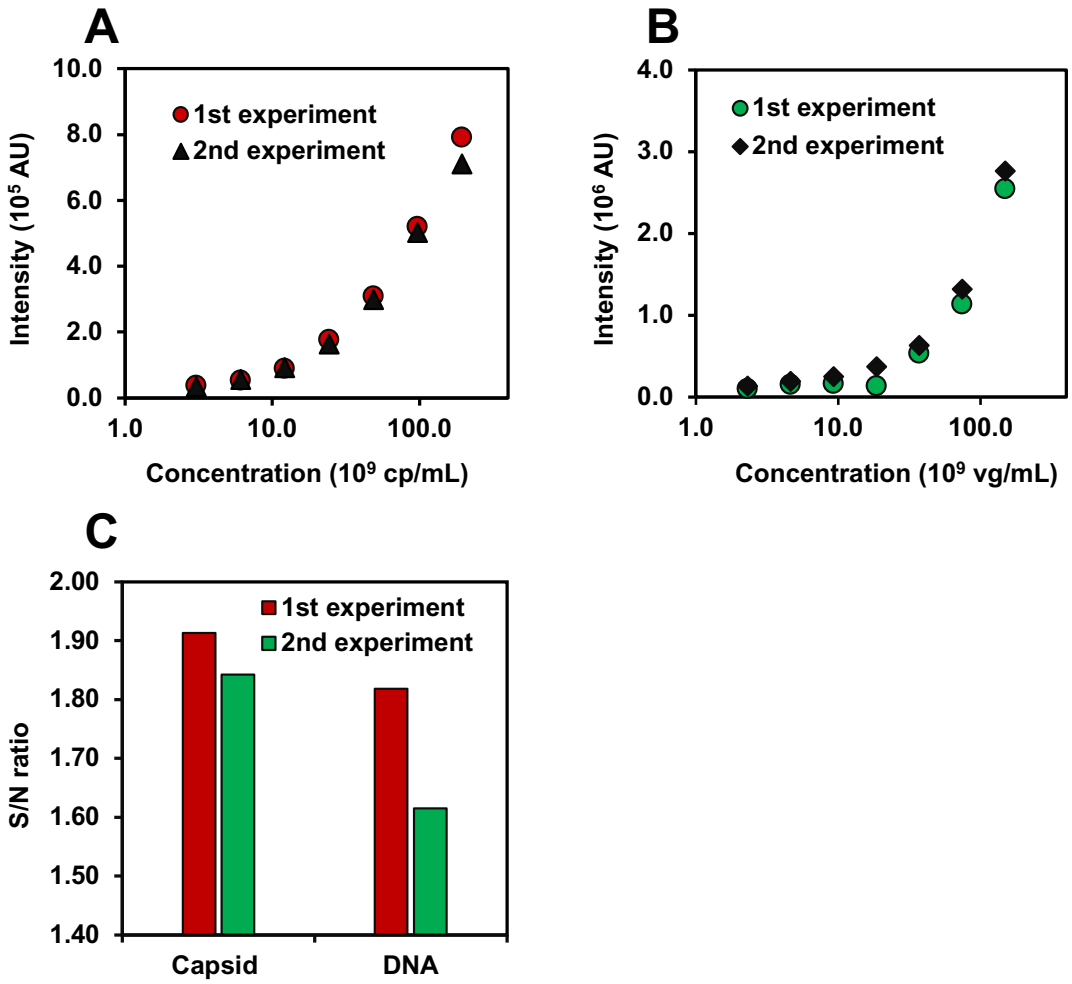

Figure 12. Optimization of antibody against AAVs by dFLISA

(A) Capsid titer quantification.

(B) Genomic titer quantification.

(C) S/N ratio of fluorescent intensity of capsid and genome of AAV vector.

Two experiments were conducted. For 1st experiment (anti-AAV VHH antibody:10 µg/mL and anti-AAV8 antibody (ADK8):1 µg/mL) and for 2nd experiment (anti-AAV VHH antibody: 20 µg/mL and anti-AAV8 antibody (ADK8): 10 µg/mL). In this quantitative analysis, only one in-house sample of serotype 8, AAV2-Lot5, was used in this quantitative analysis. The sample was originally formulated in 1 × PBS with 200 mM NaCl and 0.001% poloxamer-188. After a 100-fold dilution, the final concentration of NaCl in the solution was 2 mM, with 0.001% poloxamer-188. The final concentration of the AAV2-Lot5 sample was 7.30×10^{10} vg/mL in 0.05% Tween 20 in 1 × PBS. Subsequently, this sample solution was serially diluted at a 1:2 ratio to generate a calibration curve. The sample was analyzed in duplicate. AU, arbitrary unit

3-2-3. Comparison of the detection wavelength for the capsid and genomic quantification of AAV vector by dFLISA

After determining the appropriate concentrations of both the anti-AAV VHH antibody (10 μg/mL) and the anti-AAV8 antibody (ADK8) (1 μg/mL) (**Figure 12**), I conducted two additional experiments using an AAV8-LotB vector with a 2521bases-genome as a standard. The AAV8-LotB vector was diluted to a concentration of 7.30×10^{10} vg/mL in 0.05% Tween 20 in 1× PBS and then serially diluted at a 1:2 ratio to generate a calibration curve. The results demonstrated that, in the 1st experiment, the S/N ratios of the capsid titer were not significantly higher than in the 2nd experiment. However, the S/N ratios of the genomic titer in the 1st experiment were significantly higher than in the 2nd experiment.

Since the higher S/N ratio is a criterion of dFLISA, the intensity of the red fluorescence from proteins labeled with goat anti-mouse IgG H&L (Alexa Fluor 647) to quantify the capsid titers, with an excitation wavelength of 652 nm and an emission wavelength of 680 nm, was selected as the optimal wavelength in the 1st experiment. For the intensity of the green fluorescence from SYBR Gold to quantify the released genome, an excitation wavelength of 500 nm and an emission wavelength of 535 nm in the 2nd experiment were selected as the optimal wavelengths for further experiments in our study (**Figure 13**).

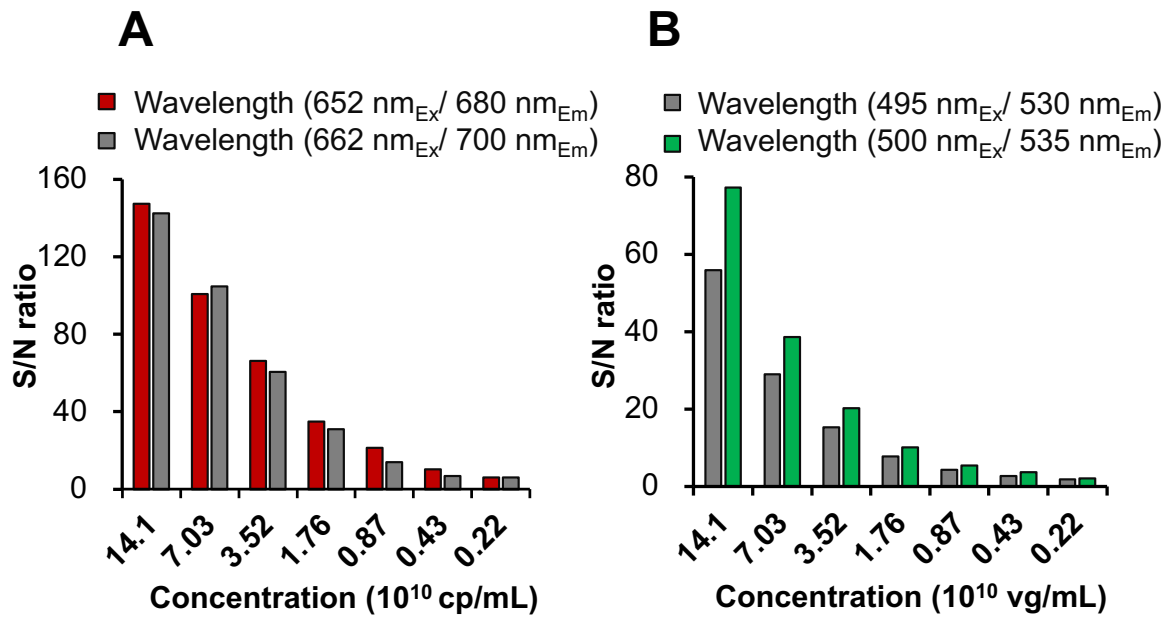

Figure 13. Comparison of detection wavelength for capsid and genome of AAV by dFLISA

(A) Wavelength for capsid titer quantification.

(B) Wavelength for genomic titer quantification.

For 1st experiment, the wavelength utilized for the detection of the capsid and genomic titer were 652 nm_{Ex}/ 680 nm_{Em} (red bar) and 495 nm_{Ex}/ 500 nm_{Em} (gray bar), respectively. For 2nd experiment, the wavelength utilized for the detection of the capsid and genomic titer were 662 nm_{Ex}/ 700 nm_{Em} (gray bar) and 500 nm_{Ex}/ 535 nm_{Em} (green bar), respectively.

In this quantitative analysis of, only one sample of serotype 8, AAV2-LotC, was used in this quantitative analysis. This sample was initially formulated in PBS, 200 mM NaCl, 0.001% poloxamer-188, and then diluted to a concentration of 7.30×10^{10} vg/mL in 0.05% Tween 20 in 1 × PBS. Subsequently, it was serially diluted at a 1:2 ratio to generate a calibration curve. The sample was analyzed in duplicate.

cp, capsid particle; Ex, excitation wavelength; Em, emission wavelength; vg, viral genome

3-2-4. dFLISA analysis

A 96-well plate was first coated with anti-AAV VHH antibody, followed by the addition of bovine serum albumin (BSA) for blocking. Standards and samples were then added to the wells. The binding efficiency of the anti-AAV VHH antibody for AAV2 vector and AAV8 vector were estimated as >98% (**Figure 7**). Mouse anti-AAV antibody was added after removal of unbound

AAVs. Then goat anti-mouse antibody conjugated to Alexa Fluor 647 was used to detect and quantify the AAV capsid proteins. The plate was washed to remove excess goat antibody and heated at 85°C for 15 min to disrupt the capsid and release the genome. SYBR gold solution was then added to each well to detect DNA. Because SYBR gold is fluorescent only when it is bound to DNA,[62] genomes can be quantified even when they are no longer immobilized on the plate and without washing out the unbound SYBR gold dye. Standard curves were generated using 4-parameter logistic regression to calculate the capsid and genome titers. The FP ratio was calculated from these values-capsid and genome titers are considered to represent total and full particle concentrations, respectively (**Figure 14**).

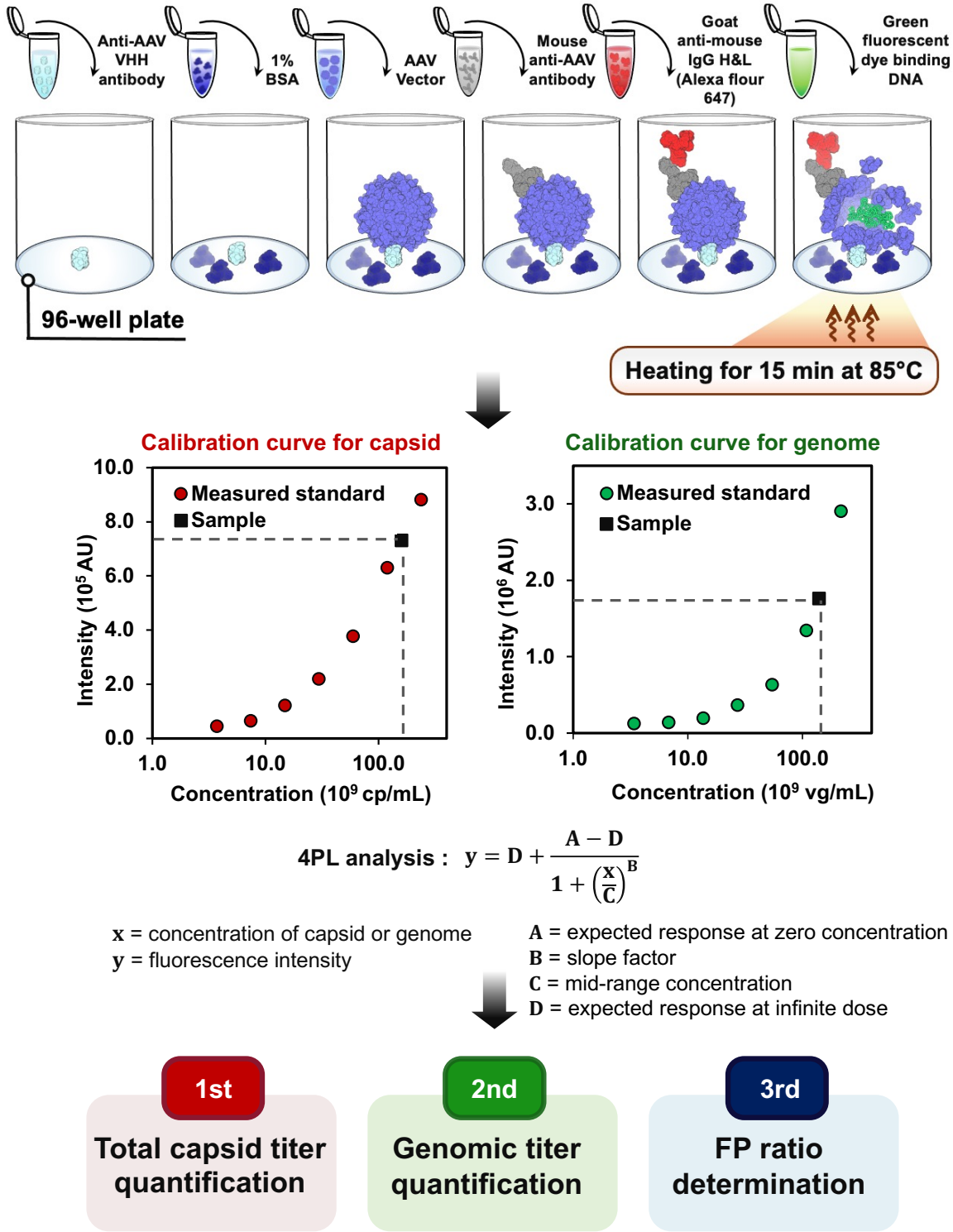

Figure 14. Schematic illustration of dFLISA analysis

The soluble biotinylated anti-AAVX conjugate VHH affinity ligand, which exhibits high affinity for AAVX, was immobilized directly onto a black 96-well plate and used as a capture protein. Subsequently, 1% BSA was added, and the individual wells were loaded with vector stocks comprising a variety of AAV samples. A mouse monoclonal antibody targeting intact AAV particles was used as the primary antibody against AAV. To enable detection, I used a goat anti-mouse IgG

H&L-labeled secondary antibody (Alexa Fluor 647). The viral capsid was disrupted, and ssDNA was released by the addition of 1 × PBS to each well, followed by incubation at 85°C for 15 min. Subsequently, I added diluted SYBR gold solution to each well and incubated the plate at room temperature for 5 min. This technique allowed us to generate the calibration curve and thus measure both red and green fluorescence, providing an assessment of the capsid and genomic titers, as well as the FP ratio, through simultaneous dual-wavelength measurements.
AU, arbitrary unit; cp, capsid particle; vg, viral genome

3-3. Validation of dFLISA

3-3-1. Precision, accuracy and LOQ of dFLISA measurement

The precision and accuracy of capsid and genomic titer quantification by dFLISA were evaluated by analyzing purified AAV8 vector samples on three separate occasions over three consecutive days (**Figure 15A** to **Figure 15C**). The capsid concentration of the original sample solution was determined in advance as 1.54×10^{11} cp/mL by BS-AUC. These samples were serially diluted at a 1:2 ratio, resulting in the series of dilutions shown in **Table 12** and **Table 13**. For precision, the coefficient of variation (%CV) of the capsid titer was less than 15% for all samples and less than 11% for Samples 1–4 (**Table 12**). The %CV of genomic titer quantification was less than 7% for Samples 1–3, and the %CV of the genomic titer of Sample 4 was 22.6% (**Table 13**). Accuracy was evaluated based on the ratio of experimental/expected values. The ratios of Samples 1–4 were consistently within the range 80–100% for both capsid and genome titers. The ratios of experimental/expected values of Samples 5–7 was lower than 80% **(Figure 15B, Figure 15C** and **Table 13)**.

According to the criteria for accuracy and precision described in the methods section, the concentration of 1–3 should be within the quantification range of dFLISA, and sample 4 (1.61×10^{10} cp/mL, 1.47×10^{10} vg/mL) met the criteria for the limit of quantification (LOQ). In addition, the concentration was calculated from fluorescence intensities of blank + 10 standard deviations (SD), which is also used to determine LOQ. The capsid titer for Sample 4 was higher than that of blank intensity + 10 SD (**Table 14**), while the genome titer for Sample 4 was lower

than that of blank intensity + 10 SD (**Table 15**). The higher values were determined as the LOQ of dFLISA for capsid and genome titer quantification: 1.61×10^{10} cp/mL for capsid titer and 1.70×10^{10} vg/mL for genomic titer.

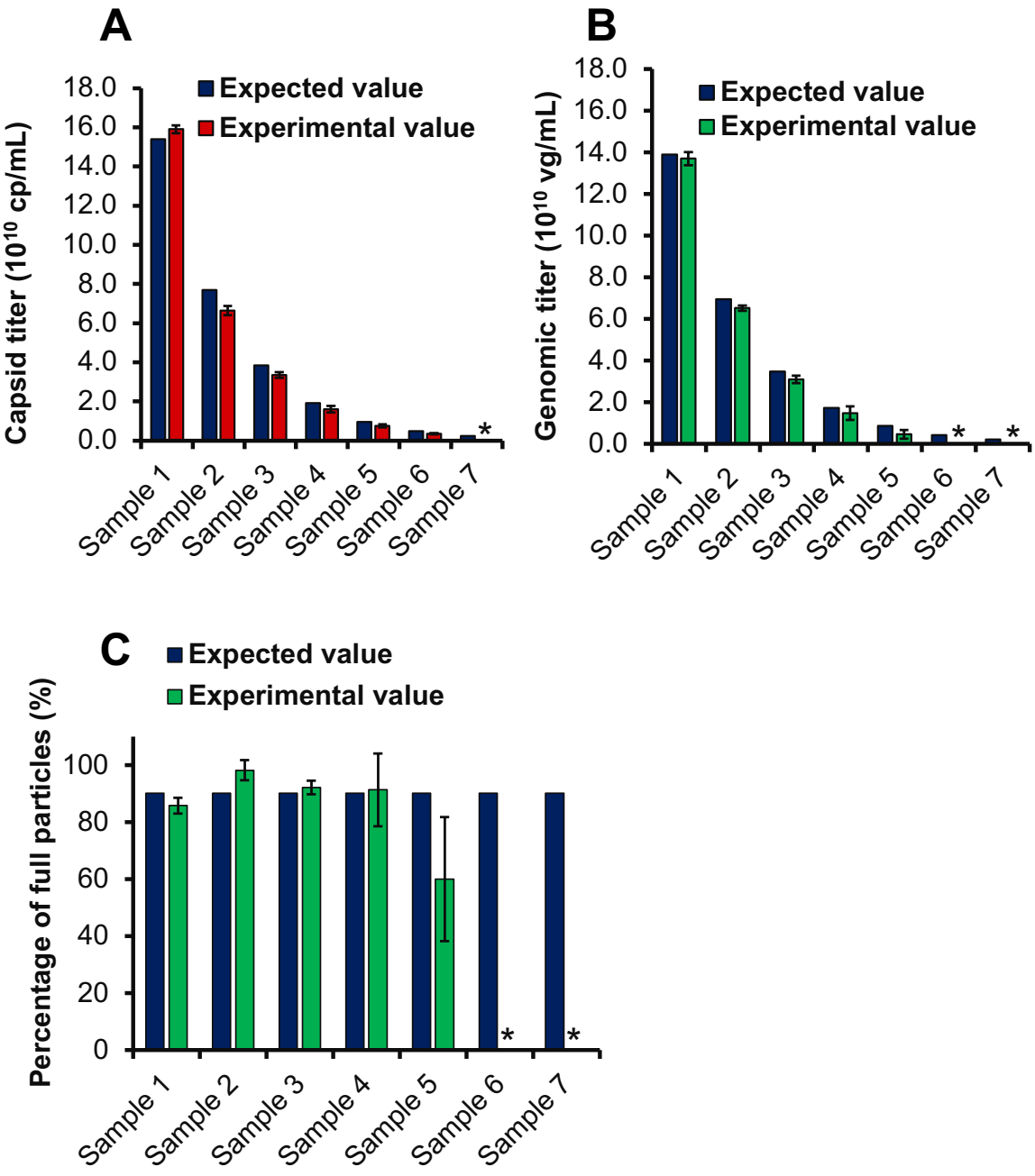

Figure 15. Quantification of capsid and genomic titers by dFLISA

(A) Capsid titer quantification.

(B) Genomic titer quantification.

(C) Percentage of full particles determination.

In this quantitative analysis, two different samples of serotype 8, AAV8-Lot1 and AAV8-Lot2, were used. Each sample was initially formulated in PBS, 200 mM NaCl, 0.001% poloxamer-188. AAV8-Lot1 was used to establish the reliability of the calibration curve and had a concentration of 1.43×10^{13} cp/ml and 1.31×10^{13} vg/mL, and then diluted 60-fold with 0.05% Tween 20 in 1 × PBS AAV8-Lot2 was used as an unknown sample and had a concentration of 6.16×10^{13} cp/ml and 5.55×10^{13} vg/ml, and then diluted 400-fold with 0.05% Tween 20 in 1 × PBS. Serial 2-fold dilutions were performed daily to obtain seven samples while avoiding freeze–thaw cycles and maintaining consistent operating conditions for a brief time. Both samples were prepared without undergoing freeze–thaw cycles. The obtained responses were plotted using dFLISA data (experimental value) and BS-AUC data (expected value). The mean values from experiments conducted over three days are presented in the results. Each sample was analyzed in duplicate wells (n=2), and error bars indicate the SD within each sample. Asterisks (*) are used to indicate cp/mL and vg/mL values that were below the limit of quantitation. cp, capsid particle; vg, viral genome

Table 12. Precision and accuracy of the dFLISA of capsid titer (cp/mL)

Sample	Expected value	Experimental value						
	Concentration (10^{10} cp/mL)	Concentration (10^{10} cp/mL)				SD (10^{10} cp/mL)	CV (%)	Accuracy (%)
		Day 1	Day 2	Day 3	Average titer			
1	15.4	15.7	15.9	16.1	15.9	0.21	1.3	102.8
2	7.70	6.98	6.48	6.45	6.64	0.29	4.4	87.6
3	3.85	3.50	3.31	3.23	3.35	0.14	4.2	87.6
4	1.93	1.81	1.53	1.50	1.61	0.17	10.6	84.1
5	0.96	0.84	0.67	0.76	0.76	0.08	10.8	76.0
6	0.48	0.29	0.39	0.35	0.34	0.04	14.4	74.3
7	0.24	0	0	0.16	0	0	0	0

Results represent the mean values from 3-day experiments, in which each sample was analyzed in duplicate wells.

The samples were initially diluted 400-fold, followed by a 2-fold serial dilution.

CV , coefficient of variation; cp, capsid particle; SD, standard deviation

Table 13. Precision and accuracy of the dFLISA of genomic titer (vg/mL)

Sample	Expected value	Experimental value							
	Concentration (10^{10} vg/mL)	Concentration (10^{10} vg/mL)				Full capsid ratio (%)	SD (10^{10} vg/mL)	CV (%)	Accuracy (%)
		Day 1	Day 2	Day 3	Average titer				
1	13.9	13.7	14.0	13.3	13.7	85.8	0.31	2.3	98.4
2	6.94	6.60	6.58	6.37	6.52	98.2	0.12	1.9	93.9
3	3.47	3.27	3.10	2.89	3.09	92.2	0.18	6.1	89.0
4	1.73	1.80	1.47	1.14	1.47	91.3	0.33	22.6	84.7
5	0.86	0.69	0.35	0.31	0.45	60.1	0.21	46.1	52.7
6	0.43	0	0	0	0	0	0	0	0
7	0.21	0	0.54	0	0	0	0	0	0

Results represent the mean values from 3-day experiments, in which each sample was analyzed in duplicate wells.

The samples were initially diluted 400-fold, followed by a 2-fold serial dilution.

CV, coefficient of variation; SD, standard deviation; vg, viral genome

Table 14. Determination LOQ of dFLISA for capsid titer detection

Blank Intensity (10^4)					Concentration calculated from
Day 1	Day 2	Day 3	Average intensity	SD	blank intensity + 10 SD (10^{10} cp/mL)
1.65	2.91	2.05	2.20	0.29	0.60

The limit of quantification (LOQ) of capsid quantification is estimated from fluorescence intensities of blank.

Results represent the mean results of 3-day experiments in which each sample was analyzed in duplicate wells.

cp, capsid particle; SD, standard deviation

Table 15. Determination LOQ of dFLISA for genomic titer detection

Blank Intensity (10^4)					Concentration calculated from
Day 1	Day 2	Day 3	Average intensity	SD	blank intensity + 10 SD (10^{10} vg/mL)
10.0	9.10	9.20	9.56	1.27	1.70

The limit of quantification (LOQ) of genome quantification is estimated from fluorescence intensities of blank.

Results represent the mean results of 3-day experiments in which each sample was analyzed in duplicate wells.

SD, standard deviation; vg, viral genome

3-4. Comparison of full particle ratio determination of AAV vector by orthogonal methods

3-4-1. Linearity of AAV8 full particle ratio in dFLISA analysis

I then investigated the linearity of the FP ratio calculated by dFLISA. Samples with different FP ratios (0%, 10.5%, 31.5%, 52.3%, 73.1%, and 90.1% of FPs) were prepared by mixing two samples: AAV8-Lot2 (FP ratio was 90.1%) and AAV8-Lot3 (FP ratio was 0%). Excellent correlation and linearity in the FP ratio were observed, with an R^2 value of > 0.99, and the slope of the plot against the expected values was 0.97. In addition, the %CV of the FP ratio was less than 25%. These results indicate that dFLISA has sufficient precision, accuracy, and linearity for FP ratio determination (**Figure 18**).

3-4-2. Determination of full particle ratios of AAV8 vector by MP

MP measurement was conducted using TwoMP. For each experiment, mixed samples (full capsids at six prepared sample ratios, specifically, 90.1%, 73.1%, 52.3%, 31.5%, 10.5%, and 0% FPs). MP's result shown that only two histogram peaks, observed Peak1 with mass corresponding to FP, while the observed peak 2 with mass corresponding to EP. Gaussian distribution fit was applied to the histogram peaks (**Figure 16**). From these Gaussian fits, the percentage of full and empty AAV8 capsids were extracted. Then the observed percentage these spike same compared with different orthogonal methods as shown in **Figure 17** and **Figure 18**.

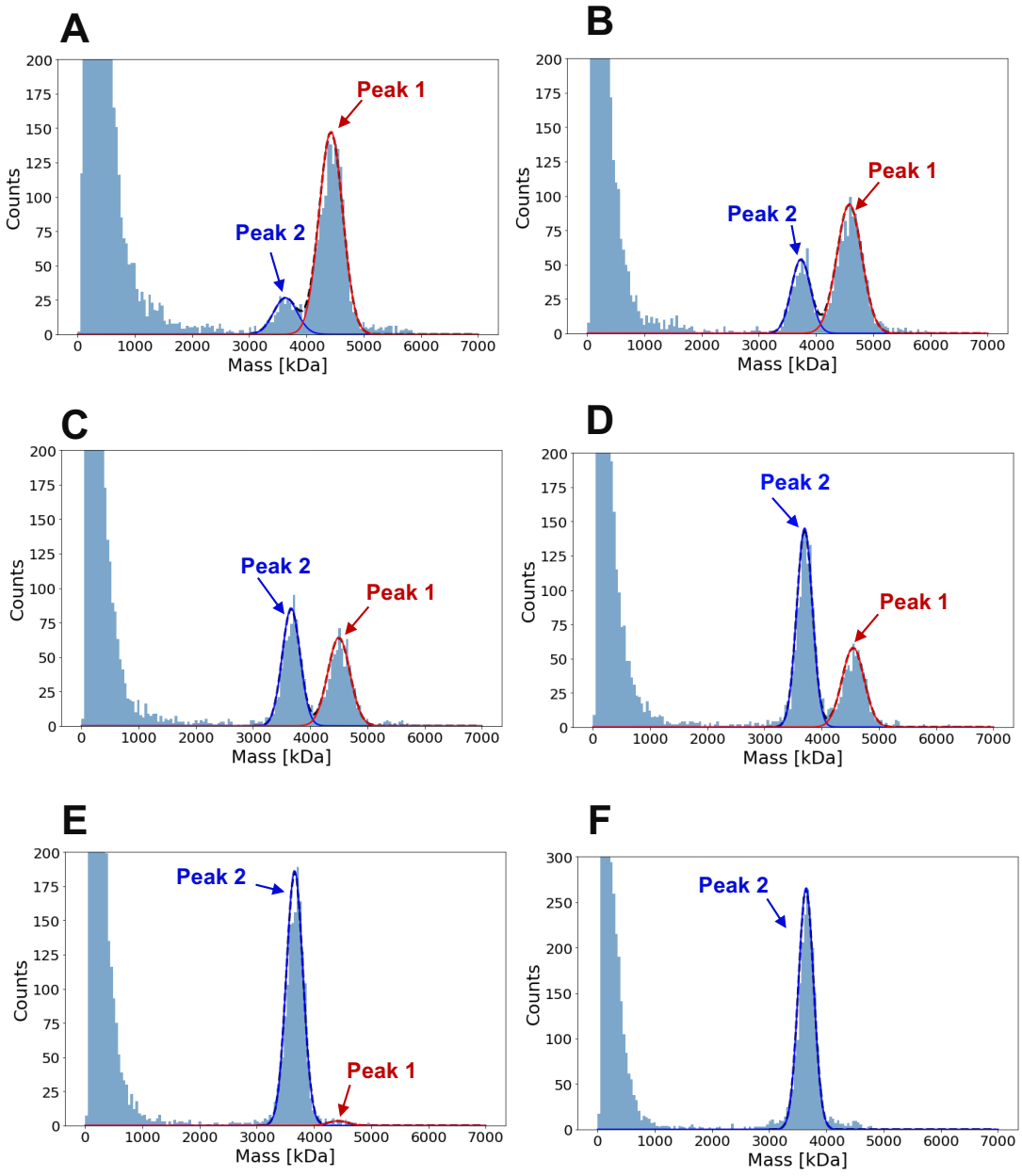

Figure 16. Histogram from MP analysis of ssDNA packaged AAV8 capsids obtained from six mixed spike samples (90.1%, 73.1%, 52.3%, 31.5%, 10.5%, and 0% FPs).

(A) Constructed mass histograms of 90.1 % full capsid.

(B) Constructed mass histograms of 73.1 % full capsid.

(C) Constructed mass histograms of 52.3 % full capsid.

(D) Constructed mass histograms of 31.5 % full capsid.

(E) Constructed mass histograms of 10.5 % full capsid.

(F) Constructed mass histogram of 0 % full capsid.

Observed Peak1 (red) with mass corresponding to FP, while the observed Peak 2 (blue) with mass corresponding to EP. For each AAV8 sample, a single representative mass histogram is displayed.

Gaussian distribution fit was applied to the histogram peaks. From these Gaussian fits, the percentage of full and empty AAV8 capsids were extracted. EP, empty particle; FP; full particle; kDa, kilodalton; MP, mass photometry

3-4-3. Linear correlation of total capsid titers and genomic titers of six mixed spike samples by orthogonal methods

I have compared the capsid titers of six mixed spike samples analyzed by three techniques: dFLISA, AUC, and ELISA (**Table 16**). Next, I also compared the genomic titers of six mixed spike samples analyzed by three techniques: dFLISA, AUC, and dPCR (**Table 17**, **Figure 17B)**.

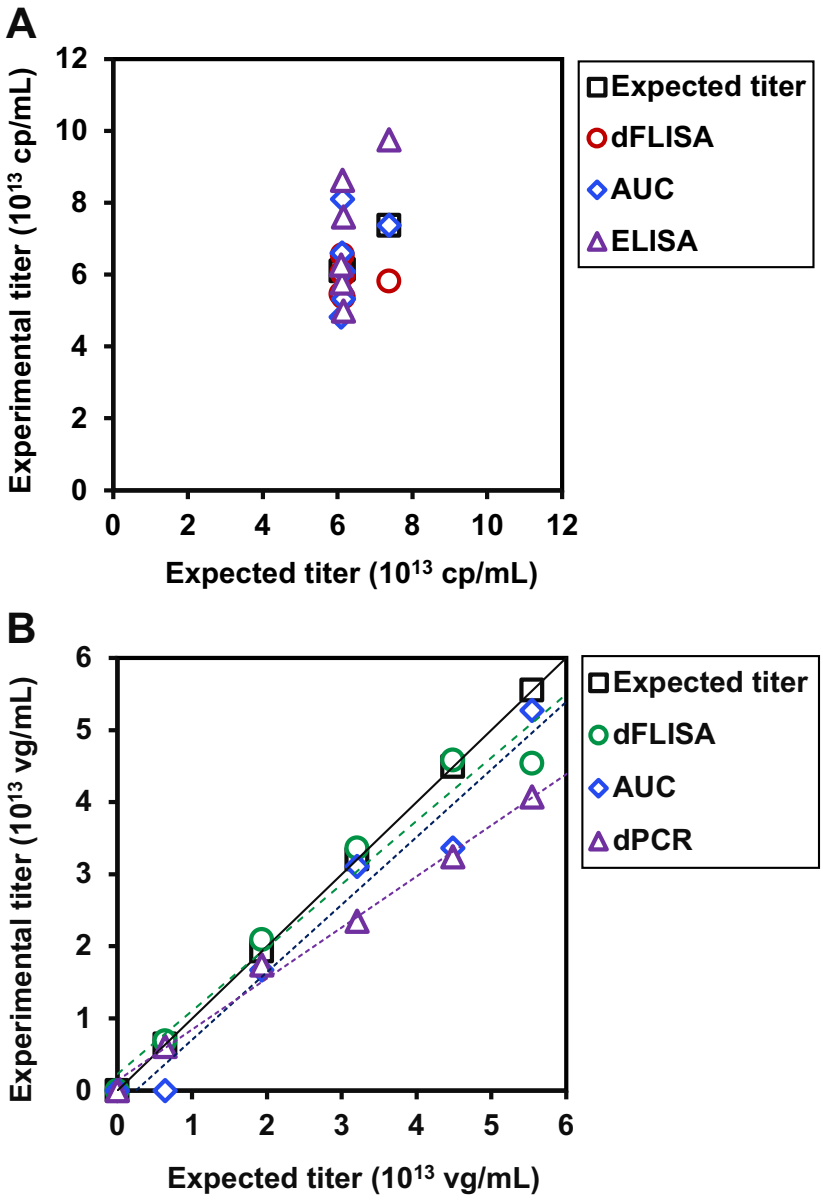

Figure 17. Linear correlation of total capsid titers (cp/mL) and genomic titer (vg/mL) of six mixed spike samples by orthogonal method.

(A) Comparison of capsid titers (cp/mL) of six mixed spike samples analyzed by three techniques: dFLISA, AUC, and ELISA. The capsid titer was adjusted to 6.16×10^{13} cp/mL for the mixed samples and to 6.09×10^{13} cp/mL for 0% FPs sample. The expected capsid titers (black square) were plotted on the horizontal axis, and the corresponding experimental capsid titer obtained by dFLISA (green circle), AUC (light blue rhombus) and ELISA (purple triangle) were plotted on the vertical axis.
(B) Comparison of genomic titers (vg/mL) of six mixed spike samples analyzed by three techniques: dFLISA, AUC, and dPCR. The linear correlation of the expected genomic titers was plotted on the horizontal axis and the corresponding experimental genomic titer obtained by dFLISA (green circle), AUC (light blue rhombus) and dPCR (purple triangle) were plotted on the vertical axis.

Table 16. Comparison of capsid titers (cp/mL) of six mixed spike samples using orthogonal techniques: dFLISA, BS-AUC, and ELISA

Sample	Expected value	Experimental value		
	AUC (10^{13} cp/mL)	dFLISA (10^{13} cp/mL)	AUC (10^{13} cp/mL)	ELISA (10^{13} cp/mL)
90.1% full	6.16	6.36	6.09	7.60
73.1% full	6.15	7.10	5.32	4.99
52.3% full	6.13	7.77	8.11	8.63
31.5% full	6.12	7.17	6.60	5.77
10.5% full	6.10	6.46	4.82	6.26
0% full	7.37	5.71	7.37	9.75

AUC, analytical ultracentrifugation; dFLISA, dual fluorescence-linked immunosorbent assay; ELISA, enzyme-linked immunosorbent assay; cp, capsid particle

Table 17. Comparison of genomic titers (vg/mL) of six mixed spike samples using orthogonal techniques: dFLISA, BS-AUC, and dPCR

Sample	Expected value	Experimental value		
	AUC (10^{13} vg/mL)	dFLISA (10^{13} vg/mL)	AUC (10^{13} vg/mL)	dPCR (10^{13} vg/mL)
90.1% full	5.55	5.46	5.27	4.07
73.1% full	4.49	5.51	3.36	3.24
52.3% full	3.21	4.04	3.11	2.35
31.5% full	1.93	2.51	1.67	1.74
10.5% full	0.64	8.39	nd[a]	0.61
0% full	0	0	0	0

AUC, analytical ultracentrifugation; dFLISA, dual fluorescence-linked immunosorbent assay; dPCR, digital chain polymerase reaction

[a]nd, not detected; vg, viral genome

3-3-5. Comparison of genomic titer by orthogonal methods using mixed samples

I evaluated the suitability of dFLISA for vector analysis by comparing it to various particle-measuring techniques, including BS-AUC, MP, and the combined digital (d)PCR/ELISA method.[69,89] As shown in **Figure 18**, dFLISA showed good correlation with the orthogonal determination of the FP ratio. The results of the MP were in good agreement with that of dFLISA, except for a 10% FP sample. BS-AUC showed lower FP values than expected, and the digital PCR (dPCR)/ELISA results were in close agreement with the expected values of 73.1%, 31.5%, and 10.5% FP. However, the dPCR/ELISA results for the 90.1% and 52.3% FP samples were very different because of variations in the PCR results.

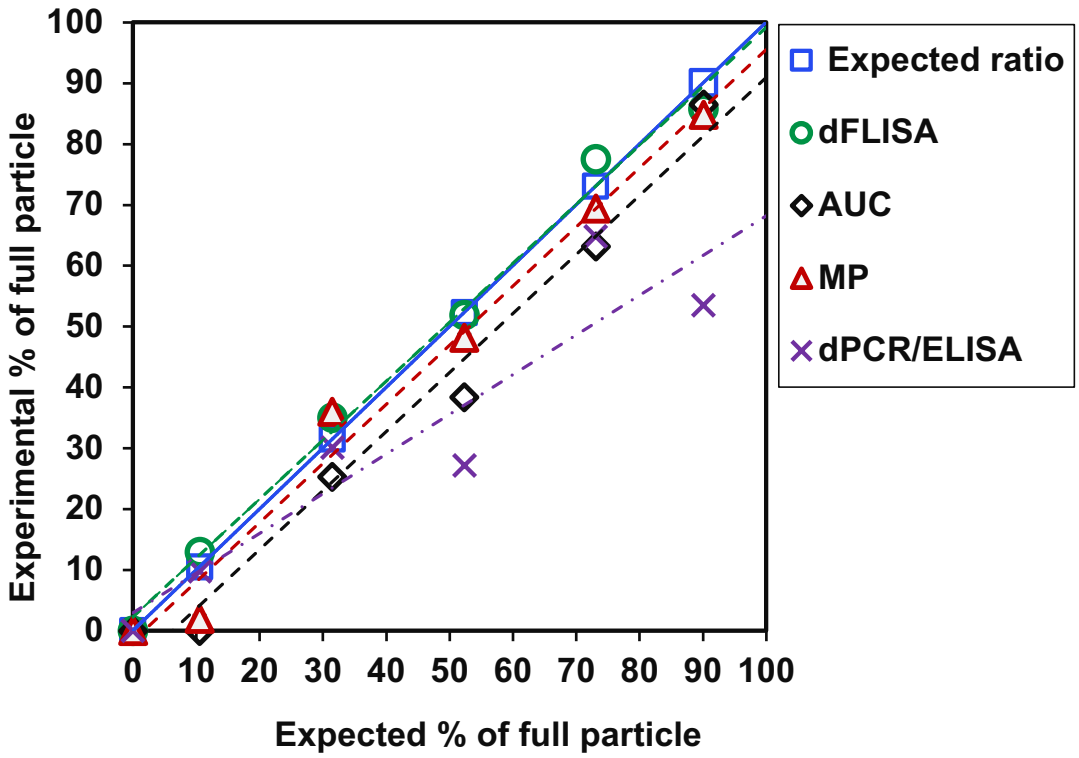

Figure 18. Determination of full-to-empty ratio by dFLISA and orthogonal method.

For the determination of the full to empty capsid ratio by dFLISA, capsid and genomic titer quantification was repeated on three consecutive days (Days 1–3) by mixing two AAV8 samples, full and empty titers, 6.16×10^{13} cp/mL and 7.37×10^{13} cp/mL, respectively, to obtain different FP ratios ranging from 0% to 90.1% FPs. A good linear correlation was obtained between the dFLISA data (experimental % full) shown on the vertical axis and the AUC data (expected % full) shown on the horizontal axis. Results are the means of 3-day experiments in which each sample was analyzed in

duplicate wells, with error bars corresponding to the SD of each population. As a comparison of genomic titer by orthogonal methods using mixed samples, the graph shows the relationship between the expected percentage of full capsids as determined by AUC (blue square) on the vertical axis and the corresponding experimental percentage of full capsids on the horizontal axis. The graph includes data points representing experimental results obtained by dFLISA (green circle) and different orthogonal methods, specifically AUC (black rhombus), MP (red triangle), and dPCR/ELISA (purple multiplication sign). All data are conducted in duplicate.

4. Discussion

4-1. Development of dFLISA

4-1-1. Screening the initial condition for assay development

The dFLISA method demonstrated successful binding efficiency, and genome release conditions were found to be appropriate for the development of this assay. For BLI was performed for efficiency of binding affinity between AAVs vector with anti-AAV VHH antibody (**Figure 7**). The result of BLI showed that the binding efficiency of VHH antibody and AAV2 was >99% over the entire range of the standard curve (**Figure 7**). It is suggested that the binding efficiency of AAV8 would be >98% even if K_D value of VHH antibody for AAV8 is 100 times larger than that for AAV2. Even though the specific affinity of VHH antibody with AAV8 vector was not available, the results indicate that the VHH coating antibody is a suitable ligand for coating microtiter plates with various AAV vectors except AAV9. In previous reports, the appropriate temperature range for AAV capsid particle disruption was found to be between 66.5°C and 89.5°C ± 0.5°C for AAV1 to AAV8 vector, excluding AAV5 vector. Therefore, in dFLISA, I used 85°C as the optimal temperature to disrupt the AAV capsid, which is the appropriate temperature range for the disruption of AAV capsid particles (as shown in **Figure 8**).

4-1-2. Development of dFLISA

This study aimed to establish a simple and reliable method of measuring AAV vector titers

and the ratio of FP. I developed dFLISA, which uses two fluorescent dyes to quantify capsid and genome titers.[64–66] The precision, accuracy, and quantification limits of dFLISA were assessed.

Importantly, in dFLSIA, appropriate wavelength detection for genome and capsid quantifications was evaluated. Additionally, both clear and black poly (styrence) microwell plates can be employed the immunosorbent assay.[90] My analysis revealed that the black well plate exhibited higher fluorescence intensity, including the S/N ratio, compared to the clear plate. This finding aligns with previous studies that suggest black polystyrene flat-bottom microplates are well-suited for fluorescence-based assays due to their ability to minimize well-to-well crosstalk and produce higher signal intensities.[90–92]

4-2. Validation of dFLISA

4-2-1. Precision, accuracy and LOQ of dFLISA analysis

The dFLISA method consistently yielded precision values below 15% across all tested samples while maintaining an accuracy of 80–100% of the expected values for both capsid and genomic titers in Samples 1–4, except in cases where the values approached or fell below the LOQ, as with Samples 5–7 **(Figure 15, Table 12** and **Table 13)**. This indicated the good precision and accuracy of my approach for obtaining capsid and genome titers, not only outperforming the combined dPCR and ELISA but also showing a significant improvement in error minimization. The relative concentrations of ExPs were relatively similar between the standard (AAV8-Lot1, 15.67%) and the sample (AAV8-Lot2, 12.95%) (**Table 10**). Because the genomic titer determined by dFLISA was the sum of FPs and ExPs, a difference in the relative concentrations of FPs and ExPs between standards and samples could result in inaccuracy and imprecision. Although the PP concentrations of samples used

were lower than the LOQ of BS-AUC^{80} and were ignored in this study, influence of PPs on the capsid and genomic titers should be considered carefully. dFLISA can simply quantify capsid and genomic titers; however, the inability to distinguish FPs from ExPs is the limitation of dFLISA. For detailed characterization, analyses using orthogonal methods that can distinguish between EPs, PPs, FPs, and ExPs are desired. I then calculated the LOQ, whose values for dFLISA were determined based on assay precision, accuracy, and background noise. It is remarkable that the LOQ values were close to those expected from the precision, accuracy, and the standard curve. Even the LOQ of dFLISA was only slightly higher than the LOQ of the ELISA. Nonetheless, it is sufficient to identify the capsid titers. Intermediate species cannot be quantified. It also indicates that further studies are needed to improve the sensitivity of the method for more accurate and precise detection and quantification of the analyte.

4-2-2. Linearity of AAV full to empty ratio in dFLISA analysis

dFLISA showed robust correlation and linearity in the FP ratio. The experimental ratio of full AAV particles was 0–85.8%, with a precision of %CV 3.26% ± 25% (**Figure 18**), demonstrating good agreement with the expected FP ratio of 0–90.1%. In addition, linearity experiments were performed using dFLISA over a range of ratios. Therefore, the reliable performance of this technique highlights its ability to discriminate between the different ratios of FPs. Furthermore, during the dFLISA demonstration, I improved the reliability and robustness of the method over multiple runs by introducing AAV vector samples at different concentrations and adjusting the FP ratio (**Figure 17A** and **Figure 17B**). This optimization not only minimized the duration of each assay, but also ensured a high level of consistency.

4-3. Comparison of the linearity of dFLISA and orthogonal methods using mixed samples

The main approach for determining both capsid and genomic titers is to choose the most

suitable analytical method for absolute quantification. BS-AUC is a standard technique used to analyze capsid content and distinguish between empty and full capsids as well as other AAV vector subspecies.[80,88,89,93] BS-AUC is based on the differential sedimentation velocities of AAV vector subpopulations under strong centrifugal force due to differences in size, density, weight, and shape. A combination of dPCR and ELISA is another standard method for the determination of the FP ratio. MP has recently gained popularity for AAV vector characterization because of its mass resolution, which allows operators to discriminate between empty and genome-filled capsids.[69,94,95]

In this study, I conducted a comparative analysis of the %FP in identical recombinant AAV samples via dFLISA, BS-AUC, MP, and dPCR/ELISA. The FP ratio determined by dFLISA was closer to the expected values than that determined by BS-AUC, MP, and dPCR/ELISA (**Figure 18**). The genomic titer determined by BS-AUC was lower than expected values (**Figure 17B**), and the FP ratio determined by BS-AUC was lower than that of dFLISA (**Figure 18**). It should be noted that FP ratio was calculated by dividing the sum of FPs and ExPs by the sum of EPs, FPs, and ExPs and different from a FP ratio calculated only from EPs and FPs.[69] According to Maruno *et al*. (2023), the relative standard deviation (%RSD) of AUC for quantification of particle concentration was less than 20%. Considering that %Full was calculated from full and empty particles and variability comes from each concentration, the results obtained in this study could be in the variability of AUC **(Figure 18)**.

Two peaks with mass corresponding to empty and full particles were observed in MP analysis, and ExP related peak was not observed **(Figure 16).** A Gaussian distribution fit was applied to the two histogram peaks and full particle ratio was calculated based on the peak area. The results of MP were consistent with that of dFLISA and both were as expected, with the exception of one sample containing 10% FPs. MP did not detect any empty particles in the

sample with 10% FPs, suggesting dFLISA has a higher sensitivity than MP. The advantages and limitations of analytical methods used in this study were summarized in **Table 19**.

Previous studies have reported evidence showing that high-performance liquid chromatography (HPLC) is a rapid and convenient method for analyzing the empty and full capsid content of purified AAV samples.[96,97] The sensitivity of HPLC was sufficient to quantify the empty and full AAV vectors in samples with capsid concentrations as low as $\sim 5 \times 10^{10}$ cp/mL,[97] whereas dFLISA was able to quantify empty and full AAV vectors at concentrations as low as 0.60×10^{10} cp/mL (**Table 14**). Notably, the sensitivity of dFLISA was higher than that of HPLC although HPLC is a promising method to determine FP ratio.

For capsid titer quantification, dFLISA demonstrated consistency with the ELISA (**Table 16**), but the LOQ of dFLISA (**Figure 17A**) was higher than that of traditional ELISA. This was probably due to differences in the detection method—the ELISA uses a horseradish-peroxidase (HRP)-conjugated streptavidin enzyme[57,98] while dFLISA uses a second antibody conjugated to red fluorescence for capsid titer quantification. For genomic titer measurement, dFLISA showed higher titers than dPCR for samples with 10.5% to 90.1% FPs. This might be due to the variability of dPCR,[99,100] and considering that the FP ratio determined by dFLISA was close to the expected values, genomic titer quantification by dFLISA should be more precise and accurate than dPCR. Another possible reason why dPCR result was lower than dFLISA result is that ExPs could contain genome without ITR, and thus dPCR could not quantify ExPs because dPCR specifically quantifies genome with ITR. The specificity of dFLISA was only for genome, not genome with ITR. The non-specificity is considered to be another limitation of dFLISA.

The dFLISA results were comparable to those of ELISA and dPCR. Thus, I believe that the

dFLISA is applicable for crude samples. Taking previous research and my routine production of AAV into account, the titer at harvest step can be higher than LOQ of dFLISA (1.61×10^{10} cp/mL, 1.70×10^{10} vg/mL), and therefore sensitivity of dFLISA is high enough to analyze crude samples whereas it would be difficult to use dFLISA for samples at the beginning of upstream process such as just after the triple transfection treatment.

Comparing the methods from the perspective of the operator, it is important to note that BS-AUC and MP require specialized equipment and high capsid titers.[89] Conversely, the reliability of dFLISA as an alternative analytical method for the precise assessment of the FP ratio that uses the same standard has been demonstrated. Thus, it is a crucial test for quantifying FP, EP, and FP ratios. In FP ratio analysis by dPCR/ELISA, data from two independent analyses are required. Therefore, the combination method generally has inherently higher variability. Moreover, dPCR-based methods show higher variability than ELISA.[101]

5. Conclusion

In this study, several investigations were conducted, including the development of antibodies to AAV capsids and the assessment of their binding efficiency. Optimal conditions for genome release were established to ensure complete and effective release of AAV genomes without degradation or loss. Wavelength detection was employed to maximize sensitivity and specificity for both capsid and genomic titers. Additionally, the type of microwell plates used for the assay was optimized.

One limitation of dFLISA is its inability to discriminate between full particle (FP), extrafilled particles (ExPs), and partial particles (PPs). However, though the inability to distinguish them is a limitation, the dFLISA results were shown as a ratio of full particle (FP) and empty particle (EP) because they are usually used as quality attributes in quality control of

gene therapy products. Furthermore, these limitations of dFLISA have been strictly demonstrated and discussed in standards and sampled quantification by BS-AUC (**Figure 9** to **Figure 11** and **Table 10** to **Table 11**). I already discussed how PP and ExP affected on the results of dFLISA based on the AUC results because AUC can quantify PP and ExP separately from EP and FP.

Ultimately, dFLISA was successfully developed. I demonstrated that it provides the determination of capsid and genome titers as well as the FP ratio in a simple way with high precision, high accuracy, and high sensitivity by using the same 96-well plate. Furthermore, the critical validation of dFLISA were evaluated such as precision, accuracy, LOQ and linearity. The capsid and genomic titers, and full capsid ratios were comparable to the expected values. For comparison with orthogonal method, the correlation between dFLISA and BS-AUC proved not only robust, but also indicating the reliability of the dFLISA results for both full and empty capsids as well. In addition, the dFLISA results also corresponded with those of other orthogonal techniques, including MP and a combination of dPCR and ELISA.

Chapter 3. Application of dFLISA

1. Introduction

In **Chapter 2**, dFLISA was successfully developed, allowing the determination of capsid and genome titers as well as the FP ratio in a simple way with high precision, high accuracy, high sensitivity and good linearity. Since the production of AAV vectors is a complex process influenced by multiple factors such as cell line or plasmid ratios. It is not only FPs that are generated, but also EPs, ExPs, and PPs. Considering this complexity, it is essential to apply the dFLISA method for the quantification of diverse AAV vectors in both purified and crude lysate samples.

In **Chapter 3**, I aim to broaden the application of dFLISA by exploring its utility in the evaluation of AAV vector development. My study focuses on two essential applications of dFLISA: the analysis of purified AAV vectors with high FP ratios and the evaluation of crude lysate samples.

For the purified AAV vectors, I demonstrated the ability of this dFLISA for quantifying the capsid and genomic titers for other AAV vector serotypes as each serotype exhibits unique characteristics affecting tissue targeting, immune response, and transduction efficiency.

Additionally, the fluorescence intensity of the AAV vector varies with different genome lengths, and this factor is also relevant to dFLISA. All AAV vectors used in other experiments had genome lengths almost identical to that of the standard AAV vector. I then conducted the dFLISA analysis to compare fluorescence intensity between AAV vectors with different genome lengths validated the value and reliability of dFLISA as a method for

evaluating AAV vector genomes.

For crude lysate analysis, firstly, the recovery efficiency of spiking levels was also assessed to see whether dFLISA can be used to analyze crude samples without purification, despite the presence of host cell DNA and proteins that could potentially interfere with measurements. Subsequently, I evaluated the ability of dFLISA for capsid/genome quantification in the presence of impurities from crude lysate and compared the results with other methods such as ELISA and dPCR.

2. Experimental materials and methods

2-1. AAV samples

Two rAAV8 vectors, including AAV8-Lot1 and AAV8-Lot2 (**Table 10)** were generated using triple-plasmid co-transfection. Briefly, pAAV-Rep&Cap (Serotype 8), pAd helper, and transgene plasmids (CMV-EGFP or AAT-FIX) were co-transfected into suspended HEK293T or VPC 2.0 (Thermo Fisher Scientific, Waltham, MA, USA) cells. The transfected cells were cultured, and the medium and cell lysate were harvested (it was collected as a crude sample). Thereafter, the samples were purified via affinity chromatography using AAVX columns (Thermo Fisher Scientific). Bulk AAV samples were purified using affinity chromatographic purification followed by a CsCl ultracentrifugation (UC) or an anion exchange column to separate full and empty particles. Purified samples (AAV8-Lot1 and AAV8-Lot2) were centrifuged at 25,000 rpm in an Optima XE-90 (Beckman Coulter, Inc., Brea, CA, USA) using a Beckman SW41Ti rotor at 20°C for 42 h. The virus bands generated by UC were collected by using a piston fractionator (BioComp Instruments Ltd., Fredericton, Canada) equipped with a UV monitoring apparatus (Triax flow cell, BioComp Instruments Ltd.). For the anion exchange chromatography, the samples were applied to a CIMmultus QA column (Sartorius,

Göttingen, Germany) and eluted with a linear gradient of 0–250 mM NaCl in bis-tris-propane buffer (pH 9.0). Then the virus fractions were dialyzed in Slide-A-Lyzer 10K (Thermo Fisher Scientific). AAV vector samples were analyzed using BS-AUC to differentiate between therapeutic products, including full particles (FPs), and product-related impurities such as empty particles (EPs), partial particles (PPs), and extrafilled particles (ExPs) (see **Figure 6**). The representative sedimentation coefficient distributions for AAV2 vector and AAV8 vector in PBS/D2O + 0.001% poloxamer-188 determined by BS-AUC, are also described in **Figure 9A** to **Figure 9B**. **Table 10** summarizes the information on the in-house AAV8 vectors used in this study.

I also used other laboratory-grade AAV vectors, including AAV2-Lot1 to AAV2-Lot4 and AAV8-Lot5 to AAV8-Lot6 manufactured in HEK293T cells, which were procured from VectorBuilder (Chicago, IL, USA). **Table11** summarizes the information on the commercial AAV2 vector and AAV8 vector used in the dFLISA experiments.

2-2. Application of dFLISA

2-2-1. Application of dFLISA for purified AAV vector samples

2-2-1.1. Application of dFLISA for quantifying different AAV serotypes

The representative dFLISA method described above was used for this experiment. AAV2-Lot3, which contained linear ssDNA, was diluted 100-fold to reach concentrations of 1.77×10^{11} cp/mL and 1.65×10^{11} vg/mL with 0.05% Tween 20 in 1 × PBS, then serially diluted 1:2 to generate a calibration curve. AAV2-Lot4 was also diluted 100-fold, resulting in final concentrations of 9.63×10^{10} cp/mL and 8.88×10^{10} vg/mL, with 0.05% Tween 20 in 1 × PBS. The AAV8-Lot5 sample containing linear ssDNA was diluted 50-fold to reach concentrations of 2.06×10^{11} cp/mL and 1.59×10^{11} vg/mL with 0.05% Tween 20 in 1 × PBS, and then serially diluted 1:2 to generate a calibration curve. AAV8-Lot6 was diluted 50-fold to achieve final

concentrations of 2.92×10^{11} cp/mL and 1.60×10^{11} vg/mL with 0.05% Tween 20 in 1 × PBS. Test samples prepared without any freeze–thaw cycles.

2-2-1.2. Fluorescence intensity of SYBR gold with different genome lengths

A ssDNA 7K ladder (PerkinElmer, Waltham, MA, USA) containing ssDNA fragments ranging from 1100 bases to 5100 bases was used. First, 2 μL of EzApplyDNA (6× loading buffer) was applied to Parafilm for each sample. Next, 10 μL of sample was added and thoroughly mixed by pipetting, and 10 μL of the mixture was loaded onto a 1% agarose gel (Funakoshi Co., Ltd, Japan). Agarose gel electrophoresis (AGE) at 70 V for 45 min, after which, the gel was stained according to the manufacturer's instructions. SYBR Gold Nucleic Acid Gel staining solution (Invitrogen, Thermo Fisher Scientific, Eugene, OR, USA) was used for gel staining. Quantitative analysis of brightness density within the stained gel was performed using an iBright 1500 instrument (Thermo Fisher Scientific) in conjunction with iBright Analysis version 4.0 software (Thermo Fisher Scientific). Image brightness adjustments were made prior to analysis.

Subsequently, the ssDNA ladder was analyzed by MP to determine the relative concentration of each ssDNA in the ladder. Before conducting MP measurements, ssDNA ladder solutions were diluted in buffer consisting of 5 mM Tris and 10 mM $MgCl_2$ (pH 8). Each measurement was recorded for 60 s, and every sample was examined a minimum of three times ($n \geq 3$). Data analysis was conducted using DiscoverMP and an in-house Python program. Histogram peaks were fitted with Gaussian distributions to extract the percentage of ssDNA ratio.

I used a DNA ladder sample consisting of a mixture of different DNA length in this experiment. To separate and obtain fluorescence intensity of each DNA, AGE was performed, and each band was dyed with SYBR gold and band intensities were measured. Because the

concentration of each DNA was different between each other and was not provided by the manufacturer, I used MP to determine relative number concertation of each DNA in the DNA ladder.

Furthermore, the fluorescence intensities obtained by agarose gel electrophoresis (AGE) with five different ssDNA ladder strands were divided by MP area (%) to obtain relative fluorescence intensity per molecule. The relative fluorescence intensity was plotted against the ssDNA ladder standard length. The expected fluorescence intensity ratio of the AAV vectors with both self-complementary DNA (scDNA) (3681 bases) and single-stranded DNA (ssDNA) (2521 bases) was also estimated from the curve.

The fluorescence intensity of AAV vector containing scDNA were examined using dFLISA and compared that of AAV vector containing ssDNA. AAV2-Lot1 containing ssDNA was diluted 100-fold to concentrations of 3.09×10^{10} cp/mL and 2.82×10^{10} vg/mL in 0.05% Tween 20 in 1 × PBS, and then serially diluted at a 1:2 ratio to generate a calibration curve. Similarly, AAV2-Lot2 containing scDNA was diluted 50-fold to concentrations of 7.47×10^{10} cp/mL and 6.66×10^{10} vg/mL in 0.05% Tween 20 in 1 × PBS and then serially diluted at a 1:2 ratio to generate a calibration curve. The dFLISA analysis method as described earlier in the Methods was used. The ratio of fluorescence intensities of ssDNA AAV8 vector and scDNA AAV2 vector were calculated.

2-2-2. Application of dFLISA for crude sample and other methods

2-2-2.1. Spike recovery test of dFLISA

A representative method for dFLISA is described above. In these experiments, AAV8-Lot1 was used as standard as described above. For the spike sample, AAV8-Lot2 was

concentrated by ultrafiltration to reach a final concentration of 6.16×10^{13} cp/mL and 5.55×10^{13} vg/mL. It was then diluted to three different spiking levels: high (Spike H) at 1.23×10^{11} cp/mL and 1.11×10^{11} vg/mL, medium (Spike M) at 0.82×10^{11} cp/mL and 0.74×10^{10} vg/mL, and low (Spike L) at 0.61×10^{11} cp/mL and 0.55×10^{11}vg/mL, all in 0.05% Tween 20 in 1 × PBS. A crude lysate sample of unknown concentration was mixed with each spike sample solution at a 1:1 volume ratio and analyzed in duplicate. The following equations were used to calculate the expected values for mixed spike samples:

Mixed spike (H – M) = $\frac{1}{2}$ (crude + Spike H) – $\frac{1}{2}$ (crude + Spike M) **(Equation 6)**

Mixed spike (H – L) = $\frac{1}{2}$ (crude + Spike H) – $\frac{1}{2}$ (crude + Spike L) **(Equation 7)**

The prepared spike sample solutions were then added to each well of the plate. The target recovery percentage (%) was within ± 25%.

2-2-2.2. Spike-recovery test of dPCR

A representative method for dPCR is described in **2-5-4** of **Chapter 2**. These experiments, the spike-recovery test by dPCR was performed using AAV8-Lot2 as the spike samples, which was concentrated by ultrafiltration to reach a final concentration of 6.16×10^{13} cp/mL and 5.55×10^{13} vg/mL. Subsequently, that was sample was spiked at three different spiking levels: high (Spike H) at 1.23×10^{11} cp/mL and 1.11×10^{11} vg/mL, medium (Spike M) at 0.82×10^{11} cp/mL and 0.74×10^{10} vg/mL, and low (Spike L) at 0.61×10^{11} cp/mL and 0.55×10^{11}vg/mL, all in 0.05% Tween 20 in 1 × PBS. A crude lysate sample of unknown concentration was mixed with each spike sample solution at a 1:1 volume ratio and analyzed in duplicate. The equations were used to calculate the expected values for mixed spike samples were the same as equations above (**Equation 6** and **Equation 7)**. The prepared spike sample solutions were then added to each well of the dPCR.

2-2-2.3. Quantification of capsid and genomic titers of crude samples by dFLISA

For this experiment, the representative dFLISA method described above was used. An AAV8 crude lysate sample of an unknown concentration was analyzed by dFLISA. The experiment, as detailed in the preceding section. The analysis was performed in triplicate. The capsid and genomic titers obtained by dFLISA were compared with ELISA and dPCR results by independent samples t-test. For capsid quantification, the dFLISA results were consistent with those of ELISA (p = 0.303), while the genomic titer measurements, dFLISA showed higher titers than dPCR (p = 0.029).

3. Results

3-1. Application of dFLISA

3-1-1. Application of dFLISA for purified AAV vector sample

3-1-1.1. Application of dFLISA analysis for divers AAVs

In this study, my next objective was to expand the applicability of the dFLISA. Specifically, I aimed to demonstrate its effectiveness in quantifying capsid and genomic titers across different AAV vector serotypes. My results clearly showed that dFLISA is not only suitable, but also highly effective in quantifying these parameters across different serotypes of AAV vectors.

Since VHH has been shown to bind to a broader range of serotypes (specifically, AAV1 to AAV8 and AAVrh10),[102–105] which is sufficient for the needs of current clinical research,[106] I further extended the applicability of the dFLISA method to facilitate the quantification of AAV vector of different serotypes. In this approach, the primary antibody was replaced by an antibody that specifically targets the serotype of interest. The capsid and genomic titers of AAV2-Lot4 were quantified by dFLISA using AAV2-Lot3 as a reference standard of AAV2 vector containing ssDNA. **Figure 19** shows that the experimental values were consistent and comparable to the expected values (± 25% of expected value). This suggests that the modified dFLISA method is effective in quantifying AAV vector of different serotypes.

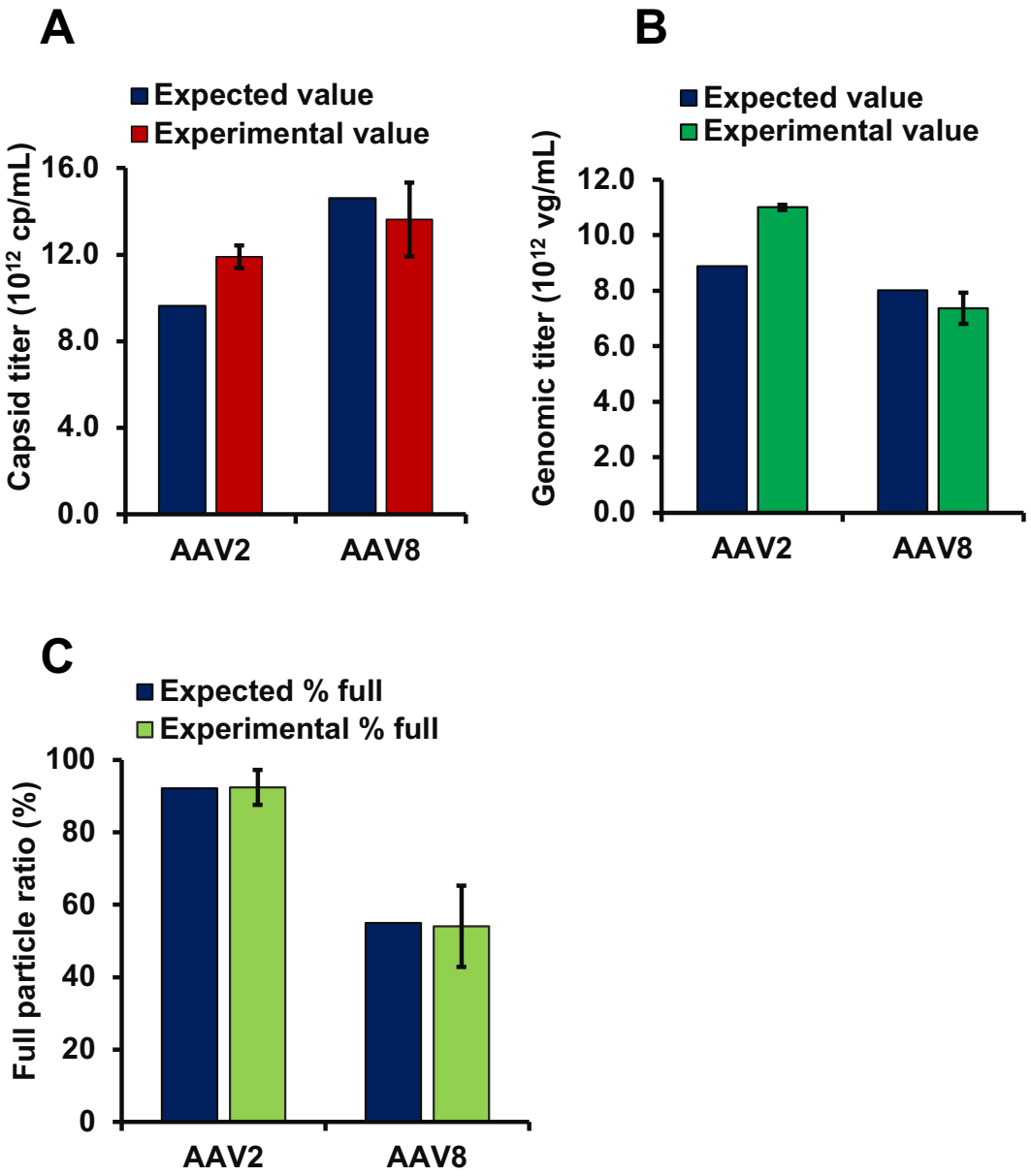

Figure 19. Application of dFLISA for quantification of different AAV serotypes

(A) Capsid titer quantification.

(B) Quantification of genome titer.

(C) Detection of FP ratio.

dFLISA experiments were performed in duplicate for AAV2 and AAV8 vector. Expected values derived from BS-AUC (dark navy blue) were compared with actual values for three parameters, specifically capsid titer (red), genomic titer (green), and FP ratio (light green). Results are the average of duplicated wells.

3-1-1.2. Fluorescence intensity with different genome lengths

Mass Photometry (MP) is a single particle analysis method and can measure the mass of individual particles (technically, ratio metric contrast, which correlates with mass, is obtained and converted to mass). Therefore, differentiate each component by the mass and provides relative number concentration of each component (% counts) was successfully measured by MP (**Figure 20A**). The result of 7200 base DNA was not used for **Figure 20** because AAV vector cannot package such a long DNA length.

I investigated the correlation between different AAV vector genome lengths and SYBR gold fluorescence intensity. First, a DNA mixture was analyzed by agarose gel electrophoresis (AGE) and dyed with SYBR gold. The intensity of each band was normalized to a relative concentration determined by MP (**Figure 20A**) and plotted against DNA length. As shown in **Figure 20B**, the fluorescence intensity correlated well with genome length. AAV2 capsids containing different genome types, specifically self-complementary DNA (scDNA) (3681 bases) and single-stranded DNA (ssDNA) (2521 bases), were analyzed by dFLISA, and their fluorescence intensities were compared (**Table 18**). The fluorescence intensity of the ssDNA AAV2 vector was approximately 1.86 times lower than that of the scDNA AAV2 vector (**Table 18**), while the fluorescence intensity of ssDNA estimated from the curve (**Figure 20B**) was approximately 1.4 times lower than that of scDNA.

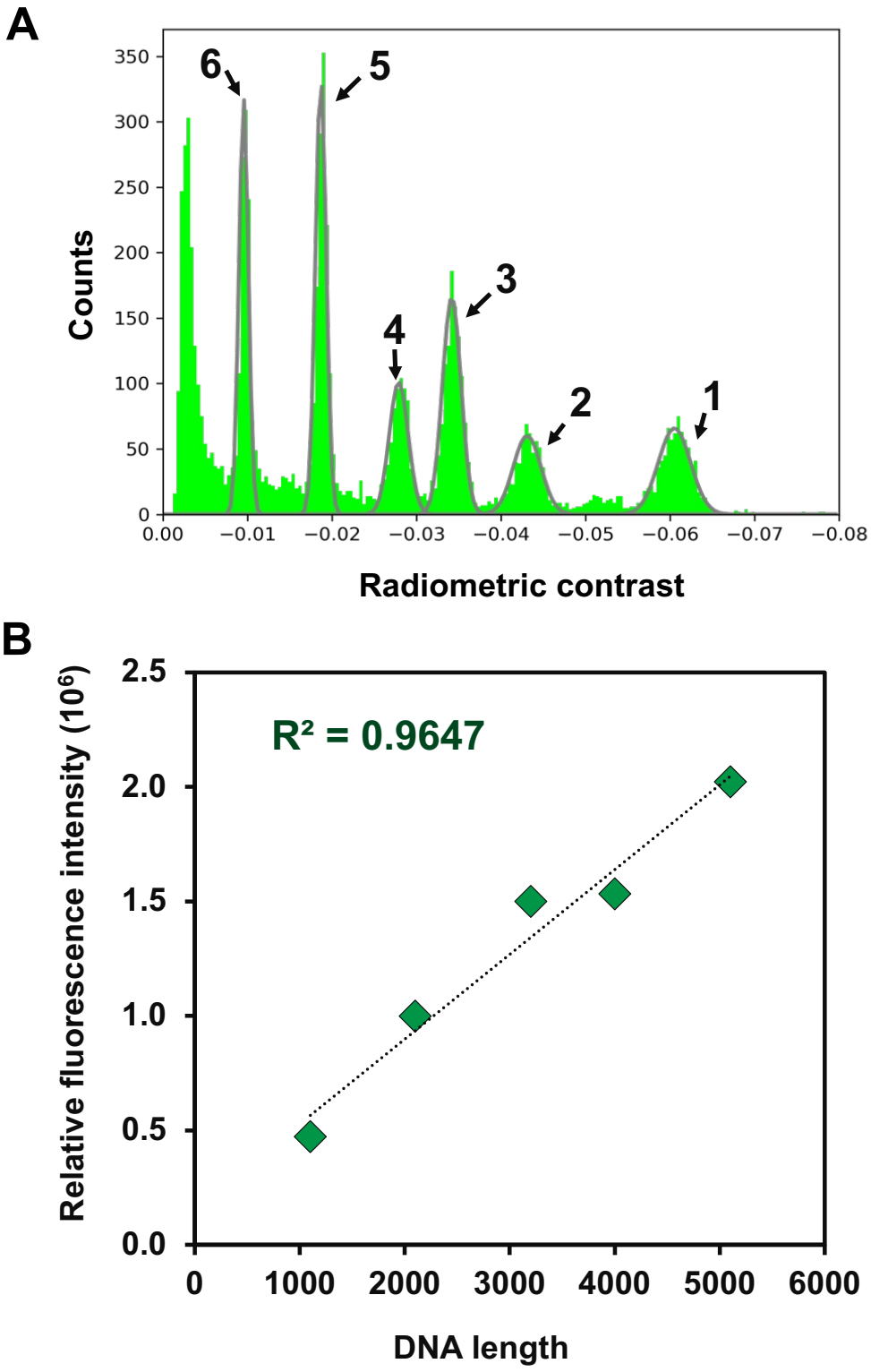

Figure 20. Fluorescence intensity of SYBR gold with different genome lengths

(A). Histogram from MP analysis of the ssDNA ladder containing 1100, 2100, 3200, 4000, 5100 and 7200 base DNA.

MP can differentiate each component by the mass and provides relative number concentration of each

component (% counts). This curve shows the relative fluorescence intensities were proportional to the genome lengths. Gray lines show results of Gaussian distribution fitting.

(B) Comparison of fluorescence intensity of AAVs with different genome lengths.

During experiment shown in this figure, relative number concentration of DNAs in the DNA ladder was obtained, and the y-axis of this figure is fluorescence intensity of ss DNAs of the DNA ladder (the result of agarose gel electrophoresis (AGE) divided by relative number concentration obtained by MP, which means relative fluorescence intensity per one molecule.

AGE, agarose gel electrophoresis; MP, mass photometry; scDNA, self-complementary DNA; ssDNA, single-stranded DNA

Table 18. Comparison of fluorescence intensity of AAV2 with different genome lengths by dFLISA

Genomic titer		Fluorescence intensity (AU)[c]			
(10^{10} vg/mL)	scDNA[a] (10^5)	ssDNA[b] (10^5)	Ratio (scDNA/ssDNA)	Average value	SD
1.41	11.11	5.93	1.87		
0.70	5.95	3.22	1.85	1.86	0.015
0.35	3.49	1.89	1.85		

[a]scDNA (3681 bases), self-complementary DNA

[b]ssDNA (2521 bases), single-stranded DNA

[c]Calculated from standard curve of AAV vectors with scDNA and ssDNA.

SD, standard deviation; AU, arbitrary unit

3-2-2. Applicability of dFLISA for crude sample

3-2-2.1. Spike recovery analysis by dFLISA

The purified sample, AAV8-Lot2, was first concentrated to final concentrations of 6.16×10^{13} cp/mL and 5.55×10^{13} vg/mL, and then diluted to three different concentrations: high (Spike H) at 1.23×10^{11} cp/mL and 1.11×10^{11} vg/mL, medium (Spike M) at 0.82×10^{11} cp/mL and 0.74×10^{11} vg/mL, and low (Spike L) at 0.61×10^{11}cp/mL and 0.55×10^{11} vg/mL. The purified samples and crude lysate were mixed at a 1:1 ratio. The recovery of the spiked purified sample was evaluated as the difference between the high minus the middle (Spike H − M) and the high minus the low (Spike H − L) concentrations because the crude lysate contained an unknown amount of AAV particles. Recovered capsid titers of the Spike H − M and Spike H − L were 1.25×10^{10} cp/mL and 2.06×10^{10} cp/mL, respectively (**Figure 21A**), and the recovered genomic titers were Spike H − M and Spike H − L of 0.91×10^{10} vg /mL and 1.61×10^{10} vg/mL, respectively (**Figure 21B**). The FP ratios of Spike H − M and Spike H − L were 73.0% and 77.9%, respectively (**Figure 21C**). Spike recovery was consistently achieved across all mixed samples. Specifically, the capsid titer recovery rate was 122.1% ± 133.8%, and the genome recovery rate was 98.8% ± 115.7%. The obtained results met the criteria written in the methods section. The results suggest the impurities in crude lysate do not interfere with capsid/genome quantification by dFLISA.

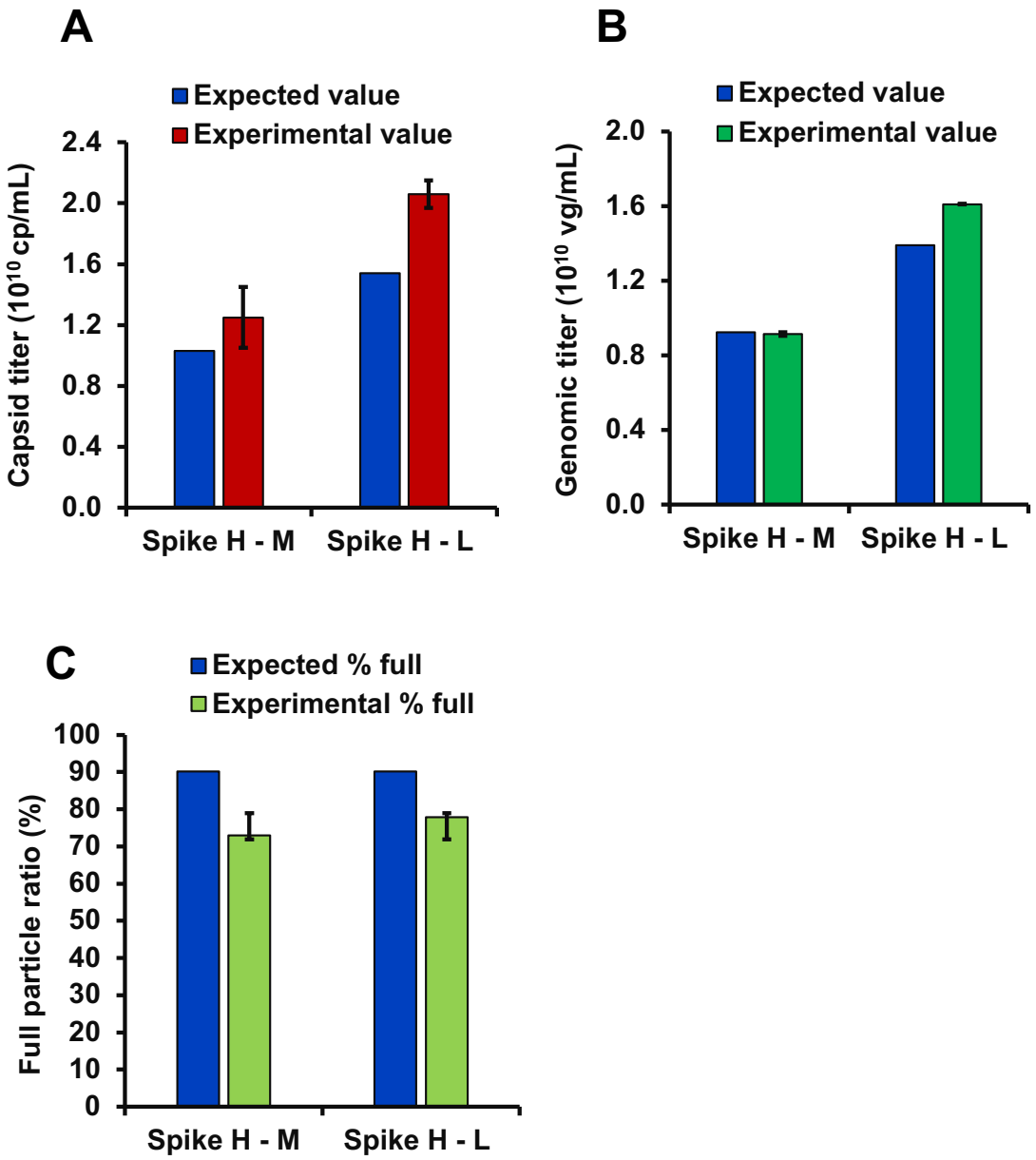

Figure 21. Applicability of dFLISA for analyzing crude samples.

(A) Capsid titer quantification.

(B) Genomic titer quantification. **(C)** Percentage of full capsids.

The various dilution factors for spike recovery were assessed by comparing the experimental values, as determined by the dFLISA method, with the expected values obtained by BS-AUC analysis. The expected values derived from BS-AUC (blue) were compared with actual values for three parameters: capsid titer (red), genomic titer (green), and FP ratio (light green). Reported results represent the average measurements from duplicate wells. All data are presented as the mean and standard deviation (n = 2).H, high concentration spike; M, middle concentration spike; L, low concentration spike

All data are presented as the mean and standard deviation (n = 2). cp, capsid; vg, viral genome

3-2-2.2. Spike-recovery test by dPCR

To determine whether the result of dFLISA was not affected by the interference of any impurities, the spike test to recovery the genomic titer, which was then analyzed by dPCR. The recovered genomic titers by dPCR were Spike H − M and Spike H − L of 0.63×10^{10} vg /mL and 0.57×10^{10} vg/mL, respectively (**Figure 22).** The result demonstrated that the spike-recovery result of dPCR was lower than expected values (1.17×10^{10} vg/mL). This is suggested the genomic titer results with dFLISA (**Figure 21**) were higher than those from dPCR. Although there is a possibility that partial genome which could not be detected by dPCR affected the dFLISA result, the high recovery rate in the spike-recovery experiment of dFLISA indicates that dFLISA results should be reliable. Another possibility is that dPCR was affected by the interference of impurities.[63,107]

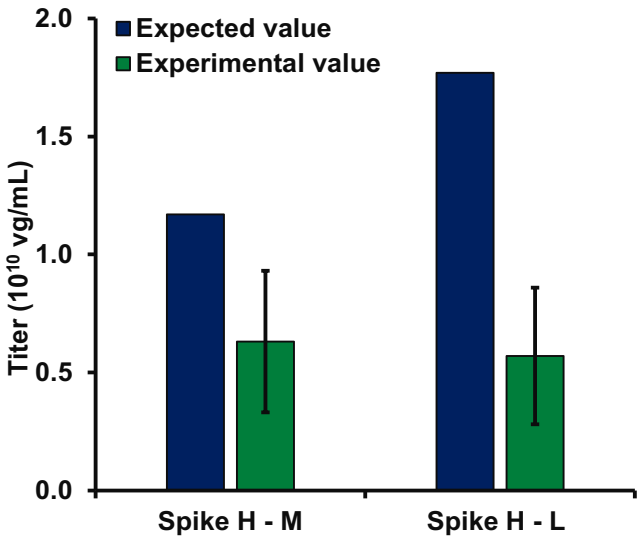

Figure 22. Spike-recovery test of dPCR

Genomic titer quantification of crude samples by dPCR were evaluated by spike-recovery test. The spike-recovery test was conducted as described in the method section 4-2-3: Quantification of crude sample by dFLISA and other methods. The various dilution factors for spike recovery were assessed by comparing the experimental values, as determined by the dPCR (dark green), with the expected values obtained by dFLISA (dark blue). The standard deviation (SD) of each parameter was obtained from the triplicated experiments. H, high concentration spike; M, middle concentration spike; L, low concentration spike; vg, viral genome

3-2-2.3. Quantification of capsid and genomic titers of crude samples by dFLISA

The results suggest the impurities in crude lysate do not interfere with capsid/genome quantification by dFLISA. Subsequently, dFLISA was applied to the quantification of capsid and genomic titers of a crude sample. A dFLISA analysis of crude AAV yielded capsid and genome titers of 3.28×10^{12} cp/mL and 7.77×10^{11} vg/mL, respectively (**Figure 23**). For capsid quantification, the dFLISA results were consistent with those of ELISA ($p = 0.303$), which is a well-established method.[36,70] In the genomic titer measurements, dFLISA showed higher titers than dPCR ($p = 0.029$) (**Figure 23**).

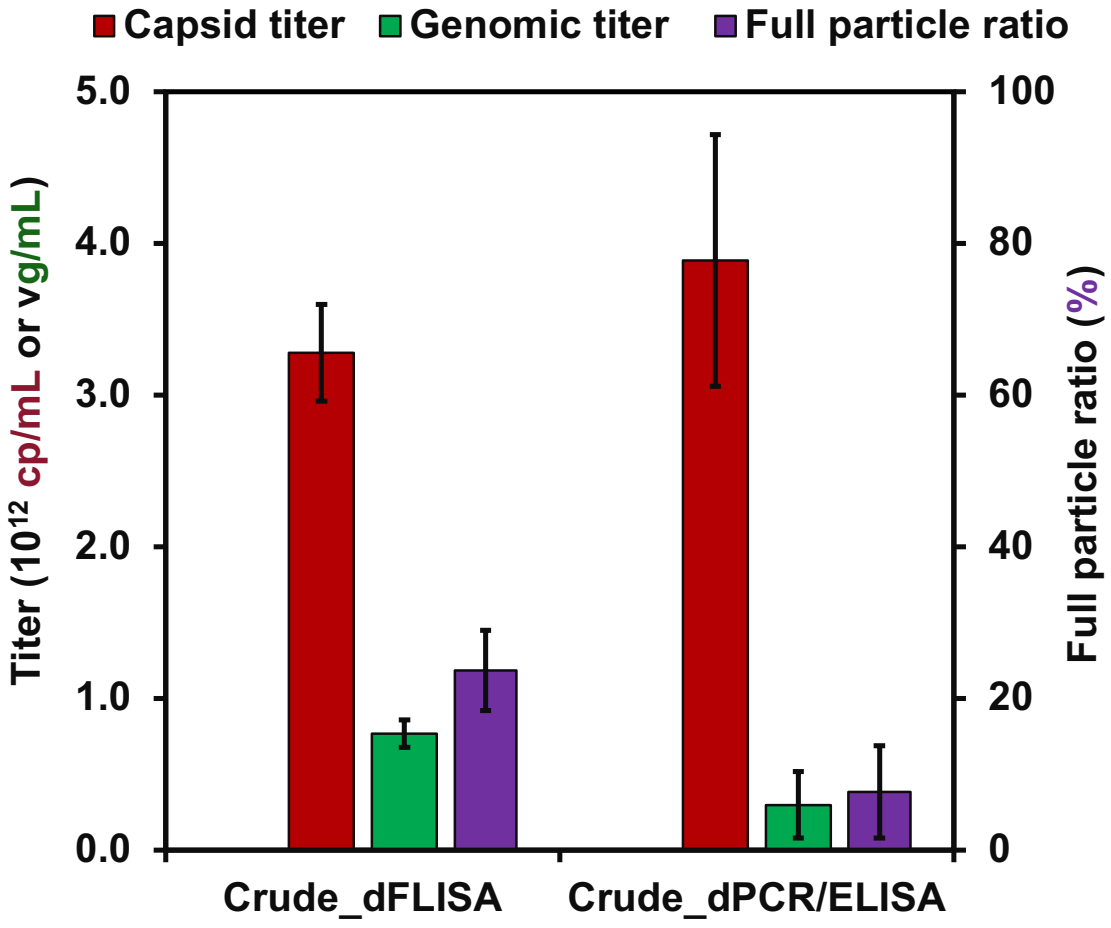

Figure 23. Determination of dFLISA's ability to quantify crude samples

AAV8 vector content in crude samples was analyzed by three methods: dFLISA (red, green and purple), ELISA (red) and dPCR (green). dFLISA was used to quantify both capsid and genomic titers and the FP ratio of AAV8 content in crude samples. ELISA was used to quantify capsid AAV8 vector

content and used the SD calculated from independent duplicate measurements (n = 2). The dPCR was used to determine the AAV8 vector content in crude samples and used the SD derived from independent triplicate measurements (n = 3). Therefore, dPCR/ELISA (purple) was used to compare FP ratios. All data presented in these experiments are the averages used to compare dFLISA and dPCR/ELISA methods' ability to quantify crude samples. The standard deviation (SD) of each parameter was obtained from the triplicated experiments.
cp, capsid particle, vg; viral genome

4. Discussion

4-1. Application of dFLISA for purified sample

4-1-1. Application of dFLISA for quantifying different AAV serotypes

dFLISA is the novel method can apply to quantifying the capsid and genomic titers for other AAV vector serotypes. In the dFLISA analysis, we used 85°C as the optimal temperature to disrupt the AAV capsid, and the appropriate temperature range for the disruption of AAV capsid particles AAV1 to AAV8 was between 66.5°C and 89.5°C ± 0.5°C, with the exception of AAV5.[87] As indicated in previous studies,[87] the specific temperature requirement for AAV5 disruption was 90°C ± 0.5°C. In addition, in our experiment, it was possible to use the AAV9 vector by simply modifying the ligand that coats the microtiter plate with the vector because the binding affinity of the VHH coating antibody is limited to the AAV9 vector.

4-1-2. Fluorescence intensity of SYBR gold with different genome lengths

The fluorescence intensity of the AAV vector varies with different genome lengths, and this factor is also relevant to dFLISA. All AAV vectors used in other experiments had genome lengths almost identical to that of the standard AAV vector. Additionally, a comparison of fluorescence intensity between AAV vectors with different genome lengths validated the value and reliability of dFLISA as a method for evaluating AAV vector genomes. To begin with I used a mixture of ssDNA to evaluate the correlation between fluorescence intensity and DNA

length. As shown in **Figure 20B**, the relative fluorescence intensities were proportional to the genome lengths. Furthermore, the differences in fluorescence intensities between two AAV vectors with different genome lengths (2521 and 3681 bases) were evaluated. According to the curve derived from the mixed DNA samples (**Figure 20B**), the ratio of fluorescence intensity of the AAV vector with scDNA to that of the AAV vector with ssDNA was expected to be 1.40; however, the experimental value was 1.86 (**Table 18**). Therefore, although the fluorescence intensity of the ssDNA mixture was proportional to genome length, an interaction of DNA released from an AAV vector with SYBR gold could be genome-dependent probably due to the high temperature for capsid disruption and/or tertiary structure of DNA. If the length of an AAV genome is different from that of the standard AAV vector, I need to evaluate the difference in SYBR gold intensity between the sample and the standard prior to dFLISA analysis.

4-2. Application of dFLSA for crude sample

4-2-1. Spike-recovery test by dFLISA

The recovery efficiency of spiking levels was also assessed to see whether dFLISA can be used to analyze crude samples without purification. The recovery percentage was within ± 25% of the expected values, which meets the criteria for acceptance (**Figure 21**). This suggests that the results of dFLISA are not affected by the matrix interferences contained in crude samples.[82,108] This highlights the suitability of the dFLISA method as a way to evaluate AAV samples that have not been purified, which offers a noteworthy advantage. Based on the results obtained, it is reasonable to conclude that the dFLISA method is well suited to the quantification of unpurified AAV vector samples. Therefore, dFLISA serves as a valuable method that can be used to accurately quantify the titers of crude samples, making it uniquely capable of directly quantifying the capsid and genomic titer and FP ratio of crude samples.

4-2-2. Spike-recovery test of dPCR

The spike-recovery result of dPCR was lower than expected values (**Figure 22**). This result also showed that the recovery percentage did not meet the acceptance criteria. Additionally, previous studies demonstrated that dPCR can be affected by the interference of impurities.[99,101,107,109,110] Therefore, dFLISA is a more accurate method for determining the concentration of AAV genomic material of crude samples compared with dPCR. This suggests that dFLISA is a reliable alternative for detecting AAV vector capsids. For genomic titer measurement, dFLISA produced better results than dPCR. This indicates that dFLISA may be a more accurate method for determining the concentration of AAV vector genomic material in a sample. It also suggests that dFLISA results are relatively unaffected by matrix interference or impurities from the crude lysate, making it a reliable analytical technique for AAV vector particle analysis. The optimization of dPCR method could provide better results, which is nevertheless beyond the scope of this study.

4-2-3. Quantification of crude sample by dFLISA and other methods

Since AUC requires the purification of crude samples prior to analysis, the capsid and genomic titers of untreated crude samples can be measured by dFLISA. The capsid titer determined by dFLISA was comparable to that determined by ELISA. However, the genomic titer results with dFLISA were higher than those from dPCR. Taking the high recovery rate in the spike-recovery experiment into consideration, dFLISA results should be reliable. Considering the LOQ of dFLISA (1.61×10^{10} cp/mL, 1.70×10^{10} vg/mL) and the concentration of AAV at the end of upstream process ($> 10^{10}$ vg/mL), sensitivity of dFLISA is high enough to analyze crude samples although it would be difficult to analyse samples at the beginning of upstream process. The dPCR/ELISA combination approach is time-consuming and exhibits low accuracy,[111] with reported coefficients of up to 36%.[108] In contrast, the entire dFLISA run was completed in less than 5 hours. The simple data evaluation procedure contributes to the

short duration, allowing for the analysis of more than 35 samples per day. Furthermore, the dFLISA allows for the straightforward quantification of purified AAV vectors as well as unpurified in-process samples. This is especially critical because there are no direct orthogonal methods available for quantifying crude samples without any purification. dFLISA was developed as a simple method to quantify full and empty particles for both purified and in-process (unpurified) samples.

It is worth to note that the inability of dFLISA to distinguish FP, PP, and ExP is a limitation of the method (**Table 19**), which may result in differences in titers from other methods such as dPCR and AUC. The most crucial performance criteria of analytical methods in this study, including the limitation of FLISA, are presented in **Table 19**.

5. Conclusion

In **Chapter 3**, I successfully explored the high-throughput capabilities of dFLISA and demonstrated its application in analyzing various aspects of AAV vectors. I found that dFLISA could not only determine the FP ratio for different AAV serotypes but also be easily modified to measure various AAV vector serotypes and genome lengths. Despite the presence of impurities such as host cell DNA and proteins in crude lysate samples, my experiments evaluating the recovery efficiency of spiking levels showed that dFLISA can effectively analyze crude samples without the need for purification. Regardless of whether purified or crude lysate samples were used, dFLISA consistently detected capsid and genome titers with high precision and without interference from the sample matrix. For the genomic result of genomic titer results with dFLISA were higher than those from dPCR. Although there is a possibility that partial genome which could not be detected by dPCR affected the dFLISA result, another possibility is that dPCR was affected by the interference of impurities. In addition, the result illustrated that dFLISA can quantify the genomic and

capsid titers of crude samples. dFLISA can be easily modified for measuring other AAV vector serotypes and AAV vectors with different genome lengths. These features make dFLISA a valuable tool for the future development of AAV-based gene therapies.

Chapter 4. General conclusion and future perspective

This study introduces a novel analytical technique that allows for the accurate and precise measurement of the abundance of both full and empty AAV vector capsids, as well as the full particle ratio. To initiate the dFLISA analysis, first, AAV samples, both purified and unpurified samples, were prepared and diluted to appropriate concentrations within the standard quantification range using a standardized buffer solution. Next, the samples were subjected to the dFLISA protocol, which involved binding specific antibodies to the AAV capsids and viral genome, followed by genome staining where two different fluorescent dyes were used to quantify full and empty AAV vector particles and the FP ratio. After the addition of a secondary antibody conjugated to one fluorescent dye, before the introduction of the second fluorescent dye, the microwell plate was subjected to heat treatment to release the genome from the capsid. Finally, dFLISA allows the determination of the FP ratio in a simple way with high precision, high accuracy, high sensitivity and good linearity, and it corresponds with the expected value.

The correlation between dFLISA and BS-AUC proved robustness and the reliability of the dFLISA for both full and empty capsids. dFLISA results also corresponded with those of other orthogonal techniques, including MP and a combination of dPCR and ELISA. Remarkably, dFLISA showed significant potential for evaluating the capsid and genome titers of unpurified samples and different AAV vector serotypes. It provides a straightforward method with high precision, requiring minimal analytical expertise. Additionally, dFLISA can be performed without specialized equipment, making it advantageous for in-process analysis. Furthermore, this simplicity facilitates high-quality viral vector production and supports in-process analytical testing, even the limitation of this dFLSA analysis is inability to distinguish full particles from extrafilled and partial particles. However, these limitations have been strictly demonstrated and

discussed in standards and sampled quantification by BS-AUC in this dissertation.

There are several promising directions for the further development and application of dFLISA. First, dFLISA application could significantly increase throughput, making it suitable for large-scale screening in pharmaceutical and clinical laboratories. Second, while this study focused on AAV vectors, the principles of dFLISA could be applied to other viral vectors such as lentiviruses (LVs) or adenoviruses, broadening its applicability in gene therapy research. Third, non-viral vectors such as lipid nanoparticles (LNPs) such as liposomes or solid lipid nanoparticles would have similar issues and could be analyzed by a method like dFLISA. Fourth, the combination of dFLISA with advanced imaging techniques or next-generation sequencing could provide comprehensive insights into viral vector characteristics and improve the precision of quantification.

In addition, the newly developed dFLISA described in this study has established itself as a critical method for the simple, accurate and precise detection of AAV vector particles. In the future, additional validation studies and clinical trials will be necessary to facilitate the transition of dFLISA from research to clinical application. In pursuit of this goal, adaptation of dFLISA protocols to specific viral targets or therapeutic proteins holds promise for enhancing its applicability in personalized medicine. This advancement will have a significant impact on gene therapy, viral diagnostics, and biopharmaceutical development, leading to improved patient outcomes and further scientific understanding.

Table 19. Most crucial performance criteria of analytical methods in this study

Methods	Target information	Purified sample	Turnaround (h)[a]	Sample volume (μL)	Sample concentration	Advantages	Limitations
BS-AUC	Particle content & aggregate	Yes	4–5	15–30	1×10^{12}–2×10^{13} cp/mL	- Capable of quantifying partially filled capsids and aggregates	- Requires specialized equipment - Purification is required prior to analysis of crude samples.
dPCR	Genomic titer	No	2–3	2–5	10^{7}–10^{10} vg/mL	- Specific and fast	- Low precision and accuracy
dFLISA	Particle content	No	4.5–5	100	2×10^{10}–10^{11} vg/mL	- High precision and accuracy - Purification is not necessary prior to analysis of crude samples	- LOQ is slightly higher than the LOQ of ELISA. However, it is high enough to detect capsid titers. - PPs and ExPs cannot be distinguished from FPs.
ELISA	Capsid titer	No	4.5–5	100	10^{8}–10^{10} cp/mL	- High specificity	- Low accuracy and precision
MP	Particle content	Yes	0.33–0.5	1–10	1×10^{11}– 1×10^{12} vg/mL	- Capable of differentiating each component by the mass and providing relative number concentration of each component (% counts). - Low material requirements	- Requires specialized equipment - Purification is necessary prior to the analysis of crude samples

[a]Turnaround time includes sample preparation and data analysis; BS-AUC, band sedimentation analytical ultracentrifugation; dPCR, digital polymerase chain reaction; dFLISA, dual fluorescence-linked immunosorbent assay; ELISA, enzyme-linked immunosorbent assay; MP, mass photometry; cp, capsid particle; vg, viral genome; ExP, extra filled particle; FP, full particle; LOQ, limit of quantification; PP, partial particle

References

1. Amrani, N., Luk, K., Singh, P., Shipley, M., Isik, M., Donadoni, M., Bellizzi, A., Khalili, K., Sariyer, I.K., Neumann, D., et al. (2024). CRISPR-Cas9-mediated genome editing delivered by a single AAV9 vector inhibits HSV-1 reactivation in a latent rabbit keratitis model. Mol Ther Methods Clin Dev. https://doi.org/10.1016/j.omtm.2024.101303.
2. Loo, L., Harris, S., Milton, M., Meena, Lembke, W., Berisha, F., Bertholet, S., Dessy, F., Dodge, R., Fang, X., et al. (2022). 2021 White Paper on Recent Issues in Bioanalysis: TAb/NAb, Viral Vector CDx, Shedding Assays; CRISPR/Cas9 & CAR-T Immunogenicity; PCR & Vaccine Assay Performance; ADA Assay Comparability & Cut Point Appropriateness (Part 3 - Recommendations on Gene Therapy, Cell Therapy, Vaccine Assays; Immunogenicity of Biotherapeutics and Novel Modalities; Integrated Summary of Immunogenicity Harmonization). Bioanalysis *14*, 737–793. https://doi.org/10.4155/bio-2022-0081.
3. Bennett, A., Gargas, J., Kansol, A., Lewis, J., Hsi, J., Hull, J., Mietzsch, M., Tartaglia, L., Muzyczka, N., Bhattacharya, N., et al. (2023). Structural and Biophysical Analysis of Adeno-Associated Virus Serotype 2 Capsid Assembly Variants. J Virol *97*. https://doi.org/10.1128/jvi.01772-22.
4. Qin, D. (2019). Next-generation sequencing and its clinical application. Cancer Biol Med *16*, 4–10. https://doi.org/10.20892/j.issn.2095-3941.2018.0055.
5. Liu, Y., Siriwon, N., Rohrs, J., and Wang, P. (2015). Generation of Targeted Adeno-Associated Virus (AAV) Vectors for Human Gene Therapy. Curr Pharm Des *21*, 3248–3256. https://doi.org/10.2174/1381612821666150531171653.
6. Summerford, C., and Samulski, R.J. (1999). Viral receptors and vector purification: New approaches for generating clinical-grade reagents. Nat Med *5*, 587–558. https://doi.org/10.1038/8470.
7. Hori, T., Fukutome, M., and Koike, C. (2019). Adeno associated virus (AAV) as a tool for clinical and experimental delivery of target genes into the mammalian retina. Biol Pharm Bull *42*, 343–347. https://doi.org/10.1248/bpb.b18-00913.
8. Yost, S.A., Firlar, E., Glenn, J.D., Carroll, H.B., Foltz, S., Giles, A.R., Egley, J.M., Firnberg, E., Cho, S., Nguyen, T., et al. (2023). Characterization and biodistribution of under-employed gene therapy vector AAV7. J Virol *97*. https://doi.org/10.1128/jvi.01163-23.
9. Chung, C.H., Murphy, C.M., Wingate, V.P., Pavlicek, J.W., Nakashima, R., Wei, W., McCarty, D., Rabinowitz, J., and Barton, E. (2023). Production of rAAV by plasmid transfection induces antiviral and inflammatory responses in suspension HEK293 cells. Mol Ther Methods Clin Dev *28*, 272–283. https://doi.org/10.1016/j.omtm.2023.01.002.
10. Smith, J., Guapo, F., Strasser, L., Millán-Martín, S., Milian, S.G., Snyder, R.O., and

Bones, J. (2024). Development of a Rapid Adeno-Associated Virus (AAV) Identity Testing Platform through Comprehensive Intact Mass Analysis of Full-Length AAV Capsid Proteins. J Proteome Res *23*, 161–174. https://doi.org/10.1021/acs.jproteome.3c00513.

11. Loeb, E.J., Havlik, P.L., Elmore, Z.C., Rosales, A., Fergione, S.M., Gonzalez, T.J., Smith, T.J., Benkert, A.R., Fiflis, D.N., and Asokan, A. (2024). Capsid-mediated control of adeno-associated viral transcription determines host range. Cell Rep *43*. https://doi.org/10.1016/j.celrep.2024.113902.
12. Samulski, R.J., and Muzyczka, N. (2014). AAV-mediated gene therapy for research and therapeutic purposes. Annu Rev Virol *1*, 427–451. https://doi.org/10.1146/annurev-virology-031413-085355.
13. Suk Lee, Y., Lee, J., Fang, K., Gee, G. V., Rogers, B., McNally, D., and Yoon, S. (2024). Separation of full, empty, and partial adeno-associated virus capsids via anion-exchange chromatography with continuous recycling and accumulation. J Chromatogr B Analyt Technol Biomed Life Sci *1242*. https://doi.org/10.1016/j.jchromb.2024.124206.
14. Huttner, N.A., Girod, A., Perabo, L., Edbauer, D., Kleinschmidt, J.A., Büning, H., and Hallek, M. (2003). Genetic modifications of the adeno-associated virus type 2 capsid reduce the affinity and the neutralizing effects of human serum antibodies. Gene Ther *10*, 2139–2147. https://doi.org/10.1038/sj.gt.3302123.
15. Wörner, T.P., Snijder, J., Friese, O., Powers, T., and Heck, A.J.R. (2022). Assessment of genome packaging in AAVs using Orbitrap-based charge-detection mass spectrometry. Mol Ther Methods Clin Dev *24*, 40–47. https://doi.org/10.1016/j.omtm.2021.11.013.
16. Bucher, K., Rodríguez-Bocanegra, E., Wissinger, B., Strasser, T., Clark, S.J., Birkenfeld, A.L., Siegel-Axel, D., and Fischer, M.D. (2023). Extra-viral DNA in adeno-associated viral vector preparations induces TLR9-dependent innate immune responses in human plasmacytoid dendritic cells. Sci Rep *13*. https://doi.org/10.1038/s41598-023-28830-7.
17. Yang, Q.-E., Walton, R.W., Kudrolli, T., Denys, N., Lance, K., and Chang, A. (2022). Rapid Quality Control Assessment of Adeno-Associated Virus Vectors Via Stunner. GEN Biotechnology *1*, 300–310. https://doi.org/10.1089/genbio.2022.0007.
18. De-Luca, R., Pupo-Correia, M., Feldhofer, M., Martins, D.L., Umprecht, A., Shahmohammadi, A., Corona, D., and von Stosch, M. (2024). Hybrid modeling of an ultracentrifugation process for separation of full and empty adeno-associated virus particles. Bioprocess Biosyst Eng *47*, 877–890. https://doi.org/10.1007/s00449-024-03014-3.
19. Blahetek, G., Mayer, C., Zuber, J., Lenter, M., and Strobel, B. (2024). Suppression of toxic transgene expression by optimized artificial miRNAs increases AAV vector yields in HEK-293 cells. Mol Ther Methods Clin Dev *32*. https://doi.org/10.1016/j.omtm.2024.101280.

20. Yin, V., Devine, P.W.A., Saunders, J.C., Hines, A., Shepherd, S., Dembek, M., Dobson, C.L., Snijder, J., Bond, N.J., and Heck, A.J.R. Spectral Interferences Impede the High-Resolution Mass Analysis of Recombinant Adeno-Associated Viruses. https://doi.org/10.1101/2022.08.27.505551.
21. McCraw, D.M., O'Donnell, J.K., Taylor, K.A., Stagg, S.M., and Chapman, M.S. (2012). Structure of adeno-associated virus-2 in complex with neutralizing monoclonal antibody A20. Virology *431*, 40–49. https://doi.org/10.1016/j.virol.2012.05.004.
22. Earley, L.F., Powers, J.M., Adachi, K., Baumgart, J.T., Meyer, N.L., Xie, Q., Chapman, M.S., and Nakai, H. (2017). Adeno-associated Virus (AAV) Assembly-Activating Protein Is Not an Essential Requirement for Capsid Assembly of AAV Serotypes 4, 5, and 11. J Virol *91*. https://doi.org/10.1128/jvi.01980-16.
23. Elmore, Z.C., Patrick Havlik, L., Oh, D.K., Anderson, L., Daaboul, G., Devlin, G.W., Vincent, H.A., and Asokan, A. (2021). The membrane associated accessory protein is an adeno-associated viral egress factor. Nat Commun *12*. https://doi.org/10.1038/s41467-021-26485-4.
24. Galibert, L., Hyvönen, A., Eriksson, R.A.E., Mattola, S., Aho, V., Salminen, S., Albers, J.D., Peltola, S.K., Weman, S., Nieminen, T., et al. (2021). Functional roles of the membrane-associated AAV protein MAAP. Sci Rep *11*. https://doi.org/10.1038/s41598-021-01220-7.
25. Schiffrin, B., Radford, S.E., Brockwell, D.J., and Calabrese, A.N. PyXlinkViewer: a flexible tool for visualisation of protein chemical crosslinking data within the PyMOL molecular graphics system. https://doi.org/10.1101/2020.06.16.154773.
26. Cole, L., Fernandes, D., Hussain, M.T., Kaszuba, M., Stenson, J., Markova, N., De Rosa, G., Campani, V., Clemente, I., and Anchordoquy, T. (2021). pharmaceutics Characterization of Recombinant Adeno-Associated Viruses (rAAVs) for Gene Therapy Using Orthogonal Techniques. https://doi.org/10.3390/pharmaceutics.
27. Issa, S.S., Shaimardanova, A.A., Solovyeva, V. V., and Rizvanov, A.A. (2023). Various AAV Serotypes and Their Applications in Gene Therapy: An Overview. Cells *12*, 1–41. https://doi.org/10.3390/cells12050785.
28. Jang, S., Shen, H.K., Ding, X., Miles, T.F., and Gradinaru, V. (2022). Structural basis of receptor usage by the engineered capsid AAV-PHP.eB. Mol Ther Methods Clin Dev *26*, 343–354. https://doi.org/10.1016/j.omtm.2022.07.011.
29. Zhang, R., Cao, L., Cui, M., Sun, Z., Hu, M., Zhang, R., Stuart, W., Zhao, X., Yang, Z., Li, X., et al. (2019). Adeno-associated virus 2 bound to its cellular receptor AAVR. Nat Microbiol *4*, 675–682. https://doi.org/10.1038/s41564-018-0356-7.
30. Mietzsch, M., Liu, W., Ma, K., Bennett, A., Nelson, A.R., Gliwa, K., Chipman, P., Fu, X., Bechler, S., McKenna, R., et al. (2023). Production and characterization of an AAV1-VP3-only capsid: An analytical benchmark standard. Mol Ther Methods Clin Dev *29*,

460–472. https://doi.org/10.1016/j.omtm.2023.05.002.

31. Sommer, J.M., Smith, P.H., Parthasarathy, S., Isaacs, J., Vijay, S., Kieran, J., Powell, S.K., McClelland, A., and Wright, F. (2003). Quantification of adeno-associated virus particles and empty capsids by optical density measurement. Molecular Therapy *7*, 122–128. https://doi.org/10.1016/S1525-0016(02)00019-9.
32. Cole, L., Fernandes, D., Hussain, M.T., Kaszuba, M., Stenson, J., and Markova, N. (2021). Characterization of recombinant adeno-associated viruses (rAAVs) for gene therapy using orthogonal techniques. Pharmaceutics *13*. https://doi.org/10.3390/pharmaceutics13040586.
33. Huttner, N.A., Girod, A., Perabo, L., Edbauer, D., Kleinschmidt, J.A., Büning, H., and Hallek, M. (2003). Genetic modifications of the adeno-associated virus type 2 capsid reduce the affinity and the neutralizing effects of human serum antibodies. Gene Ther *10*, 2139–2147. https://doi.org/10.1038/sj.gt.3302123.
34. Sommer, J.M., Smith, P.H., Parthasarathy, S., Isaacs, J., Vijay, S., Kieran, J., Powell, S.K., McClelland, A., and Wright, F. (2003). Quantification of adeno-associated virus particles and empty capsids by optical density measurement. Molecular Therapy *7*, 122–128. https://doi.org/10.1016/S1525-0016(02)00019-9.
35. Nyberg, W.A., Ark, J., To, A., Clouden, S., Reeder, G., Muldoon, J.J., Chung, J.Y., Xie, W.H., Allain, V., Steinhart, Z., et al. (2023). An evolved AAV variant enables efficient genetic engineering of murine T cells. Cell *186*, 446-460.e19. https://doi.org/10.1016/j.cell.2022.12.022.
36. Wobus, C.E., Hügle-Dörr, B., Girod, A., Petersen, G., Hallek, M., and Kleinschmidt, J.A. (2000). Monoclonal Antibodies against the Adeno-Associated Virus Type 2 (AAV-2) Capsid: Epitope Mapping and Identification of Capsid Domains Involved in AAV-2–Cell Interaction and Neutralization of AAV-2 Infection. J Virol *74*, 9281–9293. https://doi.org/10.1128/jvi.74.19.9281-9293.2000.
37. Barnes, L.F., Draper, B.E., Kurian, J., Chen, Y.T., Shapkina, T., Powers, T.W., and Jarrold, M.F. (2023). Analysis of AAV-Extracted DNA by Charge Detection Mass Spectrometry Reveals Genome Truncations. Anal Chem *95*, 4310–4316. https://doi.org/10.1021/acs.analchem.2c04234.
38. Bee, J.S., O'Berry, K., Zhang, Y. (Zoe), Phillippi, M.K., Kaushal, A., DePaz, R.A., and Marshall, T. (2021). Quantitation of Trace Levels of DNA Released from Disrupted Adeno-Associated Virus Gene Therapy Vectors. J Pharm Sci *110*, 3183–3187. https://doi.org/10.1016/j.xphs.2021.06.010.
39. Werle, A.K., Powers, T.W., Zobel, J.F., Wappelhorst, C.N., Jarrold, M.F., Lyktey, N.A., Sloan, C.D.K., Wolf, A.J., Adams-Hall, S., Baldus, P., et al. (2021). Comparison of analytical techniques to quantitate the capsid content of adeno-associated viral vectors. Mol Ther Methods Clin Dev *23*, 254–262. https://doi.org/10.1016/j.omtm.2021.08.009.

40. Halder, S., Van Vliet, K., Smith, J.K., Duong, T.T.P., McKenna, R., Wilson, J.M., and Agbandje-McKenna, M. (2015). Structure of neurotropic adeno-associated virus AAVrh.8. J Struct Biol *192*, 21–36. https://doi.org/10.1016/j.jsb.2015.08.017.
41. Deverman, B.E., Ravina, B.M., Bankiewicz, K.S., Paul, S.M., and Sah, D.W.Y. (2018). Gene therapy for neurological disorders: Progress and prospects. Nat Rev Drug Discov *17*, 641–659. https://doi.org/10.1038/nrd.2018.110.
42. Xu, G., Zhang, R., Li, H., Yin, K., Ma, X., and Lou, Z. (2022). Structural basis for the neurotropic AAV9 and the engineered AAVPHP.eB recognition with cellular receptors. Mol Ther Methods Clin Dev *26*, 52–60. https://doi.org/10.1016/j.omtm.2022.05.009.
43. West, A.C., Federspiel, J.D., Rogers, K., and Khatri, A. (2023). Complement activation by AAV-neutralizing antibody complexes. 1–29. https://doi.org/10.1089/hum.2023.018.
44. Barnes, C., Scheideler, O., and Schaffer, D. (2019). Engineering the AAV capsid to evade immune responses. Curr Opin Biotechnol *60*, 99–103. https://doi.org/10.1016/j.copbio.2019.01.002.
45. Hiemenz, C., Pacios-Michelena, A., Helbig, C., Vezočnik, V., Strebl, M., Nikels, F., Hawe, A., Garidel, P., and Menzen, T. (2023). Characterization of Virus Particles and Submicron-Sized Particulate Impurities in Recombinant Adeno-Associated Virus Drug Product. J Pharm Sci *112*, 2190–2202. https://doi.org/10.1016/j.xphs.2023.05.009.
46. Grande, A.E., Li, X., Miller, L.M., Zhang, J., Draper, B.E., Herzog, R.W., Xiao, W., and Jarrold, M.F. (2023). Antibody Binding to Recombinant Adeno Associated Virus Monitored by Charge Detection Mass Spectrometry. Anal Chem *95*, 10864–10868. https://doi.org/10.1021/acs.analchem.3c02371.
47. Ebberink, E.H.T.M., Ruisinger, A., Nuebel, M., Thomann, M., and Heck, A.J.R. (2022). Assessing production variability in empty and filled adeno-associated viruses by single molecule mass analyses. Mol Ther Methods Clin Dev *27*, 491–501. https://doi.org/10.1016/j.omtm.2022.11.003.
48. Yarawsky, A.E., Zai-Rose, V., Cunningham, H.M., Burgner, J.W., DeLion, M.T., and Paul, L.N. (2023). AAV analysis by sedimentation velocity analytical ultracentrifugation: beyond empty and full capsids. European Biophysics Journal *52*, 353–366. https://doi.org/10.1007/s00249-023-01646-z.
49. Riccardi, C., Carlson, D.P., Graham, K.S., Shameem, M., and Kamen, D.E. (2023). Evaluation of the In-Use Stability of Monoclonal Antibody IV Admixtures Prepared from Drug Products Containing Polysorbate 20 Degraded by Host-Cell Lipases. J Pharm Sci *112*, 3045–3055. https://doi.org/10.1016/j.xphs.2023.08.020.
50. Sternisha, S.M., Wilson, A.D., Bouda, E., Bhattacharya, A., and VerHeul, R. (2023). Optimizing high-throughput viral vector characterization with density gradient equilibrium analytical ultracentrifugation. European Biophysics Journal *52*, 387–392. https://doi.org/10.1007/s00249-023-01654-z.

51. Hajba, L., and Guttman, A. (2020). Recent Advances in the Analysis Full/Empty Capsid Ratio and Genome Integrity of Adeno-associated Virus (AAV) Gene Delivery Vectors. Curr Mol Med *20*, 806–813. https://doi.org/10.2174/1566524020999200730181042.
52. Selvaraj, N., Wang, C.K., Bowser, B., Broadt, T., Shaban, S., Burns, J., Saptharishi, N., Pechan, P., Golebiowski, D., Alimardanov, A., et al. (2021). Detailed Protocol for the Novel and Scalable Viral Vector Upstream Process for AAV Gene Therapy Manufacturing. Hum Gene Ther *32*, 850–861. https://doi.org/10.1089/hum.2020.054.
53. Wörner, T.P., Snijder, J., Friese, O., Powers, T., and Heck, A.J.R. (2022). Assessment of genome packaging in AAVs using Orbitrap-based charge-detection mass spectrometry. Mol Ther Methods Clin Dev *24*, 40–47. https://doi.org/10.1016/j.omtm.2021.11.013.
54. Werling, N.J., Satkunanathan, S., Thorpe, R., and Zhao, Y. (2015). Systematic Comparison and Validation of Quantitative Real-Time PCR Methods for the Quantitation of Adeno-Associated Viral Products. Hum Gene Ther Methods *26*, 82–92. https://doi.org/10.1089/hgtb.2015.013.
55. Wu, D., and Piszczek, G. (2021). Standard protocol for mass photometry experiments. European Biophysics Journal *50*, 403–409. https://doi.org/10.1007/s00249-021-01513-9.
56. Lai, S.H., Tamara, S., and Heck, A.J.R. (2021). Single-particle mass analysis of intact ribosomes by mass photometry and Orbitrap-based charge detection mass spectrometry. iScience *24*. https://doi.org/10.1016/j.isci.2021.103211.
57. Gardner, M.R., Mendes, D.E., Muniz, C.P., Martinez-Navio, J.M., Fuchs, S.P., Gao, G., and Desrosiers, R.C. (2022). High concordance of ELISA and neutralization assays allows for the detection of antibodies to individual AAV serotypes. Mol Ther Methods Clin Dev *24*, 199–206. https://doi.org/10.1016/j.omtm.2022.01.003.
58. Klumpp-Thomas, C., Kalish, H., Drew, M., Hunsberger, S., Snead, K., Fay, M.P., Mehalko, J., Shunmugavel, A., Wall, V., Frank, P., et al. (2021). Standardization of ELISA protocols for serosurveys of the SARS-CoV-2 pandemic using clinical and at-home blood sampling. Nat Commun *12*. https://doi.org/10.1038/s41467-020-20383-x.
59. Sanmiguel, J., Gao, G., and Vandenberghe, L.H. (2019). Quantitative and digital droplet-based AAV genome titration. In Methods in Molecular Biology (Humana Press Inc.), pp. 51–83. https://doi.org/10.1007/978-1-4939-9139-6_4.
60. François, A., Bouzelha, M., Lecomte, E., Broucque, F., Penaud-Budloo, M., Adjali, O., Moullier, P., Blouin, V., and Ayuso, E. (2018). Accurate Titration of Infectious AAV Particles Requires Measurement of Biologically Active Vector Genomes and Suitable Controls. Mol Ther Methods Clin Dev *10*, 223–236. https://doi.org/10.1016/j.omtm.2018.07.004.
61. Veldwijk, M.R., Topaly, J., Laufs, S., Hengge, U.R., Wenz, F., Zeller, W.J., and Fruehauf, S. (2002). Development and optimization of a real-time quantitative PCR-based method for the titration of AAV-2 vector stocks. Molecular Therapy *6*, 272–278.

https://doi.org/10.1006/mthe.2002.0659.

62. SAITO, S., KONDO, A., and UCHIDA, K. (2023). Investigating critical thermal parameters for pre-analytical preparation of adeno-associated virus vector genome titration by droplet digital polymerase chain reaction. Translational and Regulatory Sciences *5*, 28–35. https://doi.org/10.33611/trs.2023-001.

63. Meierrieks, F., Kour, A., Pätz, M., Pflanz, K., Wolff, M.W., and Pickl, A. (2023). Unveiling the secrets of adeno-associated virus: novel high-throughput approaches for the quantification of multiple serotypes. Mol Ther Methods Clin Dev *31*. https://doi.org/10.1016/j.omtm.2023.101118.

64. He, X.Z., Powers, T.W., Huang, S., Liu, Z., Shi, H., Orlet, J.D., Mo, J.J., Srinivasan, S., Jacobs, S., Zhang, K., et al. (2023). Development of an icIEF assay for monitoring AAV capsid proteins and application to gene therapy products. Mol Ther Methods Clin Dev *29*, 133–144. https://doi.org/10.1016/j.omtm.2023.03.002.

65. Fu, Q., Lee, Y.S., Green, E.A., Wang, Y., Park, S.Y., Polanco, A., Lee, K.H., Betenbaugh, M., McNally, D., and Yoon, S. (2023). Design space determination to optimize DNA complexation and full capsid formation in transient rAAV manufacturing. Biotechnol Bioeng. https://doi.org/10.1002/bit.28508.

66. Aebischer, M.K., Bouvarel, T., Barrozo, E., Kochardt, D., Elger, C., Haindl, M., Ruppert, R., Guillarme, D., and D'Atri, V. (2023). Boosting the Separation of Adeno-Associated Virus Capsid Proteins by Liquid Chromatography and Capillary Electrophoresis Approaches. Int J Mol Sci *24*. https://doi.org/10.3390/ijms24108503.

67. Overturf, K. (2009). Quantitative PCR. Molecular Research in Aquaculture, 39–61. https://doi.org/10.1002/9780813807379.ch3.

68. Blasco, H., Lalmanach, G., Godat, E., Maurel, M.C., Canepa, S., Belghazi, M., Paintaud, G., Degenne, D., Chatelut, E., Cartron, G., et al. (2007). Evaluation of a peptide ELISA for the detection of rituximab in serum. J Immunol Methods *325*, 127–139. https://doi.org/10.1016/j.jim.2007.06.011.

69. Xu, R., Janson, C.G., Mastakov, M., Lawlor, P., Young, D., Mouravlev, A., Fitzsimons, H., Choi, K.L., Ma, H., Dragunow, M., et al. (2001). Quantitative comparison of expression with adeno-associated virus (AAV-2) brain-specific gene cassettes. Gene Ther *8*, 1323–1332. https://doi.org/10.1038/sj.gt.3301529.

70. Kuck, D., Kern, A., and Kleinschmidt, J.A. (2007). Development of AAV serotype-specific ELISAs using novel monoclonal antibodies. J Virol Methods *140*, 17–24. https://doi.org/10.1016/j.jviromet.2006.10.005.

71. Eichhoff, A.M., Börner, K., Albrecht, B., Schäfer, W., Baum, N., Haag, F., Körbelin, J., Trepel, M., Braren, I., Grimm, D., et al. (2019). Nanobody-Enhanced Targeting of AAV Gene Therapy Vectors. Mol Ther Methods Clin Dev *15*, 211–220. https://doi.org/10.1016/j.omtm.2019.09.003.

72. Fu, Y., Choudhary, D., Liu, N., Moon, Y., Abdubek, P., Sweezy, L., Rosconi, M., Palackal, N., and Pyles, E. (2023). Comprehensive biophysical characterization of AAV-AAVR interaction uncovers serotype- and pH-dependent interaction. J Pharm Biomed Anal *234*. https://doi.org/10.1016/j.jpba.2023.115562.
73. Kolbeck, P.J., Vanderlinden, W., Gemmecker, G., Gebhardt, C., Lehmann, M., Lak, A., Nicolaus, T., Cordes, T., and Lipfert, J. (2021). Molecular structure, DNA binding mode, photophysical properties and recommendations for use of SYBR Gold. Nucleic Acids Res *49*, 5143–5158. https://doi.org/10.1093/nar/gkab265.
74. Tuma, R.S., Beaudet, M.P., Jin, X., Jones, L.J., Cheung, C.Y., Yue, S., and Singer, V.L. (1999). Characterization of SYBR gold nucleic acid gel stain: A dye optimized for use with 300-nm ultraviolet transilluminators. Anal Biochem *268*, 278–288. https://doi.org/10.1006/abio.1998.3067.
75. Maruno, T., Ishii, K., Torisu, T., and Uchiyama, S. (2023). Size Distribution Analysis of the Adeno-Associated Virus Vector by the c(s) Analysis of Band Sedimentation Analytical Ultracentrifugation with Multiwavelength Detection. J Pharm Sci *112*, 937–946. https://doi.org/https://doi.org/10.1016/j.xphs.2022.10.023.
76. Schuck, P. (1998). Sedimentation analysis of noninteracting and self-associating solutes using numerical solutions to the Lamm equation. Biophys J *75*, 1503–1512. https://doi.org/10.1016/S0006-3495(98)74069-X.
77. Philo, J.S. (2023). SEDNTERP: a calculation and database utility to aid interpretation of analytical ultracentrifugation and light scattering data. European Biophysics Journal *52*, 233–266. https://doi.org/10.1007/s00249-023-01629-0.
78. Maruno, T., Usami, K., Ishii, K., Torisu, T., and Uchiyama, S. (2021). Comprehensive Size Distribution and Composition Analysis of Adeno-Associated Virus Vector by Multiwavelength Sedimentation Velocity Analytical Ultracentrifugation. J Pharm Sci *110*, 3375–3384. https://doi.org/10.1016/j.xphs.2021.06.031.
79. Brautigam, C.A. (2015). Calculations and Publication-Quality Illustrations for Analytical Ultracentrifugation Data 1st ed. (Elsevier Inc.) https://doi.org/10.1016/bs.mie.2015.05.001.
80. Maruno, T., Ishii, K., Torisu, T., and Uchiyama, S. (2023). Size Distribution Analysis of the Adeno-Associated Virus Vector by the c(s) Analysis of Band Sedimentation Analytical Ultracentrifugation with Multiwavelength Detection. J Pharm Sci *112*, 937–946. https://doi.org/10.1016/j.xphs.2022.10.023.
81. Kolbeck, P.J., Vanderlinden, W., Gemmecker, G., Gebhardt, C., Lehmann, M., Lak, A., Nicolaus, T., Cordes, T., and Lipfert, J. (2021). Molecular structure, DNA binding mode, photophysical properties and recommendations for use of SYBR Gold. Nucleic Acids Res *49*, 5143–5158. https://doi.org/10.1093/nar/gkab265.
82. Jenkins, R., Duggan, J.X., Aubry, A.F., Zeng, J., Lee, J.W., Cojocaru, L., Dufield, D.,

Garofolo, F., Kaur, S., Schultz, G.A., et al. (2015). Recommendations for Validation of LC-MS/MS Bioanalytical Methods for Protein Biotherapeutics. AAPS Journal *17*, 1–16. https://doi.org/10.1208/s12248-014-9685-5.

83. Jarand, C.W., Baker, K., Petroff, M., Jin, M., and Reed, W.F. (2024). DNA Released by Adeno-Associated Virus Strongly Alters Capsid Aggregation Kinetics in a Physiological Solution. Biomacromolecules *25*, 2890–2901. https://doi.org/10.1021/acs.biomac.4c00027.
84. Xu, Y., Guo, P., Zhang, J., Chrzanowski, M., Chew, H., Firrman, J.A., Sang, N., Diao, Y., and Xiao, W. (2020). Effects of Thermally Induced Configuration Changes on rAAV Genome's Enzymatic Accessibility. Mol Ther Methods Clin Dev *18*, 328–334. https://doi.org/10.1016/j.omtm.2020.06.005.
85. Bee, J.S., O'Berry, K., Zhang, Y. (Zoe), Phillippi, M.K., Kaushal, A., DePaz, R.A., and Marshall, T. (2021). Quantitation of Trace Levels of DNA Released from Disrupted Adeno-Associated Virus Gene Therapy Vectors. J Pharm Sci *110*, 3183–3187. https://doi.org/10.1016/j.xphs.2021.06.010.
86. Kolbeck, P.J., Vanderlinden, W., Gemmecker, G., Gebhardt, C., Lehmann, M., Lak, A., Nicolaus, T., Cordes, T., and Lipfert, J. (2021). Molecular structure, DNA binding mode, photophysical properties and recommendations for use of SYBR Gold. Nucleic Acids Res *49*, 5143–5158. https://doi.org/10.1093/nar/gkab265.
87. Bennett, A., Patel, S., Mietzsch, M., Jose, A., Lins-Austin, B., Yu, J.C., Bothner, B., McKenna, R., and Agbandje-McKenna, M. (2017). Thermal Stability as a Determinant of AAV Serotype Identity. Mol Ther Methods Clin Dev *6*, 171–182. https://doi.org/10.1016/j.omtm.2017.07.003.
88. Hirohata, K., Yamaguchi, Y., Maruno, T., Shibuya, R., Torisu, T., Onishi, T., Chono, H., Mineno, J., Yuzhe, Y., Higashiyama, K., et al. (2024). Applications and Limitations of Equilibrium Density Gradient Analytical Ultracentrifugation for the Quantitative Characterization of Adeno-Associated Virus Vectors. Anal Chem *96*, 642–651. https://doi.org/10.1021/acs.analchem.3c01955.
89. Bepperling, A., and Best, J. (2023). Comparison of three AUC techniques for the determination of the loading status and capsid titer of AAVs. European Biophysics Journal *52*, 401–413. https://doi.org/10.1007/s00249-023-01661-0.
90. North, S.H., Lock, E.H., Cooper, C.J., Franek, J.B., Taitt, C.R., and Walton, S.G. (2010). Plasma-based surface modification of polystyrene microtiter plates for covalent immobilization of biomolecules. ACS Appl Mater Interfaces *2*, 2884–2891. https://doi.org/10.1021/am100566e.
91. Bee, J.S., O'Berry, K., Zhang, Y. (Zoe), Phillippi, M.K., Kaushal, A., DePaz, R.A., and Marshall, T. (2021). Quantitation of Trace Levels of DNA Released from Disrupted Adeno-Associated Virus Gene Therapy Vectors. J Pharm Sci *110*, 3183–3187.

https://doi.org/10.1016/j.xphs.2021.06.010.

92. Hao, X., Yang, X., Zou, S., and Cao, X. (2023). Surface modification of poly(styrene) 96-well plates using aptamers via a dendrimer-templated strategy to enhance ELISA performances. Colloids Surf B Biointerfaces *221*. https://doi.org/10.1016/j.colsurfb.2022.113003.

93. Onishi, T., Nonaka, M., Maruno, T., Yamaguchi, Y., Fukuhara, M., Torisu, T., Maeda, M., Abbatiello, S., Haris, A., Richardson, K., et al. (2023). Enhancement of recombinant adeno-associated virus activity by improved stoichiometry and homogeneity of capsid protein assembly. Mol Ther Methods Clin Dev *31*. https://doi.org/10.1016/j.omtm.2023.101142.

94. Barnes, L.F., Draper, B.E., Chen, Y.T., Powers, T.W., and Jarrold, M.F. (2021). Quantitative analysis of genome packaging in recombinant AAV vectors by charge detection mass spectrometry. Mol Ther Methods Clin Dev *23*, 87–97. https://doi.org/10.1016/j.omtm.2021.08.002.

95. Li, Y., Struwe, W.B., and Kukura, P. (2020). Single molecule mass photometry of nucleic acids. Nucleic Acids Res *48*, E97. https://doi.org/10.1093/nar/gkaa632.

96. Gagnon, P., Goricar, B., Mencin, N., Zvanut, T., Peljhan, S., Leskovec, M., and Strancar, A. (2021). Multiple-monitor HPLC assays for rapid process development, in-process monitoring, and validation of AAV production and purification. Pharmaceutics *13*, 1–14. https://doi.org/10.3390/pharmaceutics13010113.

97. Khatwani, S.L., Pavlova, A., and Pirot, Z. (2021). Anion-exchange HPLC assay for separation and quantification of empty and full capsids in multiple adeno-associated virus serotypes. Mol Ther Methods Clin Dev *21*, 548–558. https://doi.org/10.1016/j.omtm.2021.04.003.

98. Cui, M., Lu, Y., Tang, C., Zhang, R., Wang, J., Si, Y., Cheng, S., and Ding, W. (2019). A generic method for fast and sensitive detection of adeno-associated viruses using modified AAV receptor recombinant proteins. Molecules *24*. https://doi.org/10.3390/molecules24213973.

99. Duong, T., McAllister, J., Eldahan, K., Wang, J., Onishi, E., Shen, K., Schrock, R., Gu, B., and Wang, P. (2023). Improvement of Precision in Recombinant Adeno-Associated Virus Infectious Titer Assay with Droplet Digital PCR as an Endpoint Measurement. Hum Gene Ther *34*, 742–757. https://doi.org/10.1089/hum.2023.014.

100. Leatham, B., Mcnall, K., Subramanian, H.K., Jacky, L., Alvarado, J., Yurk, D., Wang, M., Green, D.C., Tsongalis, G.J., Rajagopal, A., et al. A rapid, multiplex digital PCR assay for EGFR, KRAS, BRAF, ERBB2 variants and ALK, RET, ROS1, NTRK1 gene fusions in non-small cell lung cancer. https://doi.org/10.1101/2023.03.09.531949.

101. Xu, Y., Guo, P., Zhang, J., Chrzanowski, M., Chew, H., Firrman, J.A., Sang, N., Diao, Y., and Xiao, W. (2020). Effects of Thermally Induced Configuration Changes on rAAV

Genome's Enzymatic Accessibility. Mol Ther Methods Clin Dev *18*, 328–334. https://doi.org/10.1016/j.omtm.2020.06.005.

102. Marino, M., Zhou, L., Rincon, M.Y., Callaerts-Vegh, Z., Verhaert, J., Wahis, J., Creemers, E., Yshii, L., Wierda, K., Saito, T., et al. (2022). AAV-mediated delivery of an anti-BACE1 VHH alleviates pathology in an Alzheimer's disease model. EMBO Mol Med *14*. https://doi.org/10.15252/emmm.201809824.
103. Fischer, M.D., McClements, M.E., Martinez-Fernandez de la Camara, C., Bellingrath, J.S., Dauletbekov, D., Ramsden, S.C., Hickey, D.G., Barnard, A.R., and MacLaren, R.E. (2017). Codon-Optimized RPGR Improves Stability and Efficacy of AAV8 Gene Therapy in Two Mouse Models of X-Linked Retinitis Pigmentosa. Molecular Therapy *25*, 1854–1865. https://doi.org/10.1016/j.ymthe.2017.05.005.
104. Miller, N.L., Raman, R., Clark, T., and Sasisekharan, R. (2022). Complexity of Viral Epitope Surfaces as Evasive Targets for Vaccines and Therapeutic Antibodies. Front Immunol *13*, 1–15. https://doi.org/10.3389/fimmu.2022.904609.
105. Gurda, B.L., Raupp, C., Popa-Wagner, R., Naumer, M., Olson, N.H., Ng, R., McKenna, R., Baker, T.S., Kleinschmidt, J.A., and Agbandje-McKenna, M. (2012). Mapping a Neutralizing Epitope onto the Capsid of Adeno-Associated Virus Serotype 8. J Virol *86*, 7739–7751. https://doi.org/10.1128/jvi.00218-12.
106. Asaadi, Y., Jouneghani, F.F., Janani, S., and Rahbarizadeh, F. (2021). A comprehensive comparison between camelid nanobodies and single chain variable fragments. Biomark Res *9*, 1–20. https://doi.org/10.1186/s40364-021-00332-6.
107. Dobnik, D., Kogovšek, P., Jakomin, T., Košir, N., Žnidarič, M.T., Leskovec, M., Kaminsky, S.M., Mostrom, J., Lee, H., and Ravnikar, M. (2019). Accurate quantification and characterization of adeno-associated viral vectors. Front Microbiol *10*. https://doi.org/10.3389/fmicb.2019.01570.
108. Heckel, J., Martinez, A., Elger, C., Haindl, M., Leiss, M., Ruppert, R., Williams, C., Hubbuch, J., and Graf, T. (2023). Fast HPLC-based Affinity Method to Determine Capsid Titer and Full/Empty Ratio of Adeno-Associated Viral Vectors. Mol Ther Methods Clin Dev, 101148. https://doi.org/10.1016/j.omtm.2023.101148.
109. Yang, Q.-E., Walton, R.W., Kudrolli, T., Denys, N., Lance, K., and Chang, A. (2022). Rapid Quality Control Assessment of Adeno-Associated Virus Vectors Via Stunner. GEN Biotechnology *1*, 300–310. https://doi.org/10.1089/genbio.2022.0007.
110. Rayaprolu, V., Kruse, S., Kant, R., Venkatakrishnan, B., Movahed, N., Brooke, D., Lins, B., Bennett, A., Potter, T., McKenna, R., et al. (2013). Comparative Analysis of Adeno-Associated Virus Capsid Stability and Dynamics. J Virol *87*, 13150–13160. https://doi.org/10.1128/jvi.01415-13.
111. McIntosh, N.L., Berguig, G.Y., Karim, O.A., Cortesio, C.L., De Angelis, R., Khan, A.A., Gold, D., Maga, J.A., and Bhat, V.S. (2021). Comprehensive characterization and

quantification of adeno associated vectors by size exclusion chromatography and multi angle light scattering. Sci Rep *11*, 1–12. https://doi.org/10.1038/s41598-021-82599-1.

Scientific publication

1. **S. Soth**, M.Takakura, M. Suekawa, T.Onishi, K. Hirohata, T. Hashimoto, T. Maruno, M. Fukuhara, Y. Tsunaka, T. Torisu, S. Uchiyama. Quantification of Full and Empty Particles of Adeno-Associated Virus Vectors by a Novel Dual Fluorescence-Linked Immunosorbent Assay. Mol Ther Methods Clin Dev. 2024, June; 32(3).

Acknowledgments

This doctoral dissertation encapsulates the entire journey of obtaining my doctoral degree in the laboratory of **Macromolecular Biotechnology**, **Department of Biotechnology**, **Graduate School of Engineering**, **Osaka University**, **Japan**. Initially, I would like to express my appreciation to the **Ministry of Education**, **Culture**, **Sports**, **Science and Technology**, **Japan (MEXT)**.

For supporting me during my Ph.D. studies, I am grateful for the grant-in-aid from "**Research and Development of Core Technologies for Gene and Cell Therapy**" supported by the Japan Agency for Medical Research and Development (AMED) [grant number JP20ae0201002].

To begin with I would like to express my sincerest gratitude to Prof. **Susumu Uchiyama** of Osaka University for sharing his expertise so willingly, and for his dedication to his supervisory role. He always gives me and everyone in our lab a lot of leadership (every year retreat and orientation). Beyond his patience, leadership, motivation, immense knowledge, and guidance, his discussions, advice, and unconditional support have motivated me to reach my study goals on this rewarding journey.

In addition, I am profoundly grateful to Associate Prof. **Tetsuo Torisu**, who has been my supervisor from my master's course through to my Ph.D. in the **Torisu team**. He was always available to give the discussion and provide guidance, even when I needed it most. One of the profound insights I gained from his slogan is the understanding that everyone is different. Consequently, interpersonal skills are crucial, regardless of our location or the individuals we are working with. Kindness, work hard, open-mindedness, and teamwork are fundamental principles essential for achieving true success in our research endeavors. Therefore, I am sincerely grateful to him for his assistance, leadership, motivation and unconditional support throughout this remarkable journey. Without his efforts, I would not have achieved the accomplishments I have today.

Furthermore, I would also like to express my sincerest gratitude to Prof. **Kazuhito Fujiyama** and Prof. **Takeshi Omasa**, Department of Biotechnology, Graduate School of Engineering, Osaka University, who kindly read this thesis and provided me with valuable guidance, comments, and suggestions for writing, the thesis presentation, and during the thesis defense.

Moreover, I would also like to give my gratitude to project assistant prof. **Mitsuko Fukuhara,** specially appointed associate prof. **Yasuo Tsunaka** for proving the purified in-house AAV8 both purified sample and crude lysate, and senior **Takayuki Onishi** for provide the purified in-house AAV8 empty particles for experiment.

I would like to express my gratitude to Assistant Prof. **Yuki Yamaguchi**, specially designated assistant prof. **Risa Shibuya**, and specially designated assistant prof. **Shigetaka Nishiguchi** for providing valuable advice regarding my paper and conference preparation. Their encouragement and kind words were a great source of motivation during challenging times.

Furthermore, I would like to express my sincerest gratitude to Mr. **Takahiro Maruno**, who has consistently supported me in my research, especially in the BS-AUC analysis. He has also dedicated his time and energy to teach about BS-AUC's data analysis and has motivated me during my study.

Additionally, I would also like to express my gratitude to Ms. **Mikako Takakura**, who contributed to the experimental analysis, investigation, and discussion for the dFLISA establishment. Her deep effort and willingness, even when she had to stay late, motivated me to persevere through lengthy experiments.

I would also like to express my gratitude to Invited Associate Prof. **Takuya Yamane** for always cheer me up whenever he meets me. Additionally, I am deeply grateful to secretary Ms. **Akiko Tsuyumine** and dispatched researcher Ms. **Karin Bandoh** for their very kind instructions and warm support, not only in my research but also in the laboratory life in general.

I would also like to express my sincerest gratitude to Mr. **Suekawa Mashahiro** for his invaluable assistance with MP measurements, and Ms. **Tamami Hashimoto** for her helpful guidance with the BLI analysis. Mr. **Kiichi Hirohata**'s insights on the BS-AUC analysis and his constructive ideas on my manuscript revision were also greatly appreciated.

During the path of the Ph.D, I have had the pleasure of working with exceptional lab-mate that have contributed to the completion of this thesis, including Mr. **Kentaro Ishii**,

Mr. **Shinji Kizuki**, Mr. **Ramy Salama**, Mr. **Tatsunori Kusube**, Ms. **Aoba Matsushita**, Mr. **Asuka Mori**, Ms. **Natsumi Wakaizumi**, Ms. **Haruka Nishiumi**, Mr. **Ekaputra Ramadhani**, Mr. **Zhuolun Yang**, Mr. **Makoto Murakami**, Mr. **Ryoji Nakatsuka**, Ms. **Satomi Kasahara**, Ms. **Mako Mori**, Mr. **Junya Mizuguchi**, Mr. **Zekun Wang**, Ms. **Zihan Zhang**, Mr. **Ryosuke Tanoue**, Mr. **Tomohiko Ikeda**, Mr. **Mark Allen Rocafort**, Ms. **Michika Nonaka**, Ms. **Rio Okada**, Ms. **Yu Nakajima**, Ms. **Shimojo Saki**, Ms. **Elga Fatima Saki**, Mr. **Shinichiro Kino**, Mr. **Yuma Furuta**, Ms. **Natsuki Shihara**, Ms. **Nana Iwamoto**, Ms. **Moe Konishi**, Ms. **Makihira Haruka**, Ms. **Amane Yamaguchi**, Mr. **Zhuofan Wang**, Ms. **Mana Yamasaki**, Mr. **Kihiro Asaka**, Mr. **Kazuto Chino**, Mr. **Shunto Kitahata**, Mr. **Koki Deguchi** and my international friends, including Ms. **Kulachatr Panyawechamontri** and Mr. **Ononugbo Chukwuebuka Maxwell** and others who have been very helpful and have always supported, shared, and kindness me through all the challenging situations of my research.

I would also like to express my sincerest gratitude to all professors, lecturers, and staff members at the **Biotechnology Department**, **Osaka University**, **Japan**, for their guidance, encouragement, and support throughout the years. I am grateful to all those who have made my studies possible.

Finally, I would like to thank my husband, **Panha Eang**, for his unwavering support and inspiration. I also thank my family for all the support received over the last three years. Being away from home is never easy, especially when "staying abroad" means being on the exact opposite side of the world. Their encouragement and faith in me have been a source of motivation and inspiration throughout this whole journey.